Accelerated Mineral Carbonation to Stabilize Non-Plastic Soils with Lime

Final Report
December 2025

Principal Investigator: Aaron Gallant

Civil and Environmental Engineering
University of Maine

Authors
Aaron Gallant; Sk Belal Hossen; Warda Ashraf; Luis Zambrano-Cruzatty; Temitope Omokinde; Andres Espinosa

Sponsored By
Transportation Infrastructure Durability Center

Transportation Infrastructure Durability Center
AT THE UNIVERSITY OF MAINE

A report from
University of Maine
Department of Civil and Environmental Engineering
5711 Boardman Hall
Orono, Maine 04469

About the Transportation Infrastructure Durability Center

The Transportation Infrastructure Durability Center (TIDC) is the 2018 US DOT Region 1 (New England) University Transportation Center (UTC) located at the University of Maine Advanced Structures and Composites Center. TIDC's research focuses on efforts to improve the durability and extend the life of transportation infrastructure in New England and beyond through an integrated collaboration of universities, state DOTs, and industry. The TIDC is comprised of six New England universities, the University of Maine (lead), the University of Connecticut, the University of Massachusetts Lowell, the University of Rhode Island, the University of Vermont, and Western New England University.

U.S. Department of Transportation (US DOT) Disclaimer

Acknowledgements

Funding for this research is provided by the Transportation Infrastructure Durability Center at the University of Maine under grant 69A3551847101 from the U.S. Department of Transportation's University Transportation Centers Program.

Technical Report Documentation Page

1. Report No.	**2. Government Accession No.**	**3. Recipient Catalog No.**
4 Title and Subtitle Accelerated Mineral Carbonation to Stabilize Non-Plastic Soils with Lime		**5 Report Date**
		6 Performing Organization Code
7. Author(s) Aaron Gallant; Sk Belal Hossen; Warda Ashraf; Luis Zambrano; Temitope Omokinde; Andres Espinosa		**8 Performing Organization Report No.**
9 Performing Organization Name and Address		**10 Work Unit No. (TRAIS)**
		11 Contract or Grant No.
12 Sponsoring Agency Name and Address		**13 Type of Report and Period Covered**
		14 Sponsoring Agency Code

15 Supplementary Notes

16 Abstract

Accelerated mineral carbonation offers a promising low-carbon alternative for stabilizing non-plastic soils traditionally treated with cement. This study investigates the feasibility of using hydrated lime and carbon dioxide to form calcium carbonate binders that enhance the strength and stiffness of sands and silts. Elemental laboratory testing evaluated the influence of density, water content, degree of saturation, and gas mobility on carbonation rate and mechanical performance. Results show that substantial strength gains—comparable to cement-stabilized soils—can be achieved through carbonation, with optimal reaction rates occurring under partially saturated conditions that maintain a continuous gas phase. Large-scale soil box experiments demonstrated the scalability of surface carbonation and assessed durability under soaking and freeze–thaw cycling. Carbonated soils exhibited strong resistance to environmental degradation, retaining improved mechanical properties. Overall, the findings demonstrate that accelerated carbonation of lime-treated non-plastic soils is a promising approach with significant potential to reduce the carbon footprint associated with soil stabilization for transportation infrastructure. The next challenge will be to develop enablement schemes such that this technology can be deployed at scales relevant to civil infrastructure.

17 Key Words		**18 Distribution Statement** No restrictions. This document is available to the public through	
19 Security Classification (of this report) Unclassified	**20 Security Classification (of this page)** Unclassified	**21 No. of pages**	**22 Price**

Form DOT F 1700.7 (8-72)

Contents

Abstract

Accelerated mineral carbonation offers a promising low-carbon alternative for stabilizing non-plastic soils traditionally treated with cement. This study investigates the feasibility of using hydrated lime and carbon dioxide to form calcium carbonate binders that enhance the strength and stiffness of sands and silts. Elemental laboratory testing evaluated the influence of density, water content, degree of saturation, and gas mobility on carbonation rate and mechanical performance. Results show that substantial strength gains—comparable to cement-stabilized soils—can be achieved through carbonation, with optimal reaction rates occurring under partially saturated conditions that maintain a continuous gas phase. Large-scale soil box experiments demonstrated the scalability of surface carbonation and assessed durability under soaking and freeze–thaw cycling. Carbonated soils exhibited strong resistance to environmental degradation, retaining improved mechanical properties. Overall, the findings demonstrate that accelerated carbonation of lime-treated non-plastic soils is a promising approach with significant potential to reduce the carbon footprint associated with soil stabilization for transportation infrastructure. The next challenge will be to develop enablement schemes such that this technology can be deployed at scales relevant to civil infrastructure.

Chapter 1: Introduction and Background

1.1 Project Motivation

Challenging subsurface conditions often dictate the need to excavate and replace shallow subgrade soils or to modify the native materials' insitu properties via soil stabilization methods to support infrastructure. This includes subbase and subgrade layers for roadways, runways, and railways, as well as foundations, embankments, erosion protection, etc. Depending on the availability and location of borrow sites, adoption of soil stabilization methods to augment the strength and stiffness of existing subgrade soils may be more suitable than excavation and replacement.

Chemical stabilization is a ground modification method, whereby chemical additives (e.g. cement, lime, fly ash) are mixed with soil and react to generate a binder that improves the mechanical properties of targeted materials (Sherwood 1993, Consoli et al. 2007, Toohey et al. 2013, Yi et al. 2014, Consoli et al. 2016, Puppala 2016, Behnood 2018, Dash et al. 2012). This method of construction is widespread globally and often adopted to stabilize soils supporting transportation infrastructure like roadways, runways, railways, etc. Conventionally, chemical additives result in hydration products that cement the soil matrix. However, there is increasing awareness of the relatively large carbon footprint associated with production of the aforementioned stabilizing agents (Worrell et al. 2001; Yi et al. 2014; Miller et al. 2018; Behnood 2018).

Accelerated mineral carbonation is a nascent approach to cement construction materials, whereby carbon dioxide is introduced with chemical additives (e.g. cement or lime) and sequestered to generate a carbonate binder. Thus, this approach has the potential to substantially decrease production-based carbon emissions and is considered a key pathway to decarbonize cemented construction materials (National Academies of Sciences et al., 2024). Production-based CO_2 emissions for cement and lime, which encompasses emissions linked to the decomposition of limestone derivatives (process-based emission) and emissions attributed to fuels used to heat kilns, are approximately 0.95 and 1.1 tonne per tonne of the chemical additive produced, respectively (Yi et al. 2013b, 2014, Higgins 2005, Cai et al. 2015, Stork 2014). However, when carbonating lime there's the potential to sequester nearly 100% of process-based emissions, which could reduce the total production-based emissions by nearly two-thirds (Hossen 2023, Gallant et al. 2025). The construction industry in the United States and Europe uses about 20% of lime produced worldwide (Dowling et al. 2015), and carbonation therefore has the potential to substantially reduce CO_2 emissions attributed to production of this chemical additive.

1.2 Background

The use of carbonate binders (De Silva 2006, De Silva et al. 2009, Ashraf 2016) shows potential to be an alternative approach to chemically stabilize soil (Fasihnikoutalab et al. 2017). Initial studies with soil focused on use of magnesium-based alkali sources, including reactive magnesia (MgO) (Yi et al. 2013, Cai et al. 2015) and olivine (Mg_2SiO_4) (Fasihnikoutalab et al. 2017). However, only 0.35 million tons of magnesium compounds, including reactive magnesia, were produced in the United States in 2020 (Merrill 2021). This is a small fraction when compared with the 16 million tons of calcium-based lime produced in the United States (Apodaca 2021), which

is more likely to be relied on as an alkali-source. Lime will carbonate under natural atmospheric conditions (e.g. Das et al. 2021, 2022, Fan et al. 2017) and this process can be accelerated to chemically stabilize soil (e.g. Hossen et al. 2020, Xu et al. 2020). Though lime is a chemical additive typically used with "reactive" high plasticity soils to generate strength gains via long-term pozzolanic reactions (Little 1999, Little and Nair 2009), it has the potential to stabilize low-plasticity or non-plastic soils via carbonation.

In typical lime stabilization, the pozzolanic reaction leads to the formation of calcium silicate hydrate (C-S-H) or calcium alumina silicate hydrate (C-A-S-H) products. These phases provide bonding between soil particles. However, due to the presence of CO_2 in our atmosphere, these phases often experience some atmospheric carbonation, forming decalcified silica gel with poorer cohesion and bonding (Haque et al. 2023). Because of this degradation to hydrate phases, carbonation has typically not been desired. However, contradictory to the traditional approach to cementation, the method investigated in this study relies on an accelerated carbonation reaction to directly form calcium carbonate ($CaCO_3$) as the bonding agent and bypass the formation of hydration products. Thus, there are no intermediate hydration reactions products where carbonates could cause performance degradation to silica gel formations associated with bond weakening. Therefore, accelerated carbonation relies on the beneficial aspects of carbonation due to the different reaction pathways.

Carbonation with hydrated lime, referred to herein as lime, may be characterized as a two-step process that requires 1.) the mixing of soil, lime, and water at a desired density (same as conventional chemical stabilization), followed by 2.) the introduction of carbon dioxide gas to accelerate the carbonation reaction. The latter step differs from conventional chemical stabilization. In a soil-lime-water mixture, the solid [s = solid] lime dissolves in pore water [l = liquid] and dissociates into aqueous-phase [aq = dissolved] cations, Ca^{2+}, and anions, OH^{-},

$$Ca(OH)_2\,[s] + H_2O\,[l] \leftrightarrow Ca^{2+}\,(aq) + 2OH^{-}\,(aq) \tag{1}$$

Carbon dioxide gas [g = gas] is then introduced into the soil matrix and dissolves in the pore water, producing a weak carbonic acid (H_2CO_3) that disassociates into H^+ and bicarbonate (HCO_3^-) or carbonate (CO_3^{2-}) ions in the pore water solution,

$$CO_2\,[g] + H_2O\,[l] \rightarrow H_2CO_3\,(aq) \leftrightarrow H^+(aq) + HCO_3^-(aq) \leftrightarrow 2H^+(aq) + CO_3^{2-}\,(aq) \rightarrow CaCO_3\,[s] \downarrow \tag{2}$$

The Ca^{2+} (aq) and CO_3^{2-} (aq) ions combine and calcium carbonate precipitates out of the pore water solution and agglomerates onto the soil grains (↓ signifies precipitation/deposition),

$$Ca^{2+}(aq) + CO_3^{2-}\,(aq) \rightarrow CaCO_3\,[s] \downarrow \tag{3}$$

If enough precipitation occurs, the carbonate minerals can bind the soil matrix. The preceding description of the exothermic carbonation reaction with lime may be summarized as,

$$\underbrace{Ca(OH)_2\,[s] + H_2O\,[l]}_{Step1:Mixing} + \underbrace{CO_2\,[g]}_{Step\ 2:Carbonation} \rightarrow \underbrace{CaCO_3\,[s]}_{Binder\ Formation} + 2H_2O\,[l] + Heat \tag{4}$$

During the reaction, there can be metastable calcium carbonate phases, including amorphous calcium carbonate (ACC), that precede the transformation to more stable, lower energy, and

crystalline polymorph phases. Formation of different polymorphs of calcium carbonate follows the Ostwald's rule of stages (Hadjittofis et al. 2022); that is, the least stable polymorph ACC is the first to nucleate, which then crystallizes to form vaterite or aragonite (also metastable), and finally, forms calcite—the most thermodynamically stable polymorph. Therefore, in such carbonation reactions, calcite is the final polymorph theoretically, which has also been confirmed experimentally for calcium hydroxide carbonation (Rodriguez-Navarro et al. 2023). While there is evidence that higher CO_2 concentrations applied during accelerated carbonation can result in strengths that are greater than carbonation under atmospheric conditions (e.g., Hay et al. 2021; Silva et al. 2021), and that the size of crystals formed may be influenced as a result (De Silva et al. 2006; Cizer et al. 2012), calcite is ultimately expected.

1.3 Research Objectives and Report Overview

The overarching objective of this study is to evaluate the feasibility of accelerated mineral carbonation as a low-carbon alternative for stabilizing non-plastic soils using hydrated lime, with particular emphasis on applications relevant to transportation infrastructure. The research is structured to quantify both the mechanical performance achieved through carbonation and the governing parameters that control the rate and extent of carbonate binder formation.

The first objective is to establish the fundamental behavior of lime-treated non-plastic soils subjected to accelerated carbonation under controlled laboratory conditions. Elemental testing was conducted to quantify the influence of index properties—including density, water content, degree of saturation, and gas-phase connectivity—on carbonation rate, binder development, and resulting strength and stiffness. These tests provide mechanistic insight into the parameters of functionality governing accelerated carbonation and allow direct comparison with conventional cement-stabilized soils.

The second objective is to assess whether the governing relationships identified at the elemental and bench scale can be extended toward field-representative conditions. This objective is addressed through large-scale soil box experiments that simulate surface-applied accelerated carbonation under near-atmospheric pressures. These experiments also evaluate the durability of carbonated soils when subjected to environmental stressors relevant to cold-region infrastructure, including soaking and freeze–thaw cycling.

This report is organized as follows. Chapter 2 presents the results of elemental and bench-scale testing, including diffusion-based carbonation experiments and controlled advective gas-flow studies that elucidate carbonation kinetics, transport mechanisms, and mechanical response. Chapter 3 describes large-scale soil box experiments and evaluates the performance and durability of carbonated soils under simulated field conditions. Chapter 4 discusses the broader benefits and challenges associated with accelerated mineral carbonation, including practical considerations for implementation. Finally, Chapter 5 summarizes the key findings, presents overall conclusions, and identifies areas where additional research is warranted.

Chapter 2: Elemental- and Bench-Scale Carbonation Behavior

The goals of elemental testing were to (a) demonstrate that carbonation of hydrated lime under low CO_2 pressures will cement non-plastic soils (sand and silt), and (b) elucidate the index properties influencing the rate of carbonation and degree of mechanical improvement under varying conditions (density and water contents). The degree of mechanical improvement and associated dependence on density and binder content are also compared with cement-stabilized non-plastic materials. The intent is to focus on stabilization applications where there is typically some attempt to control the water content and (or) density of soils mixed with chemical additives, like shallow subgrade or subbase stabilization for surface transportation infrastructure.

An understanding of how the reaction occurs lends insight behind the parameters expected to influence the rate of binder formation during soil carbonation. One consideration is that enough pore water must be present such that lime is in contact with, and dissolves into, the pore water (eq. 1). The pore water is effectively a host medium for dissolved lime and dissolved CO_2 gas (eq. 2) that leads to precipitation of binding carbonate minerals (eq. 3). The more water that is present, the more lime and CO_2 that can be dissolved at any given moment, which is expected to influence the rate of mineral precipitation and binder formation.

However, a unique feature of soil carbonation is the need to introduce and transport CO_2 through the soil matrix where lime is present. Soils with a low degree of saturation have a continuous gas phase and pockets of water. Gas diffusion and mobility through soil increase significantly with air content (Olesen et al. 1996, 1999; Schjønning et al. 1999; Moldrup et al. 2001; Fredlund et al. 2012). Thus, a continuous gas-phase can facilitate the conveyance of CO2 gas. Gas mobility is reduced as the degree of saturation and corresponding air content increase and decrease, respectively. For high degrees of saturation, CO_2 gas mobility is obstructed by a continuous water phase and gas mobility is governed, to a large extent, by diffusion of dissolved CO_2 through pore water. Diffusion of dissolved gas is comparatively slow (e.g., Mahmoodi and Gallant 2020, 2021). The soil's water content must balance water's influence on the dissolution of chemical constituents and gas mobility——competing mechanisms that can influence the rate of carbonate mineral precipitation in the soil matrix (Rodriguez-Navarro et al. 2023). Thus, the water content, associated degree of saturation, and volumetric air content are of particular interest with respect to the rate of binder formation.

From a mechanical perspective, the relationship between density and gains in strength and stiffness after accelerated carbonation—and how that relationship varies for different non-plastic soil types—has not been explored. This study seeks to link the combinations of densities and binder contents to the degree of mechanical improvement in sand and silt and to understand how the influence of binder content and density on strength compares with cement, the most widely used additive for non-reactive soils.

Based on the preceding descriptions, it is expected that the gravimetric water content (ω), density, and associated volumetric water content (θ_w), void ratio (e_o), volumetric air content (θ_a), and degree of saturation (S_r) will influence the rate of carbonation and degree of mechanical improvement. These index properties are varied in the elemental testing program.

2.1 Diffusion-Based Elemental Testing

Materials and Methods

U.S. Silica company, referred to herein as sand and silt, were used to investigate the influence of carbonation on the mechanical properties of lime-mixed non-plastic soils. The sand and silt contained 99.7% SiO2 with a specific gravity, *G*s, of 2.65 and the gradations shown in Figure 1a, which conform to ASTM C778 (ASTM 2017*c*). According to the unified soil classification system (ASTM 2017*a*), the Ottawa sand is classified as poorly graded sand (SP) and silt with low plasticity (ML). Commercial grade hydrated lime from Acros Organics, USA, was approximately 85%–90% pure calcium hydroxide with a *G*s of 2.24. For reference, Figure 1b shows the standard compaction curves (ASTM 2012) for the 10% lime mixed soils.

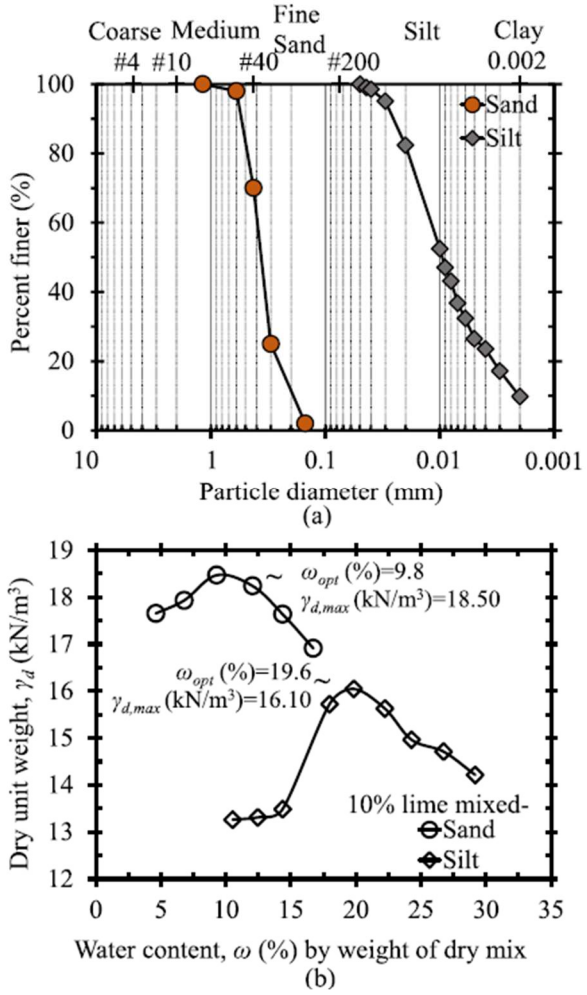

Figure 1. (a) Soil gradation curves for the Ottawa sand and nonplastic silt from the U.S. Silica company; (b) standard proctor compaction curves for the Ottawa sand and non-plastic silt containing 10% lime by dry weight of soil.

To prepare samples, dry lime and soil were mixed in a mechanical mixer for at least 2 min or until the mixture appeared uniform in color. Deionized water was then added to the mix to achieve a target gravimetric water content and degree of saturation with an associated volumetric water content and volumetric air content; note that "volumetric air content" is used here generically to

signify the volume fraction containing gas, not just "air". The moist materials were then mixed again for at least 5 min to achieve uniformity. All soil–lime–water mixtures were immediately transferred to air-tight plastic bags for 24 h to achieve moisture equalization (ASTM 2017*b*). Afterwards, reconstituted specimens 50 mm in diameter and 100 mm in height were prepared to achieve a desired dry density (γ_d), void ratio, and porosity (η). Specimens were prepared in four lifts using a two-part split aluminum mold (ASTM 2009). Each lift was uniformly compacted with a wooden tamper and soil at the top of each lift was lightly scarified so that additional soil was not compacted against a uniformly flat surface during subsequent lifts.

Specimens were then placed in a plastic box (gas chamber) and continuously fed CO2 gas. The specimens were initially carbonated in the mold because most specimens could not stand unsupported at most targeted water contents considered in this study. After 3 hours, the molds were removed because some carbonation had occurred, and the specimens could then stand unsupported. A small vent in the box prevented the buildup of pressure and effectively allowed carbonation of the specimens in a CO_2 environment under atmospheric pressure.

All soil specimens were mixed with a target gravimetric lime content (β_L), defined as the ratio of the dry mass of lime, m_L by dry mass of soil, m_s. A target value of β_L = 10% was chosen because it is toward the upper bound of lime contents typically added for shallow subgrade stabilization (Little and Nair 2009). Varying binder contents were achieved by varying the amount of time that reconstituted specimens were left in the CO_2 gas chamber. The gravimetric binder content (β_B) is defined as

$$\beta_B = \frac{m_b}{m_s} \tag{5}$$

where m_B is the mass of calcium carbonate binder formed during the reaction. The volumetric binder content (θ_B) is defined as

$$\theta_B = \frac{V_B}{V_t} = \frac{m_B/(G_B\rho_w)}{V_t} \tag{6}$$

where V_B and V_t are the volumes of carbonate binder and total soil volume, respectively. The specific gravity of the calcium carbonate (typically calcite) binder, GB, and density of water, ρ_w, can be used to compute the volume of the binder. The degree of carbonation (DoC) is defined as the ratio of calcium carbonate formed to the maximum amount possible based on the amount of chemical additive mixed in the soil, or,

$$DoC = \frac{B}{B,max} = \frac{\theta_B}{\theta_{B,max}} \tag{7}$$

where $\beta_{B,max}$ and $\theta_{B,max}$ assumes all lime has been converted to calcium carbonate via carbonation. The theoretical maximum binder content is

$$\beta_{B,max} = \frac{m_L}{m_s} \times \frac{100}{74} = \beta_L \times \frac{100}{74} \tag{8}$$

where 100/74 is the ratio of molecular masses of $CaCO_3$ and $Ca(OH)_2$.

To evaluate the influence of index properties (previously discussed) on the rate of carbonation and improved mechanical properties of carbonated lime-mixed non-plastic soil, displacement-controlled (0.5 mm/min.) unconfined compression strength (UCS) tests were performed on reconstituted samples of carbonated sand and silt; tests were conducted in general accordance with ASTM D5102 (ASTM 2009) using an Instron 5900 apparatus. Immediately after UCS testing, representative samples were collected for each batch of conditions tested and oven-dried to measure the water content and prevent any further carbonation. Water contents measured after UCS testing were approximately the same as the targeted water content during sample preparation (i.e., changes in moisture content were negligible during carbonation).

After drying, thermogravimetric analyses (TGAs) were performed on select 25–50 mg samples using a "TGA 55" from TA instruments. Samples were heated over a temperature range spanning from 0–900+ ◦C, and the weight changes that occurred due to the decomposition of calcium carbonate and hydrated lime, which initiates at different temperatures, were recorded. These measurements were used to assess the mass of soil, calcium carbonate, and any remaining hydrated lime in a sample, as well as the associated binder content and DoC.

A total of 132 UCS tests and 88 TGA tests were performed on sand and silt specimens. At least three UCS tests were performed for each condition. Table 1 summarizes the UCS test conditions and amount of time specimens were carbonated beforehand.

Table 1. Summary of test conditions and number of UCS and TGA tests performed on sand and silt specimens.

ID	Soil Type	t_c (hr.)	e_o	γ_d (kN/m^3)	ω (%)	S_r (%)	UCS Tests	TGA Tests
SP1	Sand (SP)	3, 24, 72, 120, 168	0.53	16.7	5.0	24.6	15	10
SP2	Sand (SP)	3, 24, 72, 120, 168	0.49	17.2	7.7	41.0	15	10
SP3	Sand (SP)	3, 24, 72, 120, 168	0.48	17.3	9.7	52.7	15	10
SP4	Sand (SP)	3, 24, 72, 120, 168	0.48	17.3	14.1	76.7	15	10
SP5	Sand (SP)	24, 72	0.65	15.5	7.3	29.4	6	4
SP6	Sand (SP)	168	0.64	15.6	13.7	56.2	3	2
SP7	Sand (SP)	24, 72	0.74	17.7	7.4	25.8	6	4
SP8	Sand (SP)	168	0.78	14.4	13.7	46.0	3	2
SP9	Sand (SP)	24, 72	0.85	13.8	7.3	22.5	6	4
ML1	Silt (ML)	3, 24	1.11	12.1	11.3	26.5	6	4
ML2	Silt (ML)	3, 24, 72	1.07	12.4	16.3	39.8	9	6
ML3	Silt (ML)	3, 24, 72, 120	1.08	12.3	20.3	49.0	12	8
ML4	Silt (ML)	3, 24, 168	1.08	12.3	25.2	60.9	9	6
ML5	Silt (ML)	24, 72	0.94	13.2	18.6	51.4	6	4
ML6	Silt (ML)	24, 72	0.80	14.2	18.7	61.4	6	4

Note: t_c = carbonation period; e_o = initial void ratio; ω = gravimetric water content; S_r = degree of saturation; γ_d = dry unit weight; UCS = unconfined compressive strength; TGA = thermogravimetric analysis.

TGA tests performed on uncarbonated lime-mixed soils consistently reflected the targeted lime content, which indicates the sample preparation methods resulted in a uniform soil–lime mixture and that TGA measurements accurately reflect the targeted initial lime content. Moreover, TGA tests performed on carbonated samples consistently indicated that increases in calcium carbonate content were proportional to observed decreases in lime content. This provided further validation that (a) materials were uniformly mixed; (b) mineral hydrates were not being generated (expected); and (c) calcium carbonate was the only binding mineral being generated. To further ensure the adequacy and reliability of TGA measurements, calcium carbonate contents for select samples

were further validated via comparison with interpretations using the standard test method for rapid determination of carbonate content of soils (ASTM 2014), which revealed consistent agreement.

Diffusion-Based Carbonation Rate

To explore the relative influence of degree of saturation and the volumetric air and water content on the rate of carbonation, both sand and silt soils were tested. A broad range of conditions were examined to elucidate the role of density and saturation on the rate of carbonation and mechanical improvement. The use of sand and silt allowed examination of upper- and lower-bound densities, and associated void ratios and porosities, for soils considered in this study; i.e., specimens with the highest and lowest densities could be reconstituted using sand and silt, respectively. The upper-bound density was tested using sand with a target void ratio of $e \approx 0.49$ and the lower-bound density was tested using the silt and a target void ratio of $e \approx 1.09$. The influence of density on mechanical improvement is discussed later.

Figure 2 shows the stress–strain curves from UCS tests performed on carbonated sand specimens at degrees of saturation, Sr = 25%, 41%, 53%, and 77%. Changes in strength—a proxy for changes in binder content—are illustrated for carbonation times, tc = 3, 24, 72, 120, and 168 hr. (Figure 2*a*–2*e*). Generally, strength gains occurred more rapidly in specimens with lower Sr values (Figure 2*b*), which may be attributed to higher volumetric air contents and a more interconnected gas-phase in the voids. For the sand soils with Sr less than 53%, similar gains in strength were achieved by tc = 72 hr. (Figure 2*c*), which did not change substantially when carbonated for longer periods (Figure 2*d* and 2*e*); i.e., binder contents didn't change substantially after tc = 72 h. However, substantial gains in strength were observed after tc = 168 h for sand specimens with Sr = 77% (Figure 2*e*). This delayed strength gain is likely attributed to the hindrance of CO_2 gas diffusion caused by the transition from a continuous gas- to water-phase within the voids expected at a higher degree of saturation.

Figure 3 shows the stress–strain curves from UCS tests performed on carbonated silt specimens at Sr = 27%, 40%, 49%, and 61% for different carbonation times. Like sand, silt specimens with relatively low Sr values (less than ≈50%) gain strength relatively quickly and a notable delay was observed for the specimen with the highest Sr (Figure 3*d*). The results from the sand and silt tests highlight the role that Sr plays on the rate of strength gain, which is linked to the rate of binder formation. Figure 4 illustrates that strength gains are associated with the amount of binder formed—the rate of which is governed largely by the degree of saturation and associated intrinsic mobility of gas in the soil matrix—not the carbonation period.

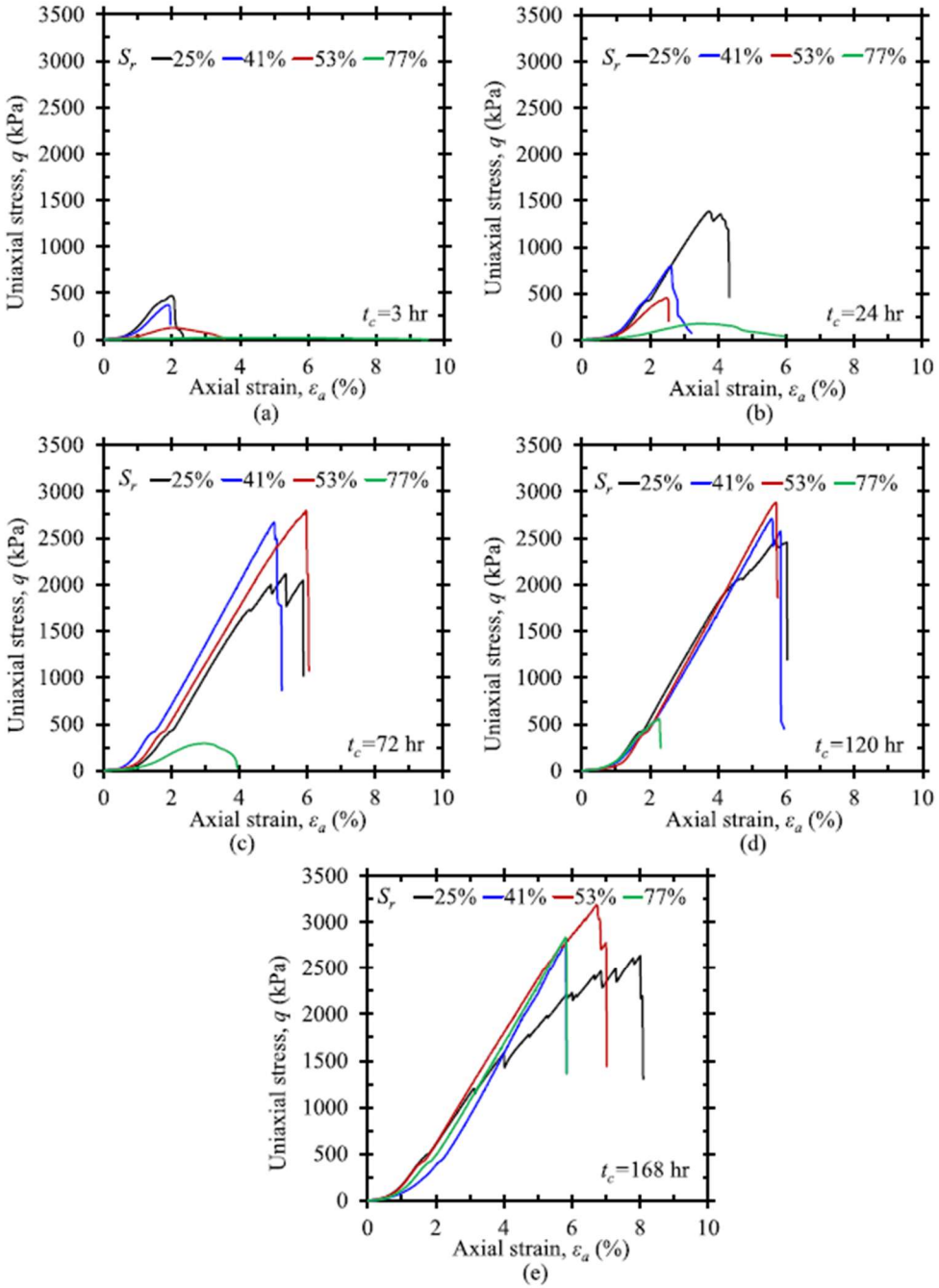

Figure 2. Temporal changes in unconfined compressive strength for sand carbonated at different degrees of saturation: (a) tc = 3 hr; (b) tc = 24 hr; (c) tc = 72 hr; (d) tc = 120 h.; (e) tc = 168 hr.

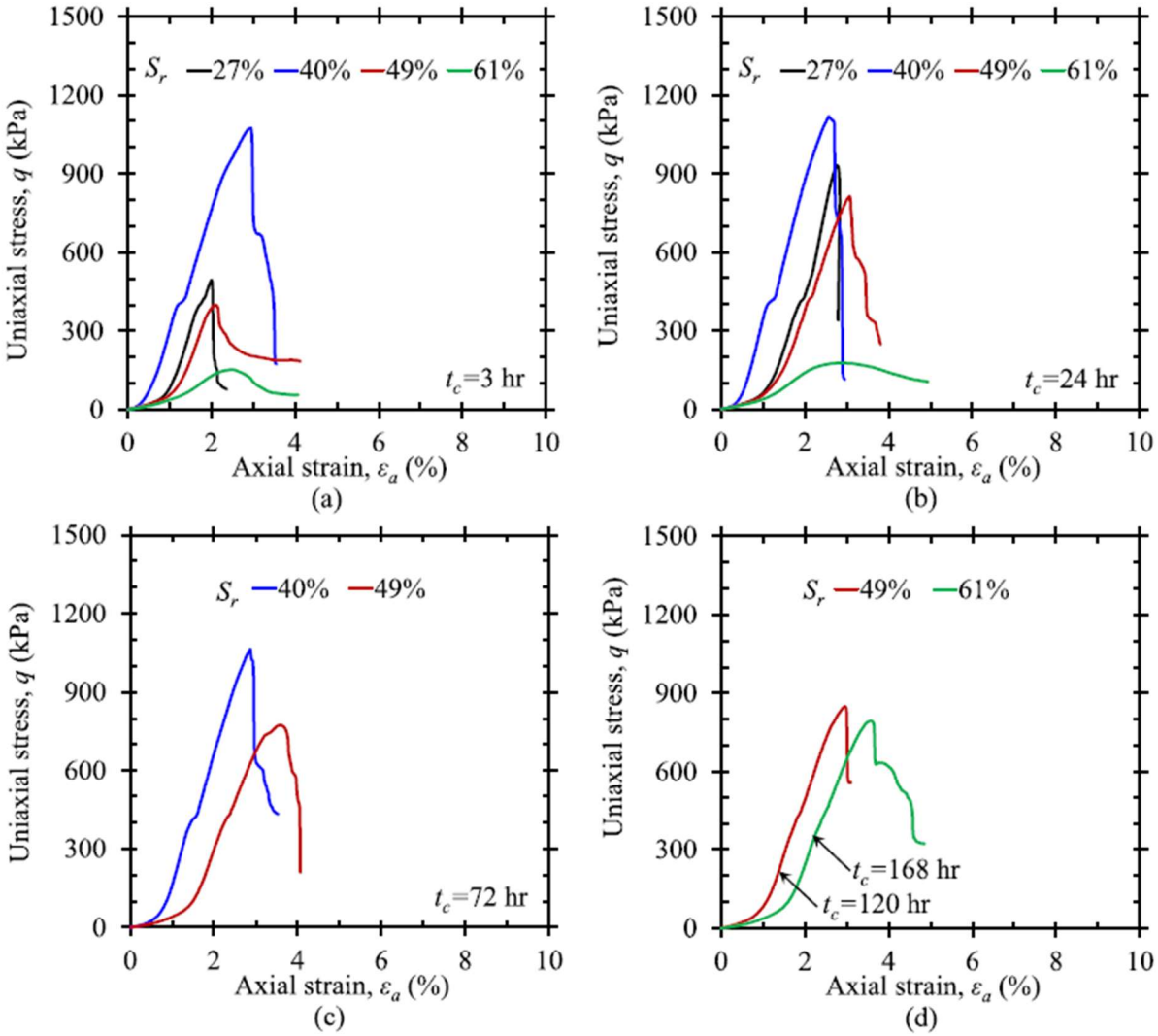

Figure 3. Temporal changes in unconfined compressive strength for silt carbonated at different degrees of saturation: (a) tc = 3 hr; (b) tc = 24 hr; (c) tc = 72 hr; (d) tc = 120 or 168 hr.

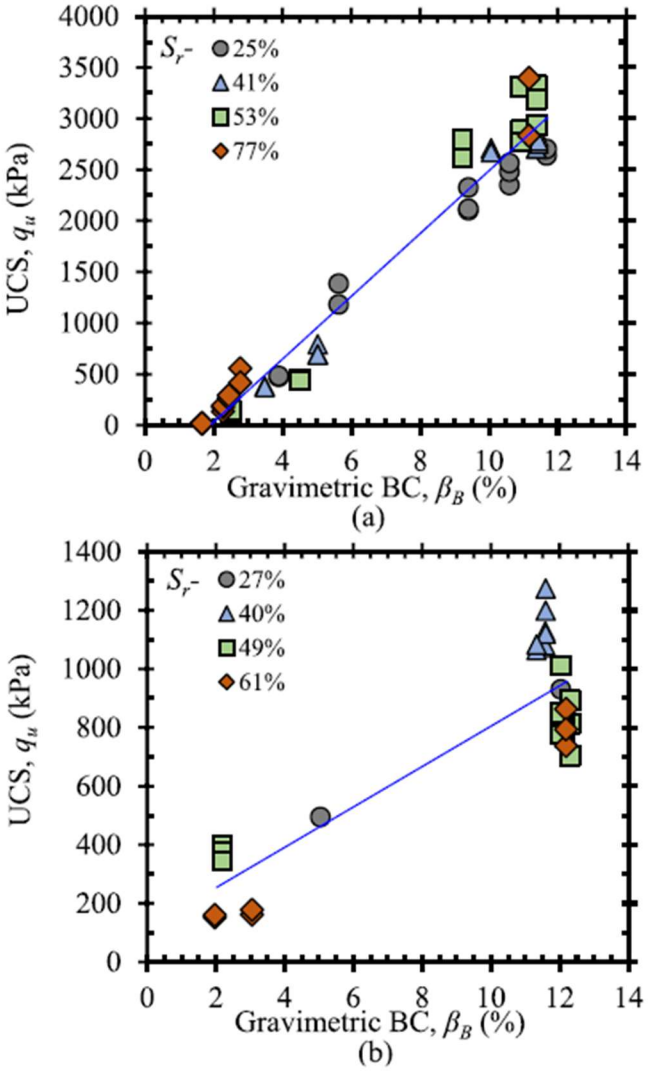

Figure 4. Unconfined compressive strength versus gravimetric binder content (BC) at the center of (a) sand specimens reconstituted at e_o = 0.49 and (b) silt specimens reconstituted at e_o = 1.09.

Figure 5 shows temporal changes in β_B and DoC at the center of sand (Figure 5*a*) and silt (Figure 5*b*) specimens carbonated at different S_r. Both soil types ultimately reached similar DoCs and gravimetric binder contents irrespective of the initial S_r. The maximum DoCs are not 100% because the lime was not pure $Ca(OH)_2$. Recall that lime used in the study was approximately 85%–90% $Ca(OH)_2$, similar to the maximum DoCs achieved. In eqs. 7 and 8, $\beta_{B,max}$ assumes that the lime is pure $Ca(OH)_2$. Thus, it can be readily observed that the maximum achievable binder content and DoC reduces according to the percent purity of the lime when that is the case; i.e., maximum achievable $\beta B = x\beta b,max$ and the maximum DoC = $x\beta_{b,max}/\beta_{B,max}$, where x is the percent purity of the lime with respect to $Ca(OH)_2$.

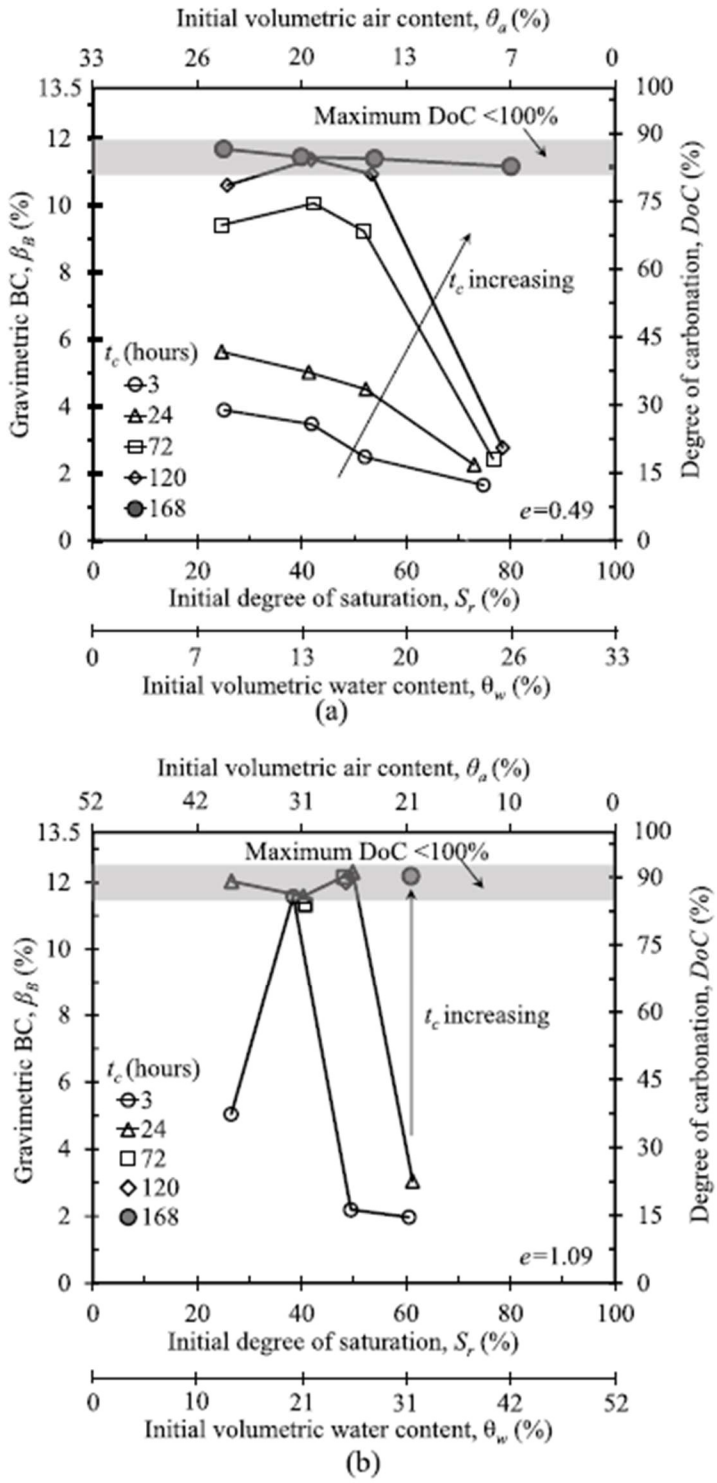

Figure 5. Temporal changes in the gravimetric binder content (BC) and degree of carbonation at the center of soil specimens for different degrees of saturation for (a) sand and (b) silt. The corresponding volumetric air contents and water contents are also shown.

Though S_r plays a role, it is not the only parameter governing the rate of carbonation. There are notable differences in the carbonation periods required to achieve the maximum strength gains observed in each soil type with the same S_r. Sand specimens reconstituted at S_r values less than

50% reached their maximum binder content and DoC within approximately 72 hr, while silt specimens with similar S_r values were near their maximum DoC within 24 hr. Also shown in Figure 5 are the corresponding volumetric air and water contents for different S_r values. Volumetric air contents were greater in the silt specimens than the denser sand specimens prepared at a similar S_r. Thus, volumetric air content, which influences the effective mobility of gas in the soil matrix, can be partly attributed to the greater rate of binder formation in silt, though not entirely (discussed more later).

Figure 6*a* compares increases in β_B with carbonation time for the sand and silt specimens carbonated at similar *S*r, but below threshold *S*r values where pore water significantly obstructed the mobility of CO_2 gas. Differences in the time required to reach $\beta_{B,max}$ are due to differences in the soils' initial condition (θ_a and θ_w), but also differences in the mass of lime that was carbonated. The mass of lime in silt was less than in the sand because the specimens were prepared at different densities, but the same β_L; i.e., a similar DoC does not imply that the same mass of $CaCO_3$ was precipitated throughout the specimen (recall eqs. 5–8).

Figure 6*b* shows how the volumetric binder content changes with carbonation time, which allows for a direct comparison of the amount of binder formed in sand and silt specimens. The maximum volumetric binder content for sand is greater than for silt because the mass of soil, and thus lime (eq. 6), was greater for the denser sand specimens. A comparison of the index properties on the carbonation rate can be made by examining the difference in volumetric binder content at the same carbonation time (e.g., red arrows in Figure 6*b*) or differences in carbonation time required to achieve the same volumetric binder content (e.g., blue arrows in Figure 6*b*). This demonstrates why the rate of increase in volumetric binder content is greater for the silt when compared with sand specimens at similar S_r values.

The conductivity of viscous fluids like water through silt, which are comprised of soil grains with higher specific surface areas than coarse grained soils, is lower than in sand. This is due in large part to higher energy losses attributed to friction and reflected in lower coefficients of hydraulic conductivity (all else being equal). This is true even when the porosity is significantly greater in silt than sand. Therefore, the higher rate of carbonation in the silt, typically considered a less permeable material than sand, may not be readily intuitive to most geotechnical engineers. However, these principles are not necessarily valid when considering mobility of non-viscous fluids, like gas. In Figure 7, temporal changes in volumetric binder content are compared for sand and silt specimens with the same amount of water (θ_w) to isolate the influence of the water-free void volume (θ_a) on the mobility of CO_2 through the soil matrix (Figure 7*a*). Silt specimens, which had a greater θ_a, carbonated more rapidly. The comparisons demonstrate that the mobility of gas—a non-viscous fluid where friction does not substantially influence gas mobility—is more heavily influenced by the water-free void volume than the soil fabric and grain size. As discussed previously in the context of the UCS tests (Figure 2 and Figure 3) and illustrated in Figure 5, while there is a threshold S_r where continuity of the water-phase in the pores begins to significantly obstruct the mobility of gas (Moldrup et al. 2000, 2001), the volumetric air content appreciably affects the degree to which the rate of carbonation is suppressed.

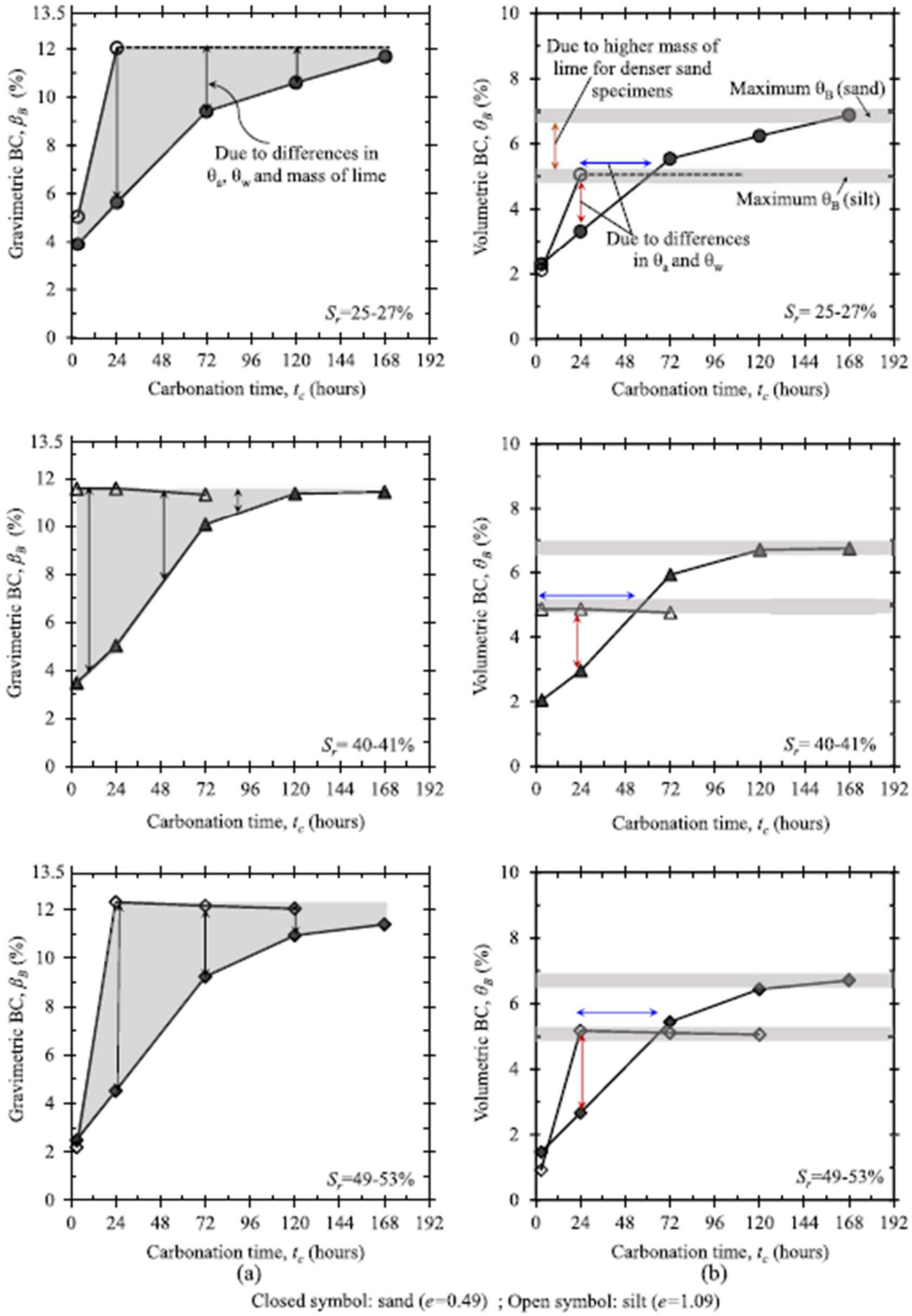

Figure 6. Differences in the rate of binder content (BC) increases in the sand and silt based on the (a) gravimetric binder content and (b) the volumetric binder content.

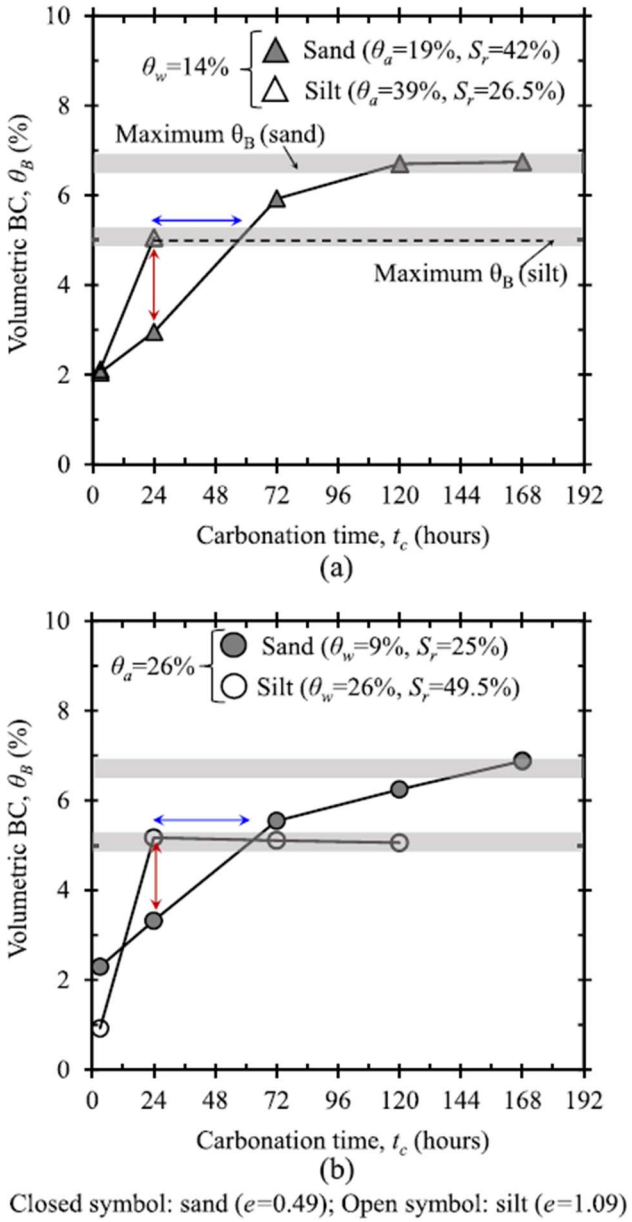

Figure 7. Comparison of increases in volumetric binder content (BC) for (a) sand and silt specimens with the same volumetric water content and Sr values associated with gas-phase connectivity throughout the pores; (b) sand and silt specimens with the same volumetric air content and Sr values associated with gas-phase connectivity throughout the pores.

Figure 7*b* compares temporal changes in volumetric binder content for sand and silt specimens where the volumetric air content for each soil type is equal to illustrate the influence of volumetric water content (Figure 7*b*). Silt specimens with a greater volumetric water content carbonated faster. Also, sand and silt specimens with the highest volumetric air content (lowest S_r) did not reach their maximum DoC fastest. When $S_r \approx 40\%$, the maximum DoC was achieved in the shortest amount of time (Figure 5). This demonstrates that the volumetric water content—a measure of the amount of water serving as a "host medium" to dissolved constituents influences the rate of carbonation; recall eqs. 1 and 2 and that more water permits the dissolution of more CO_2 gas and lime that facilities the reaction kinetics during carbonation.

For soils examined here, S_r served as a proxy to establish threshold conditions where the water-phase substantially obstructs the mobility and diffusion of carbon dioxide gas in the soil. Assuming continuity (or near continuity) of the gas phase, the volumetric air content is a proxy for gas mobility and the amount of CO_2 gas (essential ingredient) that can be conveyed to lime-mixed soil. The volumetric water content is a proxy for the instantaneous amount of lime and CO_2 gas that can dissolve and react throughout the carbonation period (i.e., reaction kinetics). There is a balance between θ_a, θ_w, and S_r that can be achieved to optimize the rate of carbonation. However, it may be difficult, if not impossible, to control this optimum condition in a field/construction setting. However, for some applications, there may be some practical control over the water content (e.g., base, subbase, and subgrade stabilization). In these cases, it would be most prudent to attempt to achieve a continuous or near-continuous gas phase within the pore network that facilitates gas mobility and diffusion in soil.

Unconfined Compressive Strength

The preceding section utilized soil types to create a significant difference in void ratio to examine the influence of volumetric air and water contents on the rate of carbonation. The influence of density across each soil type was explored separately to evaluate its influence on the degree of mechanical improvement in the sand and silt. Figure 8 shows representative stress–strain curves from UCS tests for sand (Figure 8*a*) and silt (Figure 8*b*) specimens carbonated at different initial void ratios. In Fig. 8, all specimens had a high DoC. Though specimens were prepared at the same β_L = 10%, the void ratios associated with similar strengths for the sand and silt differ significantly; silt specimens achieve similar strengths at lower densities (higher void ratios).

Figure 9*a* summarizes the UCS tests performed on sand specimens at different void ratios, which are categorized as “loose”, “medium dense”, and “dense”. The volumetric binder contents (top) and corresponding gravimetric binder contents (bottom) in each density range are also shown. The comparisons clearly demonstrate the substantial increase in carbonated strength as void ratio decreases and density increases for relatively high DoCs ranging between 68% and 93%, which are the tan-colored symbols where θ_B = 5.4%– 6.8%. For the “dense” sands, even subtle changes in void ratio have a significant influence on the UCS when θ_B was greater than 5.4%; i.e., density has an exponential influence as it increases (and void ratio decreases). The results in Figure 9*a* also illustrate that the degree of strength improvement is influenced by the binder content, though its relative influence is dependent on the density. Though the densities for finer grained silt specimens differ, Figure 9*b* illustrates that the influence of void ratio on strength improvement is like sand. However, to achieve similar strengths in silt as achieved in the sand, the density and volumetric binder content in silt are lower.

For cement stabilized soils, Consoli et al. (2007) demonstrated that changes in UCS with the void volume versus cement volume are significantly different, but recognized that unifying the influence of each to predict strength improvement was critical to streamlining predictive models. They were the first to develop a relationship between UCS and the influence of density and binder content using an adjusted porosity and volumetric binder content ratio, $\nabla = \eta/(\theta_B)^b$, where

$$q_u = \left(\frac{\eta}{(\theta_B)^b}\right)^{-B} = A \cdot \nabla^{-B} \quad (9)$$

and where $\eta = e/(1 + e)$ is porosity expressed as a percentage, and A, B, and b are scalars that relate to the soil type (e.g., coarse- vs. fine-grained) and the soil's critical state condition and strength of the binder phase (Diambra et al. 2017). The latter strength component, the binder phase, is by far the most influential and primarily governs in low-stress environments (this study). Use of an adjusted porosity and volumetric binder content ratio has been shown to work well to predict the influence of density and binder content across many soil types and for several chemical additives used to generate a binder (e.g., Consoli et al. 2009, 2011*a*, 2011*b*, 2016, 2018, 2020, 2021; dos Santos et al. 2022).

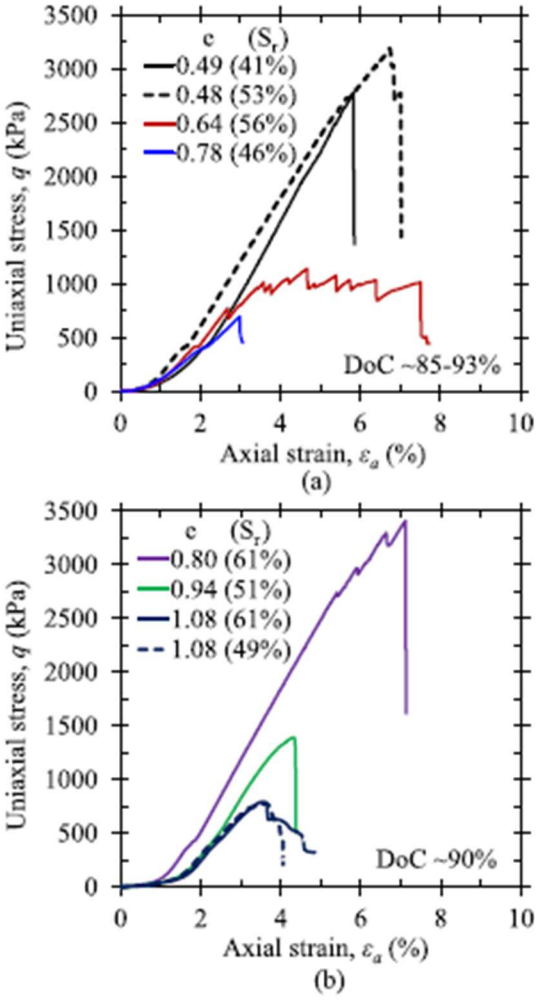

Figure 8. Representative stress–strain curves from unconfined compression strength (UCS) tests performed on (a) sand and (b) silt specimens at different densities. Specimens were carbonated sufficiently such that the maximum DoC attainable was achieved.

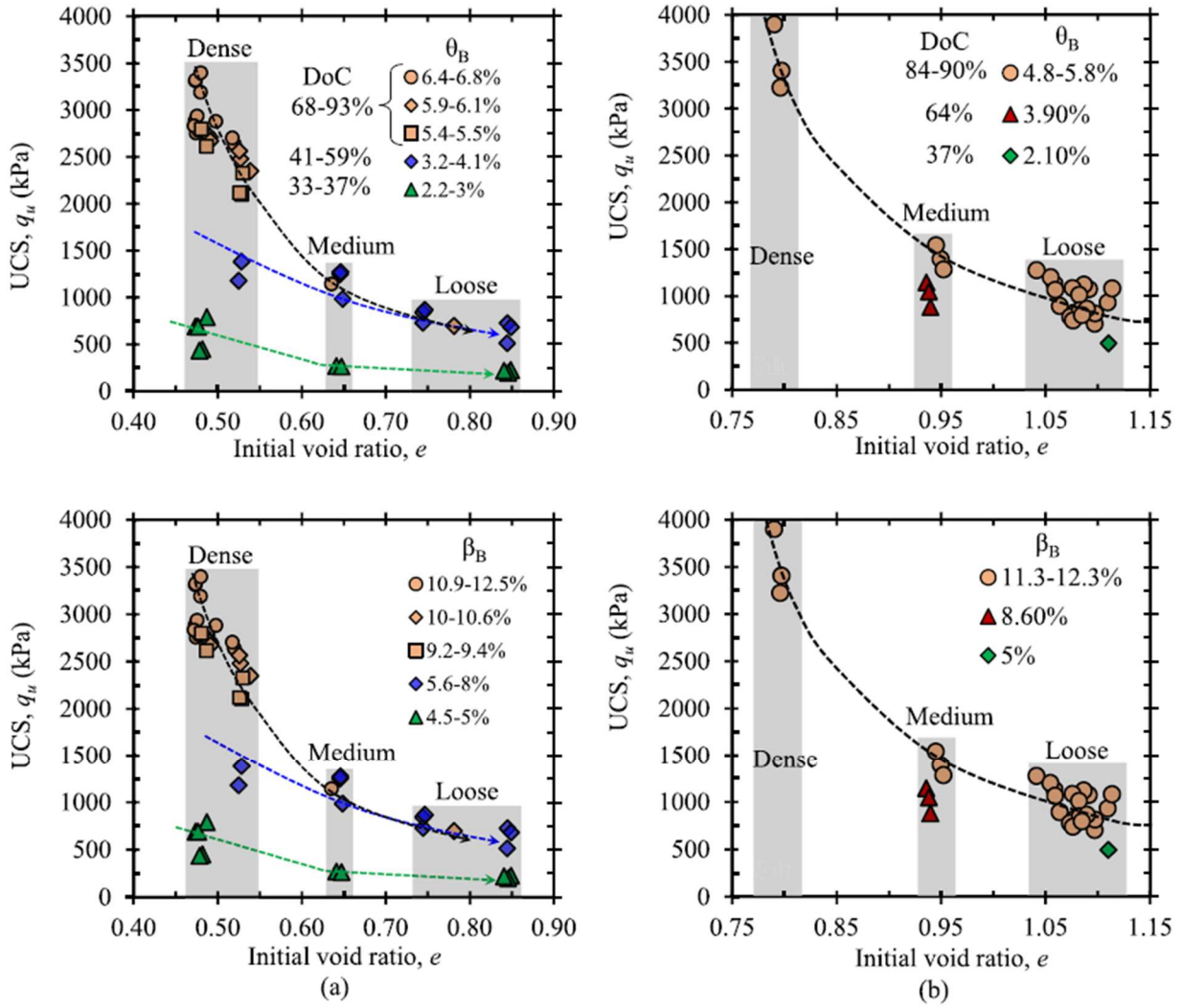

Figure 9. Influence of void ratio (i.e., density) on carbonated unconfined compressive strength in (a) sand and (b) silt. The void ratio ranges considered loose, medium-dense, and dense for each soil type are shown. The top and bottom figures indicate volumetric binder content and the corresponding gravimetric binder content, respectively. Only carbonated specimens with θ_B greater than 2% were considered due to substantial non-homogeneity of the binder phase in soils with very low binder contents.

Diambra et al. (2017) demonstrated a theoretical basis for eq. 9 and showed that $b = 1/B$, but with the simplifying assumptions that cemented materials are isotropic, contributions of soil and binder strength can be superimposed, and that there is strain-compatibility of the soil and binder phases in the composite soil material. Enforcing this condition, Figure 10 shows the power law relationship between ∇ and UCS. The optimized coefficients were $b = 1/B = 0.34$ or the sand and $b = 1/B = 0.13$ for the silt, with the coefficients of determination, R^2, equal to 0.91 and 0.94, respectively. As soil becomes more fine-grained, the optimized model coefficients b and A are expected to decrease and increase, respectively (Diambra et al. 2017)—which was the case for the carbonated soils in this study.

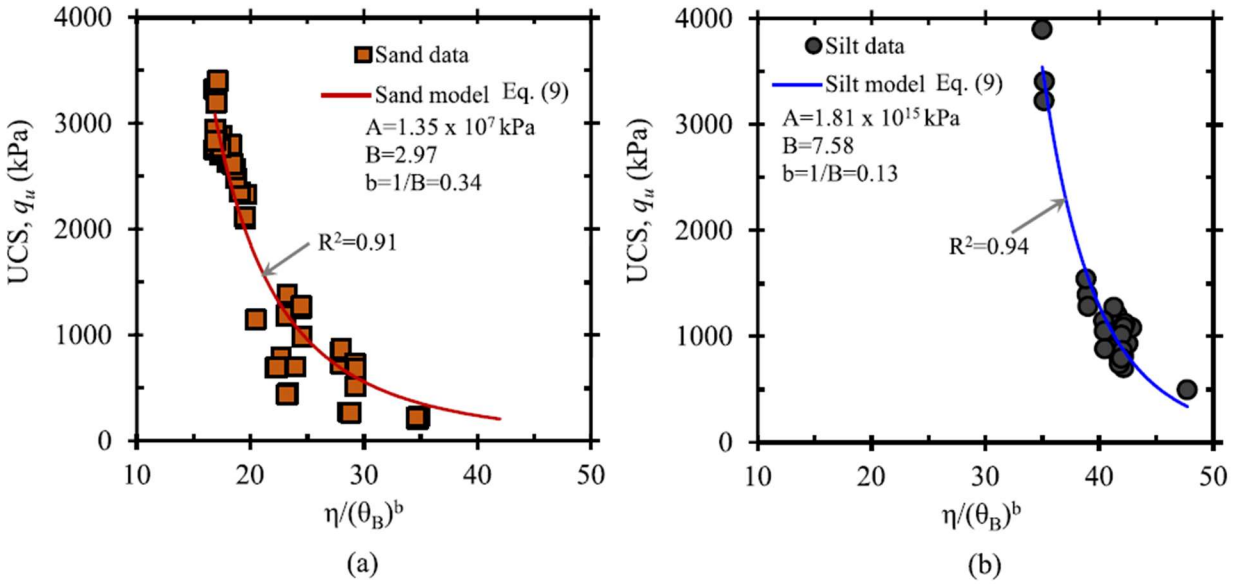

Figure 10. Unconfined compressive strength and the adjusted porosity and volumetric binder content ratio ($\nabla = \eta/(\theta_B)^b$) for (a) carbonated sand and (b) carbonated silt soils in this study.

In their original study, Consoli et al. (2007) used a value of b = 0.28 acting on the volumetric binder content, which has since been used in other studies examining cement-stabilized soils (e.g., Consoli et al. 2016). Figure 11a shows the optimized power–law relationship for the sand and silt when b = 0.28 so that carbonated soils from this study could be compared with cement-stabilized soils. For the carbonated sand, optimized parameters were A = 1.77 × 108 kPa and B = 3.73. For the carbonated silt, A = 1.03 × 1013 kPa and B = 6.62. Changes in R^2 for the optimized conditions were negligible. Thus, optimizing using b = 0.28 is reasonable for the carbonated soils. Also shown in Figure 11a is the cement-stabilized clayey sand presented by Consoli et al. (2007), which align with data and relationship presented for the carbonated sand.

However, the silt data are shifted right of the carbonated and cement-stabilized sand data, which is expected. The shift in the silt data reflects the lower densities (higher porosities) and lower volumetric binder contents needed to achieve similar strengths as that of sand (recall Figure 10). Figure 11*b* shows the power–law relationships for the carbonated sand and silt plotted with data for cement-stabilized fine-grained soils (silts and clays) presented by Consoli et al. (2016), which are also shifted from right from the Consoli et al. (2007) relationship. The comparison between carbonated and cement-stabilized soils demonstrates that similar strengths can be achieved via carbonation under similar conditions (i.e., density and binder content).

It should be acknowledged that the cement-stabilized specimens were soaked prior to UCS testing to limit the effects of matric suction on strength (Consoli et al. 2007, 2016), which was not done for the carbonated specimens in this study. However, as previously discussed, the vast majority of specimens were prepared at water contents where they could not stand unsupported until some carbonation had occurred, including specimens prepared and tested at degrees of saturation where the highest UCS values were observed. Only silt specimens tested at the lower range of water contents could stand temporarily unsupported. Three UCS tests were performed on uncarbonated silt specimens at a low degree of saturation (38%) associated with conditions near residual matric

suction values (i.e., high suction) in silt; this is also near the lower bound of degrees of saturation used in testing. UCS values for these uncarbonated specimens had an average UCS of 51 kPa, which is a low percentage of the strengths measured for all carbonated specimens. Generally, it has been widely established that shear strength increases linearly with suction up to the air-entry-value (AEV), but increases nonlinearly beyond the AEV and ceases to increase (or even decreases) as suction levels increase and approach residual values (Escario and Saez 1986; Fredlund et al. 1996; Vanapalli et al. 1996; Cunningham et al. 2003). Thus, any influence of matric suction on the UCS of carbonated specimens was negligible or small for the carbonated non-plastic sands and silts tested.

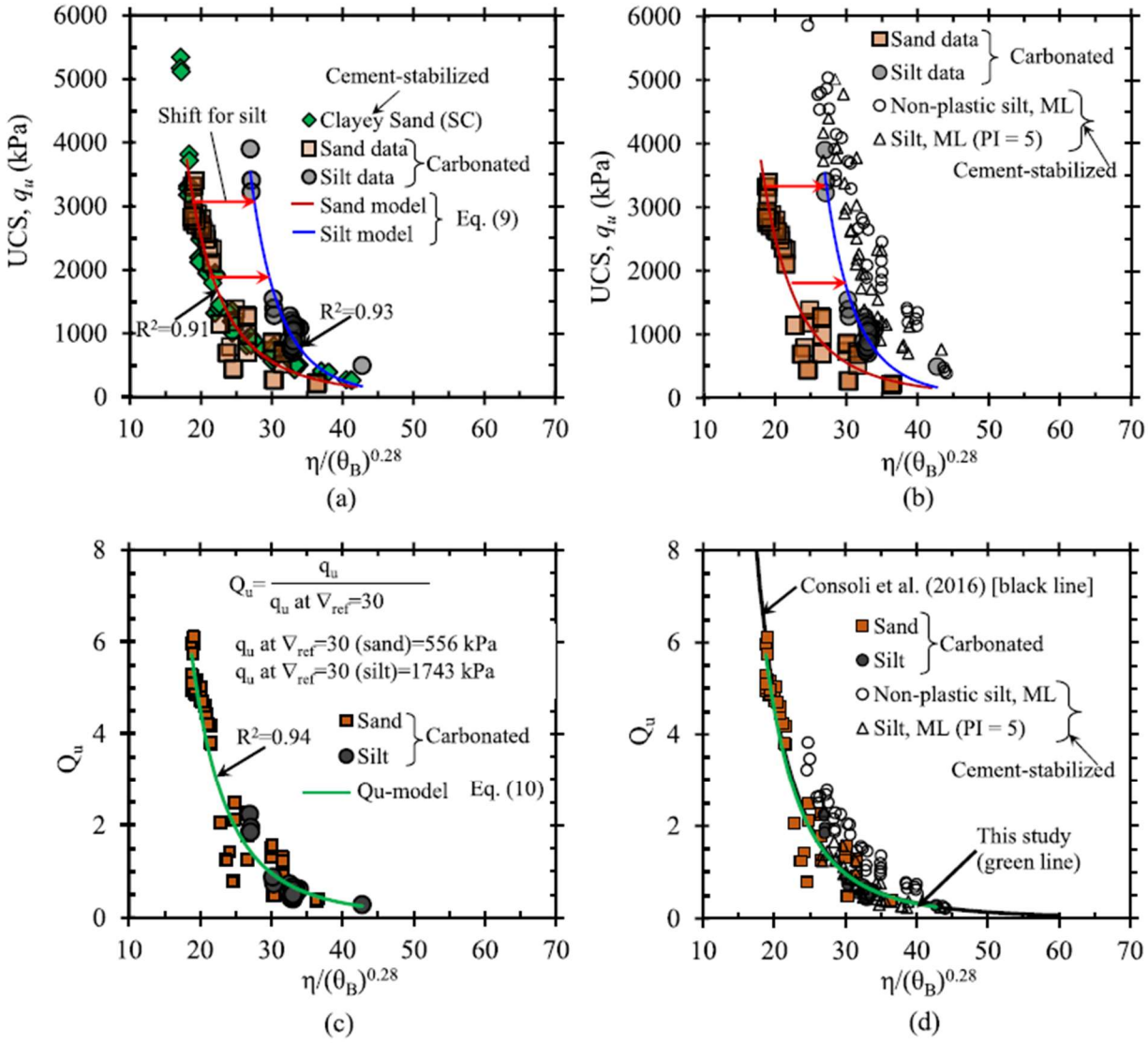

Figure 11. The upper plots show the unconfined compressive strength and the adjusted porosity and volumetric binder content ratio ($\nabla = \eta/(\theta_B)^{0.28}$) for carbonated sand and silt soils shown with data for cement-stabilized soils: (a) clayey sand data presented by Consoli et al. (2007); (b) fine-grained silt soils presented by Consoli et al. (2016). Note that θ_B is the volumetric cement content for Consoli et al. (2007, 2016) data. The lower plots show (c) optimized normalized unconfined compressive strength relationship for all carbonated soils sand and silt soils with θB greater than 2%; (d) optimized normalized unconfined compressive strength relationship for all carbonated soils compared with many cement-stabilized soils presented in Consoli et al. (2007, 2016). A $\nabla ref = 30$ and b = 0.28 was used for both the carbonated and cement-stabilized soils presented by Consoli et al. (2007, 2016).

A benefit of using the same adjusted porosity and volumetric binder content ratio is that it opens the possibility to develop a unique relationship applicable to several soil types (Consoli et al. 2016). A unique relationship for the carbonated soils can be made by normalizing their UCS at a reference ratio, ∇_{ref}, that is common to all soil types. For the sand and silt, this was case for $\nabla ref = 30$ when $b = 0.28$. The dimensionless UCS, Qu, is then evaluated as

$$Q_u = \frac{q_u}{q_u @ \nabla_{ref}} = C\left(\frac{\eta}{(\theta_B)^{0.28}}\right)^{-D} \approx \left(\nabla_{ref}\right)^{D} \cdot (\nabla)^{-D} \quad (10)$$

where C is a scalar dependent on the reference adjusted porosity and volumetric binder content ratio, and D is a scalar similar to B in eq. 9. For a normalized relationship to work well across multiple soil types, the optimized parameters should result in $\eta/(\theta_B)^{0.28} \approx (\nabla_{ref})^D$. Figure 11*c* shows Q_u for a $\nabla ref = 30$, where data for the sand and silt collapse to the same line defined by eq. 10, where $C = 4.05 \times 105 \approx (\nabla_{ref})^D$, $D = 3.81$, and $R^2 = 0.94$. The normalized Q_u relationship for carbonated soils in this study is practically identical to cement-stabilized materials, as illustrated by the comparison with a broad range of non-plastic cement-stabilized soils shown in Figure 11*d*. Note that more soils than clayey sand and silt were used to develop the Qu relationship presented by Consoli et al. 2016 and shown on Figure 11*d*, but only sand and silt are shown here. This comparison further highlights that similar performance can be expected due to soil carbonation with lime as conventional mixing with cement.

From a practical perspective, a normalized UCS relationship is also useful when it is shown to be applicable to both coarse-grained and fine-grained silt soils, because an understanding of the influence that density and volumetric binder content have on any soil type can theoretically be achieved with a limited number of tests. In theory, testing at one value of ∇ would provide an understanding of strength across the entire ∇-domain. Though the relationship shown in Figure 11*d* agrees well with the data, Consoli et al. (2016) stopped short of demonstrating how the normalized Qu model performed for the individual cement-stabilized soils considered in their study. In some cases, normalization in this manner can be deceptive and provide an unfounded sense of reliability with respect to predictive capabilities. Figure 12 shows how the optimized Qu model predicts strength for the carbonated sand and silt, which provides good agreement with both soil types. Better agreement was observed with the sand, for which there was more data used to optimize the Q_u model parameters. Though this demonstrates that the utility of Q_u is promising for carbonated soils, a limited number of soil types were investigated. More soil types will need to be tested across a broader range of conditions to verify the relationship shown in Figure 11*c* is applicable to materials not investigated in this study.

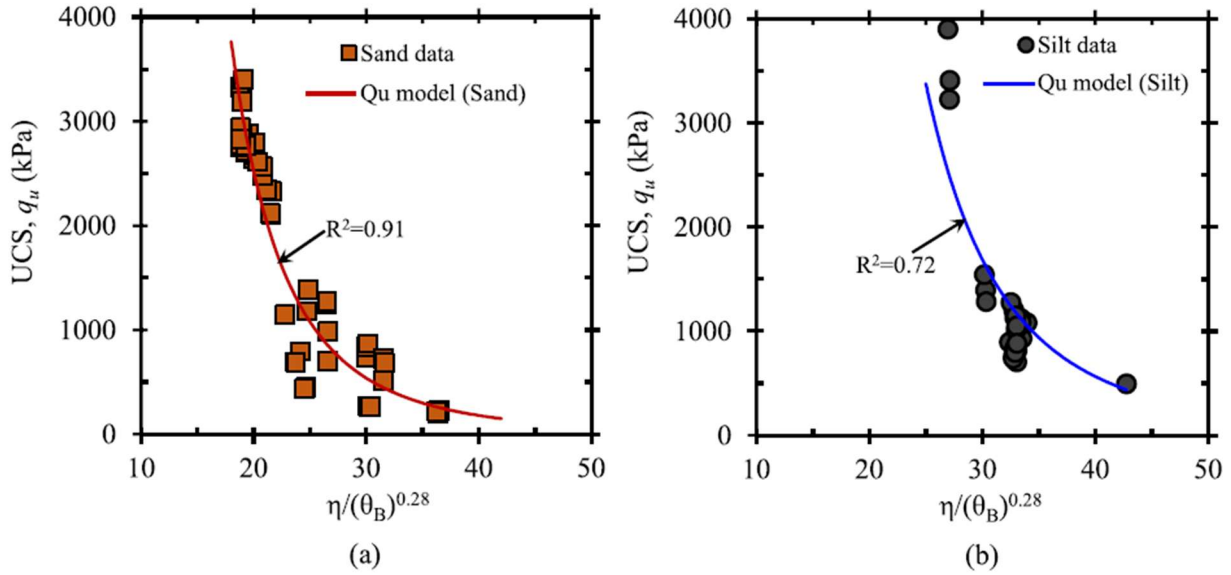

Figure 12. Unconfined compressive strength predicted using the optimized Qu model developed for (a) carbonated sand and (b) carbonated silts.

Relationship Between Strength and Stiffness

The influence of accelerated carbonation on soil stiffness was also examined. Stiffness was interpreted using global end-to-end vertical specimen displacements, where the surface roughness of end-platens and seating effects influences the initial part of stress–strain curves obtained from the UCS tests. However, based on studies that utilize on-specimen instrumentation, it is reasonable to expect that soils deform in a nearly uniform manner prior to the onset of shear band formation and development of a rupture surface (e.g., Burland 1990; Mooney et al. 1998). Once seating effects are overcome, incremental strains evaluated from global displacement measurements are similar to those interpreted from on-specimen instrumentation that capture strains locally (e.g., Perbawa et al. 2021). After an apparent soft response initially due to seating, a significantly stiffer response was observed thereafter prior to an abrupt failure in these brittle materials, as expected. Throughout the testing program, a stiffer response was always observed when carbonated specimens had mobilized 50% of the peak strength. Thus, Young's modulus was interpreted as the tangent modulus at 50% of the ultimate strength (E_{50}).

Figure 13 illustrates the relationship between UCS and E_{50}. The stiffness of carbonated soil increases significantly until $q_u \approx 1$ MPa, and then increases marginally with increasing UCS thereafter (Figure 13*a*). Similarity of the relationship between E_{50} and UCS for both the sand and silt implies that the binder-phase and interparticle bonding is primarily governing stiffness of the carbonated sands and silts. Recall that similar strengths were achieved in the silt at lower densities (higher void ratios) than carbonated sand (Figure 9); i.e., if the voids volume substantially influenced compressibility, it would be reflected by a difference in stiffness at similar strengths.

Figure 13*b* shows the empirical power law relationship between UCS and $E50/qu$ for the sand and silt ($R^2 = 0.89$). The strong relationship between UCS and normalized $E50$ is useful, as it expands the utility of the predictive models for strength.

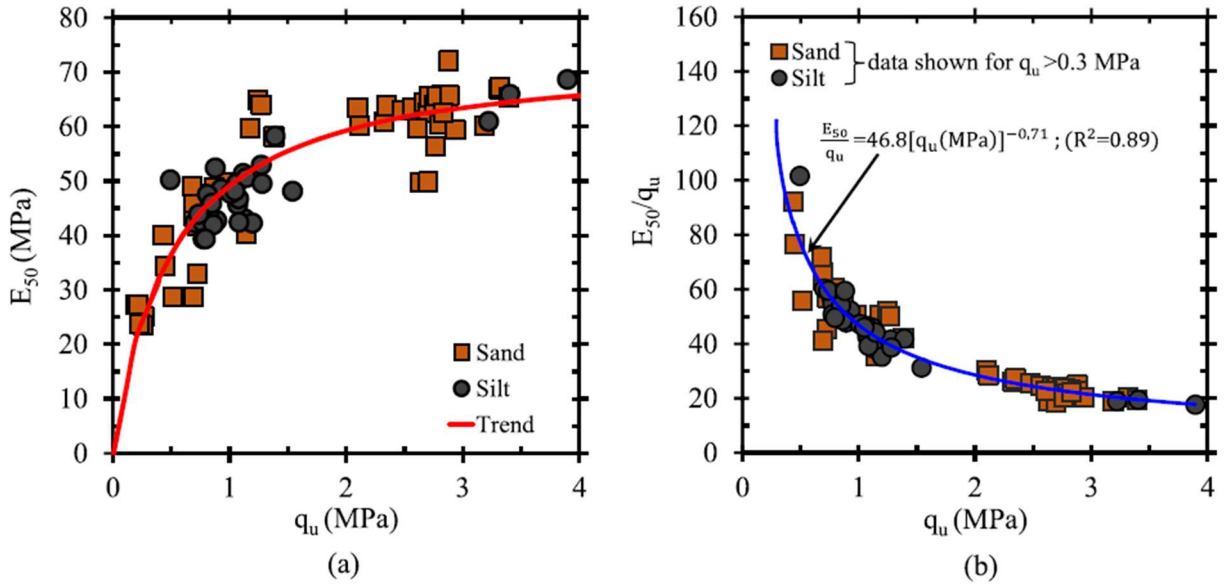

Figure 13. Relationship between unconfined compressive strength and (a) stiffness at 50% of the ultimate strength, E_{50}; and (b) stiffness normalized by the unconfined compressive strength. Data in part (b) only considered for specimens with strengths greater than 0.3 MPa.

Practical Applications

The preceding UCS relationships can be applied to predict strength and stiffness, with an understanding that a broader range of conditions and soil types must be investigated to further validate the applicability of q_u–∇ and "generalized" Q_u–∇ models. In practice, specifications are typically based on a targeted volumetric lime content for shallow subgrade stabilization. The gravimetric lime content is related to the final volumetric binder content, and thus predicted strength (Figure 11*a* and Figure 11*b*) and stiffness (Figure 13) of carbonated non-plastic sands and silts from this study at different densities, where

$$\theta_B = \frac{B/G_B}{(1+e_f)\left(\frac{1}{G_s}+\frac{\beta_B}{G_B}+\frac{B_{LF}}{G_L}\right)} \tag{11}$$

and where Gs, GB, and GL are the specific gravities of the soil particles, calcium carbonate binder (calcite), and lime, respectively. $\beta_{Lf} = \beta_L - (74/100)\beta_B$ is any unreacted lime and e_f is the final void ratio after carbonation,

$$e_f = \frac{\left(\frac{1}{G_s}+\frac{\beta_L}{G_L}\right)(1+e_o)}{\left(\frac{1}{G_s}+\frac{\beta_{Lf}}{G_L}+\frac{\beta_B}{G_B}\right)} - 1 \tag{12}$$

For typical lime contents, the void volume only decreases 1%–3% due to carbonation (i.e., $e_o \approx e_f$).

Figure 14 synthesizes the predicted strengths (top row) and stiffness (middle row) for a broad range of gravimetric lime contents, which are based on relationships presented from this study. Figure 14 also shows the approximate ideal water contents and degrees of saturation to carbonate sand

and silt (bottom row); the limits where the water-phase in the void volume is not expected to obstruct the mobility of gas and significantly suppress the rate of carbonation are shown. Understanding the parameters of functionality are essential to scale accelerated carbonation. For shallow subgrade stabilization, development of techniques to enable accelerated carbonation in the field will need to consider the influence of water content and compaction from both a mechanical and gas mobility perspective.

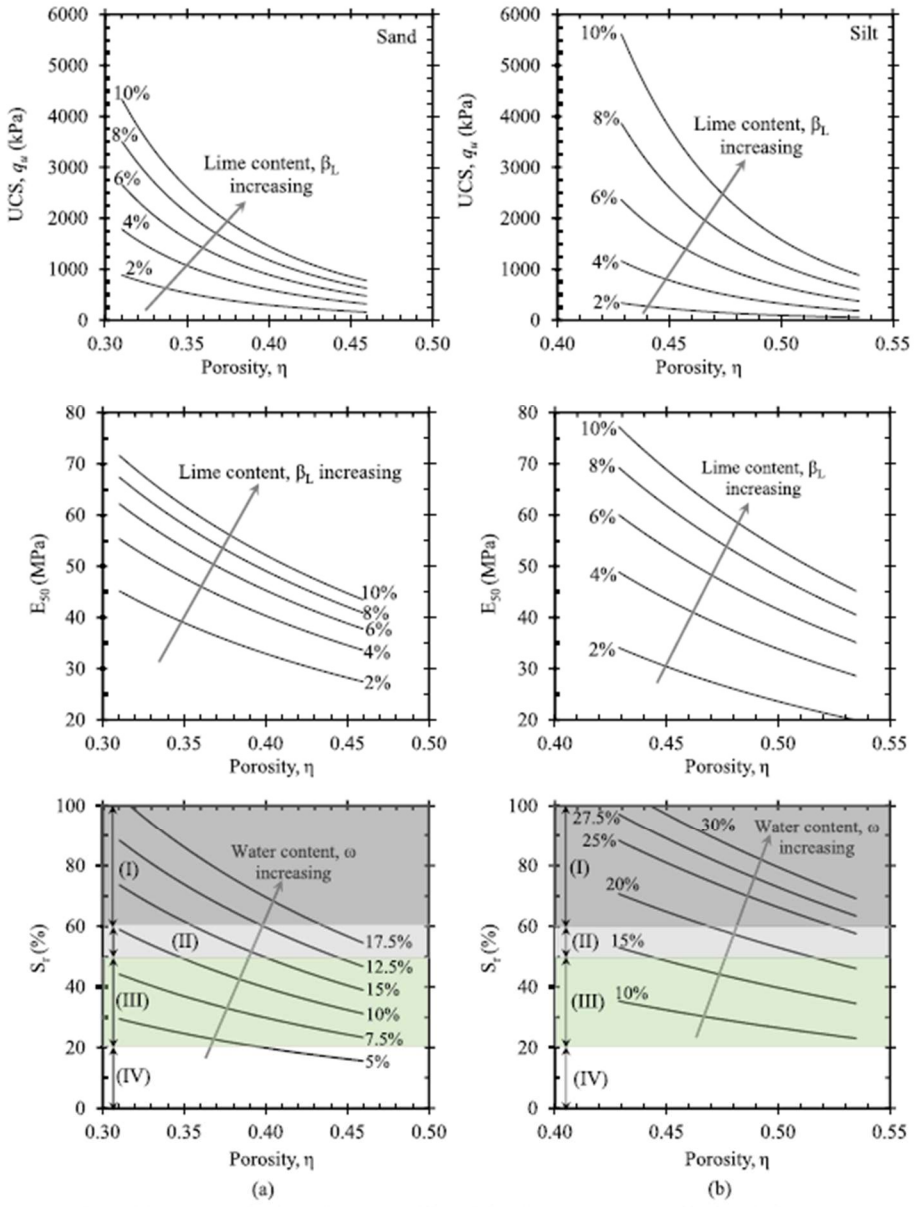

Notes: (I) Suppressed carbonation rate anticipated (continuous water-phase in the voids);
(II) Transition zone; (III) Efficient carbonation rate (continuous gas-phase in the voids); (IV) Untested

Figure 14. Influence of porosity and lime content on the predicted unconfined compressive strength (top row) and stiffness (middle row), as well as the influence of water content on the degree of saturation at different porosities, showing the approximate ideal limits to carbonate (bottom row) for (a) sand and (b) silt. Lime contents refer to the amount of $Ca(OH)_2$ that has fully reacted to form $CaCO_3$.

2.2 Bench-Scale Advective Gas Flow Tests

Previous elemental testing demonstrated that accelerated mineral carbonation can generate substantial strength gains in lime-treated non-plastic soils when carbon dioxide transport is governed by diffusion, with carbonation rate and binder development strongly influenced by moisture condition and gas-phase connectivity (e.g., Liska et al. 2008; Gallant et al. 2025). While diffusion-dominated processes can achieve high degrees of carbonation given sufficient time, they inherently limit the rate at which CO_2 can be supplied to the soil matrix, particularly at higher degrees of saturation where gas mobility is restricted (Olesen et al. 1996; Moldrup et al. 2000; Mahmoodi and Gallant 2020).

Actively introducing CO_2 under an advective gas-flow regime provides a means to increase CO_2 delivery rates and potentially reduce carbonation times. However, under advective conditions, carbonation effectiveness is no longer governed solely by gas availability, but also by the ability of local reaction kinetics to utilize CO_2 before it migrates through the soil. In particular, aqueous-phase diffusion distances associated with water films and the spatial distribution of lime may limit lime utilization even when CO_2 is abundantly supplied (Gallant et al. 2024; Moore et al. 2025).

To investigate these mechanisms, the bench-scale experiments presented in this section examine accelerated carbonation of lime-treated silt under low-pressure ($\leq$10 kPa) advective CO_2 flow. The tests are designed to isolate carbonation behavior under controlled gas-flow conditions, with emphasis on reaction-front development, degree of carbonation, and CO_2 utilization efficiency. The influence of lime content and water content is evaluated explicitly, as these parameters are expected to govern reaction kinetics and are critical for interpreting carbonation performance prior to field-scale implementation.

Figure 15 conceptually illustrates the role of a connected gas phase in facilitating bulk CO_2 transport through the soil matrix. Under advective flow conditions, CO_2 movement is driven by pressure gradients, and carbonation reactions must occur rapidly enough to ensure effective utilization of both lime and CO_2. If reaction kinetics are insufficient relative to the imposed gas flow, CO_2 may migrate through the soil without reacting, resulting in incomplete carbonation and reduced lime utilization.

In contrast, when gas transport is governed primarily by diffusion, CO_2 movement occurs in response to concentration gradients rather than pressure gradients. This mode of transport is inherently slower, which increases the likelihood that CO_2 will be consumed by reactions with available alkali additives before advancing beyond reactive zones. As a result, diffusion-dominated carbonation is expected to promote higher utilization of reactive additives, albeit over longer timescales.

As illustrated in Figure 15, carbonation reactions occur at the intergranular scale within water films that host the dissolved chemical species required for carbonate precipitation, including calcium and carbonate ions. Following dissolution, these constituents must diffuse through the water films before reacting to form a carbonate binder. Consequently, the local rate of carbonation is influenced by water film thickness, which governs local aqueous-phase diffusion distances and reaction times (i.e. rate of alkali ion conversion to carbonates).

Lime particles located closer to the gas–water interface are expected to react first, followed by lime distributed deeper within the water films at greater distances from the CO_2 dissolution front. Although water films are thin, diffusion of dissolved CO_2 and calcium species through the aqueous phase is several orders of magnitude slower than gas transport under advective flow conditions. As a result, CO_2 may be supplied to the soil matrix at rates that exceed the capacity of local reaction processes, particularly at higher degrees of saturation.

The experimental program described in this section is designed to evaluate how degree of saturation, used as a proxy for water film thickness, and lime content, representing the amount of reactive material present, influence the degree of carbonation, lime utilization, and overall CO_2 uptake.

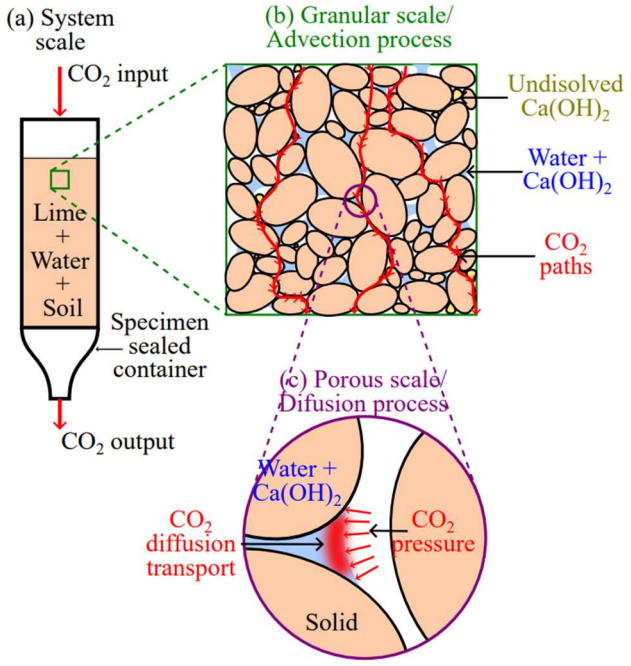

Figure 15. a) Schematic of accelerated mineral carbonation experiments showing inter-granular level scales illustrating the influence of: b) water content on the bulk mobility and permeability of gas in soil; c) water film thickness on aqueous-phase CO2 and lime diffusion process required for the carbonation reaction kinetics to occur. Note: The purpose of this figure is illustrative, and the depiction of the grains does not represent the actual shape of the silt used for these experiments.

Experimental Design and Methods

Bench-scale carbonation experiments were conducted using a one-dimensional soil column designed to impose controlled advective carbon dioxide (CO_2) flow through a lime-treated soil specimen. The experimental apparatus consisted of a transparent polyvinyl chloride (PVC) tube with an internal diameter of 76 mm and a total height of 312 mm, as shown in Figure 16. The soil specimen occupied a height of 203 mm, leaving a headspace of approximately 109 mm above the specimen for gas distribution. The column was hermetically sealed at both ends to prevent gas leakage.

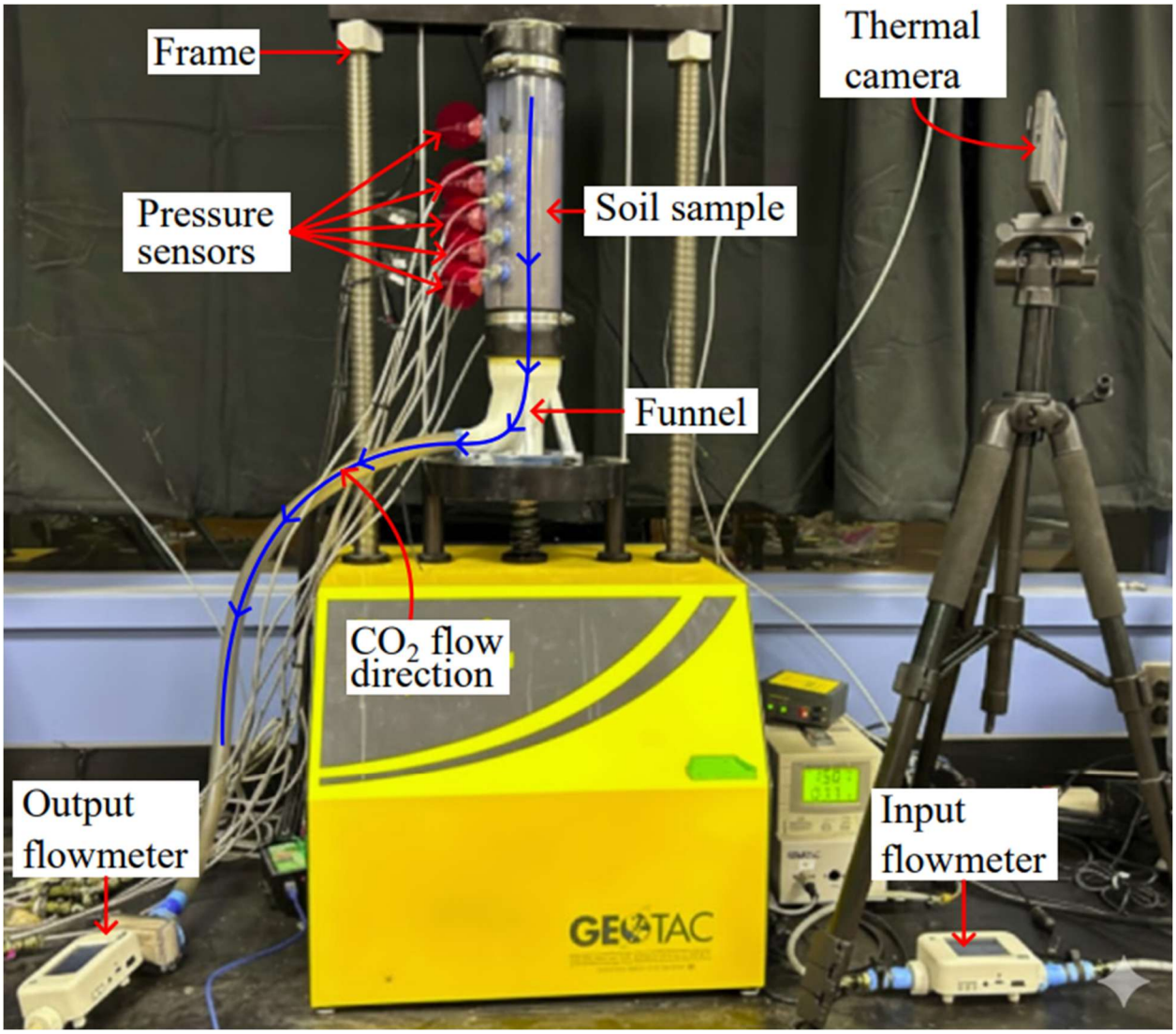

Figure 16. Picture of the experimental setup illustrating components and CO_2 flow direction.

Carbon dioxide gas was injected at room temperature (approximately 23 °C) from a high-pressure industrial CO_2 cylinder equipped with a calibrated manual regulator. Gas was introduced at the top of the column and flowed downward through the specimen under low injection pressures not exceeding 10 kPa. The base of the column was connected to a custom 3D-printed funnel to minimize abrupt changes in cross-sectional area and reduce flow disturbances. The entire assembly was placed in a mechanical frame to prevent seal failure or specimen displacement caused by pressurization of the headspace.

Mass flowmeters were installed at both the inlet and outlet of the specimen to continuously monitor the mass of CO_2 entering and exiting the column. These measurements allowed direct quantification of reacted CO_2 and identification of gas breakthrough at the outlet. Pressure transducers were embedded within the column, including one sensor in the headspace and four sensors installed at 38 mm vertical intervals along the specimen height. These sensors recorded boundary pressures and internal pressure gradients during carbonation.

Continuous thermal imaging was performed throughout each test to monitor the progression of the exothermic carbonation reaction. Because heat generation occurs nearly instantaneously upon reaction between dissolved CO_2 and lime, thermal imaging provided real-time visualization of the advancing reaction front. Test termination was based on a combination of thermal and gas-flow observations. Specifically, tests were ended when either the thermal front reached the desired depth or CO_2 breakthrough was detected at the outlet flowmeter. Recognizing that reactions may continue beyond these indicators, post-carbonation measurements were used to quantify final carbonate formation.

Following carbonation, specimens were dismantled and sectioned to measure calcium carbonate content as a function of depth using standardized calcimetry procedures in accordance with ASTM D4373. These measurements were used to compute the degree of carbonation, defined as the ratio of measured carbonate binder content to the theoretical maximum binder content corresponding to complete conversion of the available lime.

The soil tested was a non-plastic silt classified as ML under the Unified Soil Classification System, with a specific gravity of 2.65 (same as Gallant et al. 2024). Hydrated lime was added at gravimetric contents of 3%, 5%, 7%, and 10%. Dry silt and lime were first blended in a mechanical paddle mixer to ensure uniform distribution, after which deionized water was added and mixing continued. Specimens were compacted in five lifts, each approximately 40 mm thick, to achieve target void ratios of approximately 0.8 or 0.9. Two degrees of saturation were investigated: approximately 30% and 55%, selected to represent conditions with contrasting gas-phase connectivity and water film thickness. Each lift was compacted uniformly, and the surface was scarified prior to placement of the subsequent lift to promote continuity between layers.

A total of eleven carbonation tests were conducted and are summarized in Table 2. In the first test series, lime content was varied while maintaining a degree of saturation of approximately 30%, a condition favorable for bulk gas transport. For these tests, the total volume of CO_2 introduced was either approximately equal to the theoretical requirement for complete carbonation or intentionally limited to assess partial carbonation and reaction-front development. In the second test series, the influence of moisture condition was examined by comparing specimens prepared at degrees of saturation of 30% and 55%.

Table 2. Summary of test conditions for advective CO_2 gas flow tests.

Test ID	Mass of soil (g)	Mass of lime (g)	Mass of water (g)	Reference CO_2 volume (STD Lt)	Introduced CO_2 volume (STD Lt)	β_L	Water content (%)	S_r (%)	Void ratio	$CO_{2,\,ratio}$	Average pressure (kPa)
T1	1343	134	128	17.2	17.2	10%	8.64%	30%	0.81	100%	11
T2	1340	93.8	130	14.2	10.2	7%	9.07%	30%	0.81	72%	6
T3	1346	94.3	125	14.2	15.9	7%	8.69%	30%	0.81	112%	8
T4	1452	102	137	17.3	8.7	7%	8.79%	30%	0.81	50%	6
T5	1427	71.3	128	17.3	17.3	5%	8.57%	30%	0.82	100%	8
T6	1430	42.9	129	11.3	5.9	3%	8.74%	30%	0.80	52%	3
T7	1430	42.9	129	11.3	11.8	3%	8.74%	30%	0.83	104%	6
T8	1388	41.6	147	10.1	12.9	3%	10.3%	30%	0.90	129%	4
T9	1382	96.7	138	18.7	29.2	7%	9.35%	30%	0.91	156%	6
T10	1385	41.5	260	7.8	12.5	3%	18.3%	55%	0.91	161%	4
T11	1375	96.3	260	32.3	32.3	7%	17.7%	55%	0.91	100%	9

This experimental design enabled systematic evaluation of carbonation behavior under advective gas flow, including reaction-front progression, lime utilization, and CO_2 uptake efficiency as functions of lime content and degree of saturation.

Test Results

Figure 17. Representative thermal imaging (top row) and pressure readings (bottom row) for Test T7 with βL = 3% and Sr = 30% at different stages of carbonation during a test: a.) 3.6 minutes; b.) 7.8 minutes; c.) 11.9 minutes. presents representative thermal imaging and pressure measurements obtained during a one-dimensional carbonation test conducted under an imposed advective CO_2 flow regime (Test T7). Thermal images show a distinct temperature contrast associated with the exothermic carbonation reaction, forming a well-defined thermal front that advanced downward through the specimen with time. The progression of this thermal front indicates rapid reaction between injected CO_2 and available lime near the gas entry boundary.

Simultaneously recorded pressure measurements reveal a linear decrease in pressure with depth that closely tracked the location of the thermal front (Figure 17. Representative thermal imaging (top row) and pressure readings (bottom row) for Test T7 with βL = 3% and Sr = 30% at different stages of carbonation during a test: a.) 3.6 minutes; b.) 7.8 minutes; c.) 11.9 minutes.). Above the front, measurable pressure gradients developed as CO_2 was introduced and consumed, whereas below the front pressure readings remained near zero, indicating that the soil was not internally pressurized by CO_2 gas. The close correspondence between the advancing thermal front and pressure gradients demonstrates that the majority of injected CO_2 was rapidly consumed by carbonation reactions as it entered the specimen.

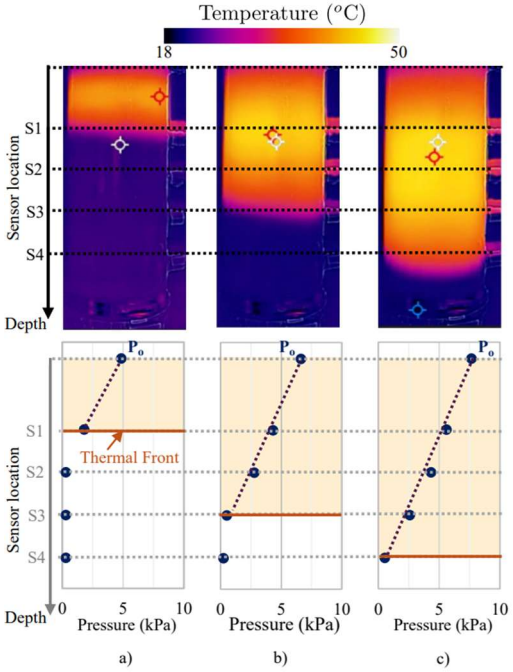

Figure 17. Representative thermal imaging (top row) and pressure readings (bottom row) for Test T7 with βL = 3% and Sr = 30% at different stages of carbonation during a test: a.) 3.6 minutes; b.) 7.8 minutes; c.) 11.9 minutes.

Figure 18 compares post-carbonation degrees of carbonation (DoC) measured along the specimen depth with the corresponding thermal fronts for tests conducted with sufficient CO_2 supply (CO_2,ratio ≈ 100%) and tests where CO_2 supply was intentionally limited (CO_2,ratio < 100%). When sufficient CO_2 was supplied, the maximum DoC was approximately uniform throughout the specimen depth for all lime contents tested, indicating that carbonation progressed through the full height of the column. In contrast, when CO_2 supply was limited, carbonation advanced only partially through the specimen. Above the thermal front, DoC values were comparable to those observed in fully supplied tests, whereas below the front DoC values decreased sharply and approached zero, indicating negligible carbonation. A small transition zone immediately below the thermal front exhibited marginal carbonation, suggesting limited post-front diffusion of dissolved species.

These observations confirm that carbonation under advective flow progressed in a predominantly top-down manner and that the thermal front effectively delineates the active carbonation reaction zone. The combined use of thermal imaging, pressure measurements, and post-carbonation DoC profiles provides consistent evidence that injected CO_2 was rapidly sequestered upon entering reactive regions of the specimen.

For specimens prepared at a degree of saturation of approximately 30%, the maximum achievable DoC decreased with increasing lime content, regardless of whether a sufficient quantity of CO_2 was supplied (Figure 18). Once this maximum DoC was reached throughout the specimen, additional injected CO_2 permeated through the soil without further reaction. This behavior suggests that, at higher lime contents, local reaction kinetics limited lime utilization under the imposed advective flow conditions. It is inferred that portions of the lime were distributed such that dissolution and aqueous-phase diffusion could not keep pace with the rate of CO_2 delivery, resulting in incomplete utilization of available lime.

Figure 19a summarizes the average DoC achieved throughout the specimen as a function of lime content and degree of saturation. While DoC decreased modestly with increasing lime content, degree of saturation exerted a stronger influence on carbonation efficiency. Specimens prepared at a higher degree of saturation ($Sr \approx 55\%$) consistently exhibited lower DoCs than those prepared at $Sr \approx 30\%$. This trend is attributed to thicker water films at higher saturation, which increase aqueous-phase diffusion distances and locally retard reaction kinetics, despite the presence of advective gas flow.

Figure 19b presents the time required for the carbonation reaction front, interpreted from thermal imaging, to traverse the full specimen height. Reaction-front advancement occurred rapidly, with total carbonation times ranging from approximately 15 to 40 minutes. Longer times were associated with higher lime contents, reflecting increased reactive demand. Comparison across degrees of saturation shows that reaction fronts advanced more quickly for specimens at $Sr \approx 55\%$ than for those at $Sr \approx 30\%$. Although higher saturation restricts gas-phase pathways, reduced lime utilization at higher saturation resulted in lower overall CO_2 uptake, allowing the reaction front to advance more rapidly through the specimen.

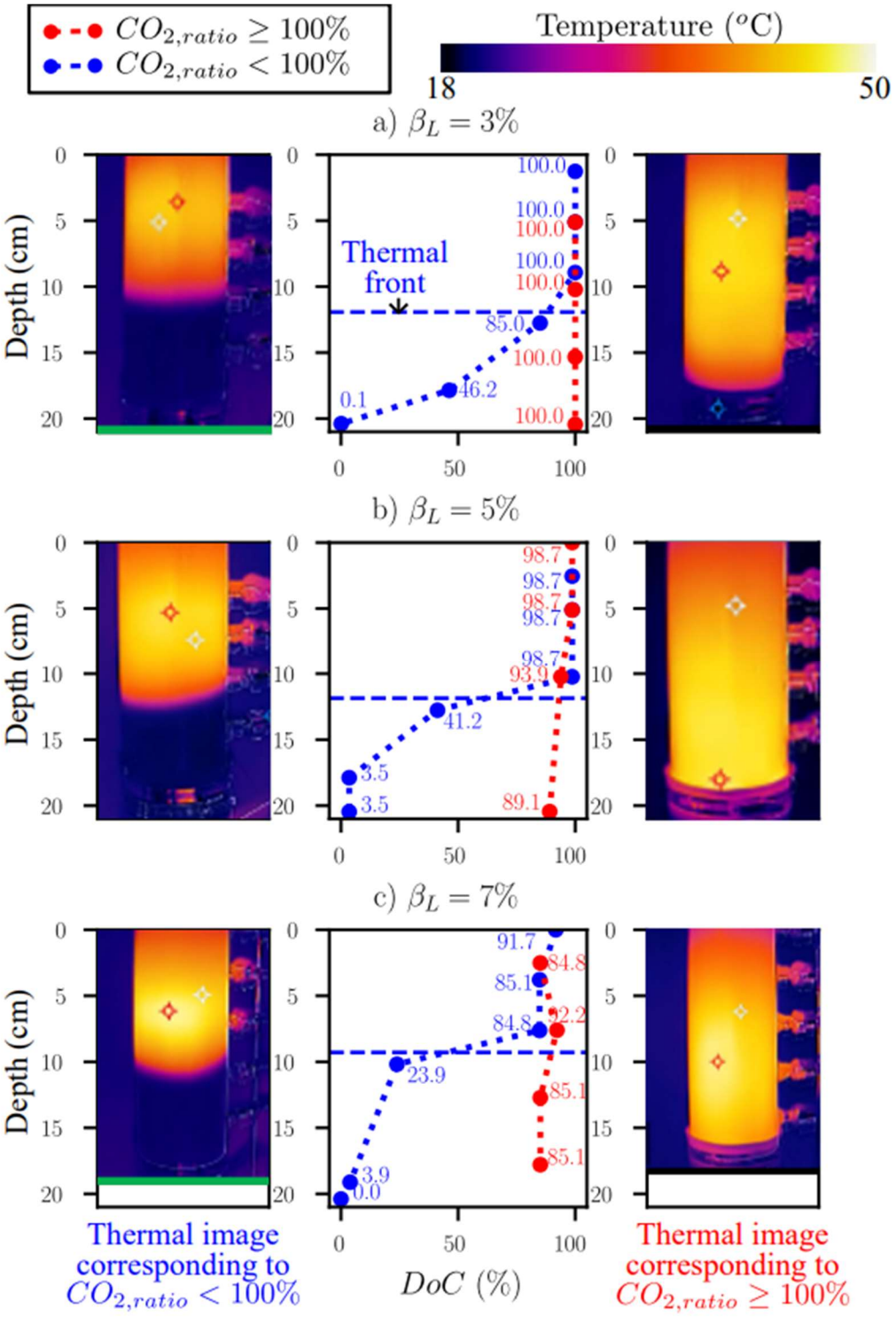

Figure 18. Comparison of the post-carbonation DoC and corresponding thermal fronts at the end of a test for the three test conditions where a sufficient supply of CO2 was injected (CO_2,ratio ≥ 100% in red) and where it was not (CO_2,ratio < 100% in blue) for: a.) βL = 3% and Sr = 30% (Test T6 and T7); b.) βL = 5% and Sr = 30% (Tests T4 and T5); c.) βL = 7% and Sr = 30% (Tests T2 and T3). The thermal images were trimmed and scaled to the sides of the vertical axis for reference.

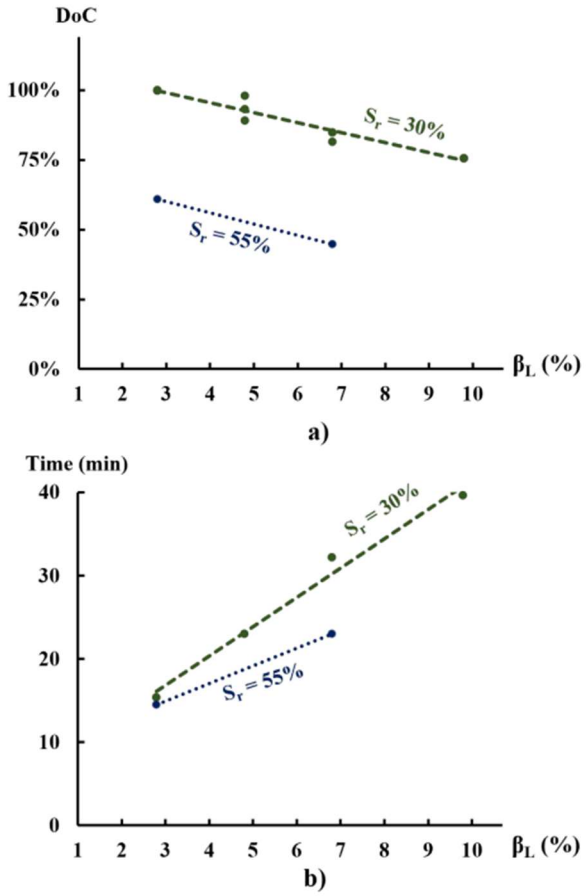

Figure 19. a.) Measured average DoCs achieved throughout a sample for different lime contents and degrees of saturation (Sr = 30% and 55%) when a carbonation reaction front advanced through the sample; b.) comparison of the time required for the carbonation reaction front interpreted from thermal imaging to advance through the entire sample.

Overall, the test results demonstrate that advective CO_2 delivery can significantly accelerate carbonation relative to diffusion-dominated processes, while also revealing clear limitations associated with lime utilization and moisture condition. Degree of saturation was found to be the dominant factor governing maximum achievable carbonation under advective flow, with higher saturation conditions leading to reduced lime utilization despite rapid reaction-front propagation.

Discussion

The bench-scale experiments demonstrate that introducing CO_2 under an advective gas-flow regime can substantially accelerate carbonation relative to diffusion-dominated processes. Thermal imaging and pressure measurements consistently showed that carbonation progressed rapidly in a top-down manner, with reaction fronts advancing through the specimen on the order of tens of minutes. This confirms that carbonation reaction kinetics are sufficiently fast to generate a carbonate binder under advective flow conditions, provided that CO_2 is delivered to regions containing reactive lime.

However, the results also reveal important limitations associated with lime utilization and CO_2 efficiency under advective transport. Once a maximum degree of carbonation was achieved within the specimen, continued CO_2 delivery resulted in gas permeation without additional reaction. This behavior indicates that carbonation effectiveness under advective flow is not governed solely by

CO_2 availability, but by the ability of local reaction processes—lime dissolution, CO_2 dissolution, and aqueous-phase diffusion—to keep pace with the imposed gas flow. In this sense, advective transport can oversupply CO_2 relative to reaction capacity, leading to diminished utilization efficiency.

The observed reduction in maximum degree of carbonation with increasing lime content further supports this interpretation. At higher lime contents, a larger fraction of lime appears to be distributed in locations where dissolution and subsequent reaction cannot occur rapidly enough under advective conditions. This may reflect limitations in lime dissolution rates, incomplete submergence of lime particles in pore water, or increased diffusion distances between dissolved CO_2 and available calcium ions. As a result, higher lime contents do not necessarily translate to higher carbonate formation under rapid gas-flow regimes.

Degree of saturation exerted an even stronger influence on carbonation performance. Specimens prepared at higher saturation consistently exhibited lower degrees of carbonation, despite rapid advancement of reaction fronts. This behavior is attributed to thicker water films, which increase aqueous-phase diffusion distances and retard local reaction kinetics. Although advective flow enhances bulk CO_2 delivery, carbonation reactions ultimately occur within the water phase; therefore, thicker water films impose a fundamental kinetic limitation. The faster advancement of reaction fronts at higher saturation reflects reduced CO_2 uptake rather than enhanced reaction efficiency.

These findings highlight a key distinction between advective and diffusion-dominated carbonation. Diffusion-based approaches, while slower, promote more complete utilization of lime and CO_2 over longer timescales, as gas transport is inherently limited and reactions are allowed to proceed toward completion. In contrast, advective gas delivery prioritizes speed but can result in underutilization of reactive additives if flow rates exceed local reaction capacity.

From an implementation perspective, the results suggest that advective carbonation is most effective as a means to rapidly initiate carbonate binder formation to a target depth, rather than as a standalone strategy for maximizing lime utilization. Hybrid approaches that combine initial advective CO_2 delivery with subsequent diffusion-controlled exposure may offer a more balanced solution, enabling both rapid strength development and efficient CO_2 sequestration. Such strategies could be particularly relevant for field-scale applications, where control over gas delivery rates, boundary conditions, and moisture states is inherently more complex.

Overall, the bench-scale results provide critical mechanistic insight into carbonation under advective flow and establish important constraints on CO_2 delivery rates, moisture conditions, and lime contents. These insights directly inform the interpretation of larger-scale experiments and underscore the need for careful control of gas transport mechanisms when designing carbonation-based soil stabilization systems.

Chapter 3: Large-Scale Soil Box Testing

Based on elemental testing (Gallant et al. 2025) the parameters of functionality and associated index properties influencing the rate of carbonation and degree of strength improvement. Generally, it was shown that a calcium carbonate binder can substantially increase the mechanical attributes of soil chemically improved via carbonation, expanding the applicability of lime as a chemical additive that can be used to treat non-plastic soils. Like other chemically stabilized soils, the strength is highly dependent on the density, volumetric binder content, and soil type. It was shown that stiffness correlates well with the unconfined compression strength and that the binder-phase primarily governs strength and stiffness. Moreover, it was shown that carbonated soil has a similar dependence on soil type, density, and binder content as cement-stabilized soils. Strengths between 3 and 4 MPa could be achieved with a gravimetric hydrated lime, $Ca(OH)_2$, content of ~9%. It's important to note that hydrated lime typically forms from quick lime (CaO) after "mellowing" in the field. The equivalent quick lime content is ~5% and this percentage is comparable to cement contents often applied in the field for non-plastic materials.

The rate of binder formation in carbonated soil is intrinsically linked to the mobility of gas in the soil matrix, which is governed largely by the degree of saturation and volumetric air content. In soils with degrees of saturation (S_r) below ~50%, a rapid increase in the binder content was observed relative to specimens with higher degrees of saturation (all else being equal). This is attributed to a continuous or near-continuous gas-phase through the voids. Soils with degrees of saturation greater than 50 to 60%—the threshold values where a transition from a continuous gas-phase to a continuous water-phase in the void space is expected—the rate of binder formation decreased substantially. If the degree of saturation was below threshold values that provided "air pipes" facilitating gas mobility through the soil matrix, then higher volumetric water contents appeared to increase the rate of carbonation. This was attributed to greater dissolution of lime and carbon dioxide gas in the pore water, which hosts chemical constituents, during the reaction.

Therefore, there is an optimum volumetric water and air content (degree of saturation) linked to the rate of carbonation. Gallant et al. (2025) showed full carbonation of specimens with a gravimetric lime content of 10% within 3 to 24 hours under optimal conditions (Sr ~ 40%). However, it may be difficult, if not impossible, to control this optimum condition in a field/construction setting. However, for some applications, there may be some practical control over the water content (e.g., base, subbase, and subgrade stabilization). In these cases, it would be most prudent to attempt to achieve a continuous or near-continuous gas-phase within the pore network that facilitates gas mobility and diffusion in soil.

The lessons learned from elemental- and bench-scale testing were carried forward to larger soil box experiments to demonstrate some field-scale applications, which are presented here.

3.1 Methods

Figure 20a shows a conceptual schematic of surface carbonation on an embankment of soil. Carbon dioxide gas is introduced beneath an impermeable gas barrier that is sealed near the perimeter of a targeted treatment area to facilitate vertical penetration of CO_2 into the soil. Figure 20b shows the large soil box that was used and is representative of a portion of the embankment near the

perimeter where some gas escape through the slope of a treated area may be expected to occur; i.e. simulation of a critical location when considering the potential for gas escape. In Figure 20b, the left edge of the box represents a vertical cut closer to the center of a hypothetical embankment, while the right edge represents a sloped portion of the embankment (see red lines in Figure 20a). The box was sealed with a plastic covering and sealed around the edges. Holes were drilled through the embankment side of the box to allow gas flow and simulate the perimeter of an embankment.

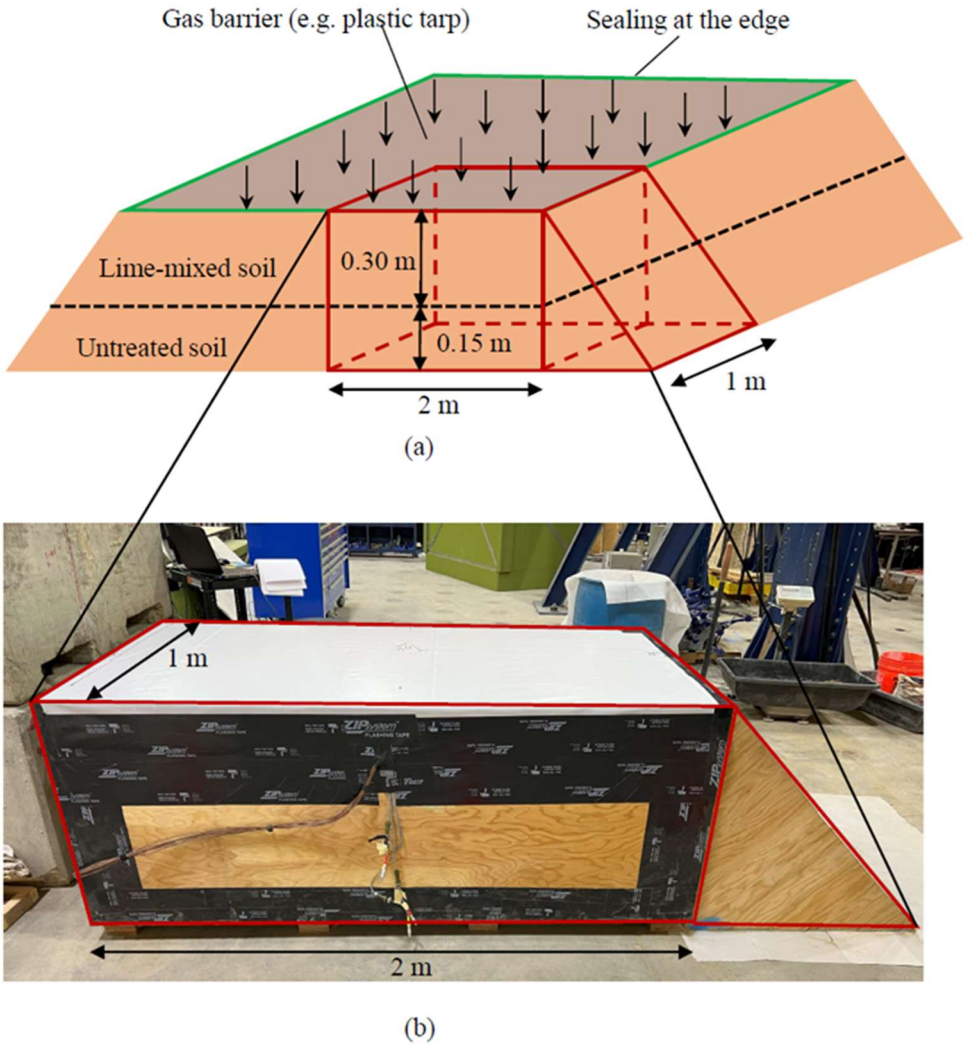

Figure 20. a.) A conceptual schematic of surface carbonation on an embankment of soil (not to scale), where car-bon dioxide gas is introduced beneath an impermeable gas barrier and sealed near the perimeter of a targeted area to enforce vertical penetration of carbon dioxide gas into the soil. b.) Large soil box intended to simulate a portion of the embankment near the perimeter where gas-escape near the perimeter/slope may occur (from Gallant et al. 2024).

Soil Box Construction and Instrumentation

Figure 21 provides an overview of the soil box construction and installation of instrumentation used to monitor carbonation of the non-plastic silt mixed with lime. The wooden box was sealed at the bottom and at jointed connections to prevent gas- and moisture-loss during experiments (Figure 21a). Perforated PVC pipes installed at the base of the box prevented pressure buildup and maintained an atmospheric gas

boundary pressure at the bottom of the soil column during carbonation; the pipes were also used later to introduce groundwater and saturate the soil for freeze–thaw durability testing (Figure 21b). The soil consisted of 22% sand, 71% silt, and 7% clay by weight, was classified according to the Unified Soil Classification System as a low plasticity silt with sand (ML). This soil type was selected because it is a highly frost-susceptible material and because it was comprised primarily of stable quartz and alumina, which are generally considered "non-reactive" from a conventional lime-stabilization perspective; i.e. no pozzolanic hydration products that would bind the soil particles were expected during the experiment, which provided the opportunity to isolate the effects of carbonation. An effective $Ca(OH)_2$ content of 6.4% by dry weight of soil was used for lime-mixed soil. The Graymont lime was only 80% pure $Ca(OH)_2$, and therefore 8% by weight of soil of the Graymont lime material was used to achieve the 6.4% $Ca(OH)_2$ content.

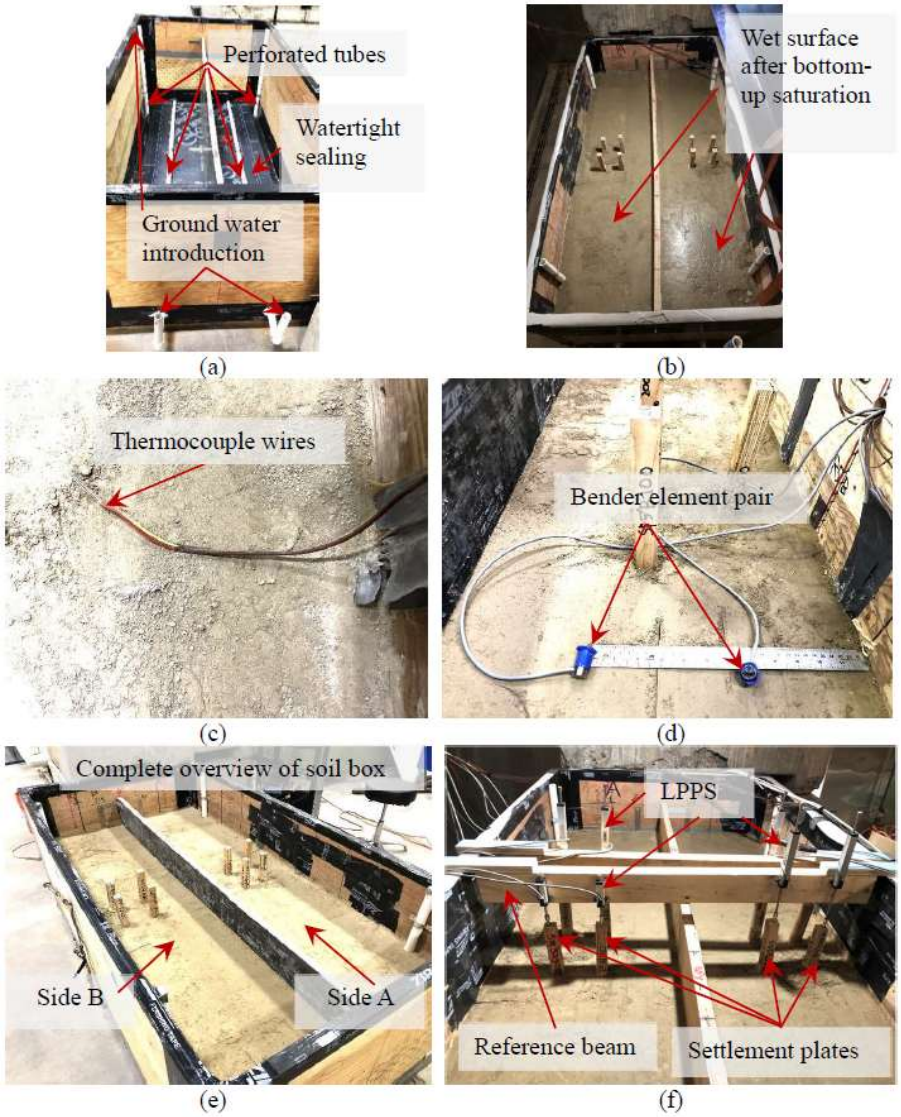

Figure 21. Overview of soil box assembly and installation instrumentation: a.) horizontal and vertical perforated pipes to saturate the soil, and water sealing on both sides of the box; b.) soil surface after carbonation and complete saturation but before freezing; c.) thermocouples embedded at depth as box is filled; (d.) bender element pairs shown as box was being filled; e.) soil box after filling for sides A and B; and f.) Lin-ear Potentiometer Position Sensor (LPSS) mounted on wooden settlement plates (adapted from Gallant et al. 2024).

The soil was hand-compacted in 50 mm lifts to a final thickness of 450 mm with a relative compaction of 86 to 88% (γ_d = 14.2 to 14.4 kN/m^3) and void ratio e = 0.8. Hydrated lime from Graymont Inc. was mixed with the non-plastic silt in the upper 300 mm of the box. Prior to filling the box, dry soil and lime were thoroughly mixed before adding water and mixing again to achieve a desired water content. To evaluate if observations from elemental testing would apply in the large soil box experiment, the box was divided into sides "A" and "B" and prepared with different S_r values. S_r = 30% and S_r = 40% were prepared on Sides A and B, respectively (Figure 21e). These Sr values were expected to: a.) provide sufficient water to facilitate the reaction; and b.) not result in moisture levels that obstruct the permeation of gas into the soil matrix. To achieve a uniform lime content, void ratio, and associated water content and degree of saturation, the weight of the moist material was measured for each 50 mm lift to ensure consistency throughout the box. Pre-carbonation cores performed in concert with California Bearing Ratio testing (discussed later) revealed gravimetric water contents were always within 1% of the target value at all depths.

Thermocouples (TCs), bender element pairs (BEs), and wooden settlement plate pedestals were embedded in the soil at varying depths as the box was filled. Five thermocouples were placed at two locations on each side of the box (20 total) to monitor temperature changes at depths z = 0, 100, 200, 300, and 400 mm during carbonation and environmental durability testing later (Figure 21c). Two bender element pairs were placed on each side of the box at z = 50 and 250 mm (the upper pair on Side A ultimately did not function). Each pair was placed 150 mm apart and the 14 mm long elements extended 3.5 mm from a titanium housing into the soil and transmitted horizontally propagating and horizontally polarized shear waves, V_s (Figure 21d). The elements were installed at the desired depth by placing soil around the tip and housing, followed by careful compaction just around the element to ensure the element was secure and in firm contact with the soil while also avoiding damage to the instrument. Linear Potentiometer Position Sensors (LPPS) were mounted to reference beams near the center of the box Sides A and B to monitor vertical deformations at depth during freeze-thaw testing (Figure 21e).

Figure 22 shows a plan and elevation view of instrumentation locations in the soils box, which was 2 m in length and 1 m wide (each side was 0.5 m wide). The TCs and LPPSs wires were connected to a USB-2416 series data acquisition system from Measurement Computing that monitored temperature and deformations continuously. Shear wave velocities were measured using a GDS bender element data acquisition system. Measurements were not continuous and taken periodically.

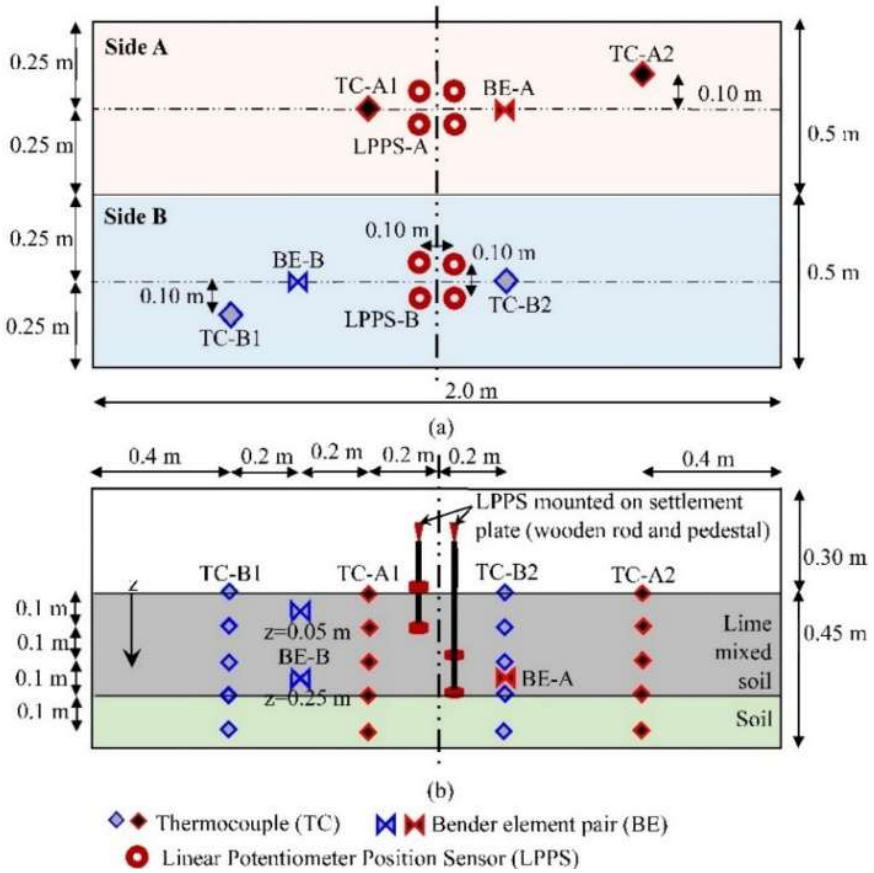

Figure 22. Soil box instrumentation plan and dimensions showing the locations of the thermocouples (TC), bender element pairs (BE), and Linear Potentiometer Position Sensor (LPSS) mounted on settlement plates (wooden rod with a circular pedestal) in a.) plan view and b.) elevation view (adapted from Gallant et al. 2024).

Destructive Testing and Sampling

Destructive testing and sampling were performed to assess changes in mechanical behavior, binder content (BC), and lime content. The field California Bearing Ratio (CBR) test was performed in general accordance with ASTM D4429-09 to assess changes in strength and stiffness throughout the soil column after carbonation and freeze-thaw testing in an environmental chamber. The field CBR equipment, which consists of a mechanical screw jack and piston that penetrates the ground, reacted off a steel beam secured by reaction blocks on each side of the box; the reaction beam spanned the length of the box and was repositioned to the centerline on each side of the box for CBR testing. The CBR is a normalized stress defined as,

$$CBR = \frac{\sigma_\delta}{\sigma_{std}} \tag{13}$$

where σ_δ is the measured stress at 2.54 or 5.08 mm of piston penetration, and σ_{std} is a standard stress of 6.9 or 10.3 MPa that corresponds to 2.54 or 5.08 mm of penetration, respectively. The CBR is the largest stress ratio arising from measurements at 2.54 and 5.08 mm of penetration. The field CBR was typically performed at five different depths (z = 0, 100, 150, 250, and 350 mm) before and after carbonation and after two freeze-thaw cycles were performed. The CBR was only performed at the soil surface after soaking (i.e. after carbonation but before freeze-thaw cycling) to help limit the number of holes drilled throughout the box.

A 75 mm thin-walled shelby tube was used to extract soil samples post-carbonation. Given the stiff nature of the soil post-carbonation, a scissor jack was used to slowly and methodically penetrate the thin-walled sampler by reacting off the steel beam. Samples were immediately extruded and oven dried to prevent any potential carbonation from atmospheric CO_2. The samples were stored in hermetically sealed plastic containers prior to TGA testing that was performed to determine the $CaCO_3$ binder content and $Ca(OH)_2$ content. CBR testing and sampling were performed in tandem; i.e. after each CBR test, sampling was performed to collect soil for chemical testing, but to also advance the hole to the next CBR test depth.

Accelerated Surface Carbonation Setup

Figure 23a provides an overview of the experimental setup, where a TSI 5300 series mass flowmeter (Figure 23b) located between the soil box and gas valve Figure 23c) measured the standard liters of gas supplied through a single manifold connected to six CO_2 cylinders (Figure 23d). The flowmeter monitored the gas flow rate and the total amount of gas supplied in the box during the carbonation experiment. The wires for thermocouples and bender elements were routed through a single sealed opening in the box and connected to a data acquisition system.

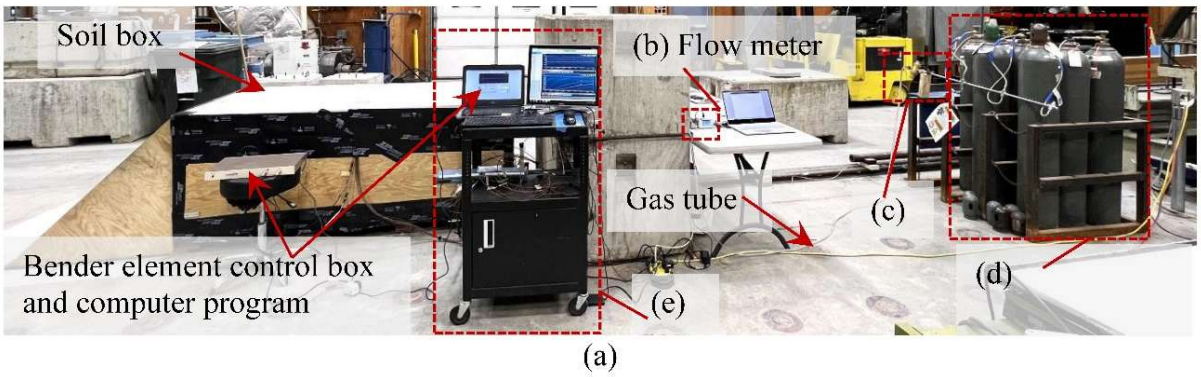

Figure 23. Overview of setup and equipment used for the large-scale surface carbonation experiment: a.) complete overview of experimental setup highlighting different components; b.) carbon dioxide mass flowmeter between the soil box and c.) gas valve located between the flowmeter and the d.) six CO2 gas cylinders connected through a single manifold to supply uninterrupted flow; e.) data acquisition system connected to thermocouples and bender elements (from Gallant et al. 2024).

Environmental Durability Testing and Freeze-Thaw Chamber

Frost action—which consists of frost heave followed by thaw weakening—is generally well understood (Konrad 1999, 2005, Konrad and Roy 2000) and the experimental configuration was designed to incorporate the three essential factors required for ice lens formation: i.) subfreezing temperature that penetrate the subgrade (i.e. 1-D freezing front); ii.) a frost-susceptible soil within the freezing zone (soaked silt in this study); and iii.) a continuous groundwater source that can feed water into the freezing zone (Konrad 1999).

After carbonating the silt, the large soil box was moved into an environmental chamber. Figure 24 shows the freeze-thaw (FT) experimental setup inside the environmental chamber (interior dimensions-6.7 m in length and width with a height of 4.3 m), which could control the temperature (T) between +50 C and -40 C. Prior to applying FT cycles, the post-carbonated soil column inside the box was saturated (soaked). Water was introduced through two conduits running the length of

the box (at the bottom) and four vertical conduits on the box sides (two on each side—see Figure 24a). Only the bottom 150 mm of the vertical conduits were perforated ensure water was introduced at the bottom of the box. Sufficient water was added to ensure saturation of the silt and later confirmed via water content measurements. The soil was also visibly soaked prior to FT cycling. The conduits provided a means to simulate an open groundwater system at depth for water uptake as freezing or thawing occurred; i.e. the water supply was maintained through the bottom conduits throughout the FT experiments so that a water source was available to feed potential ice lens formation or fill voids created during thaw periods.

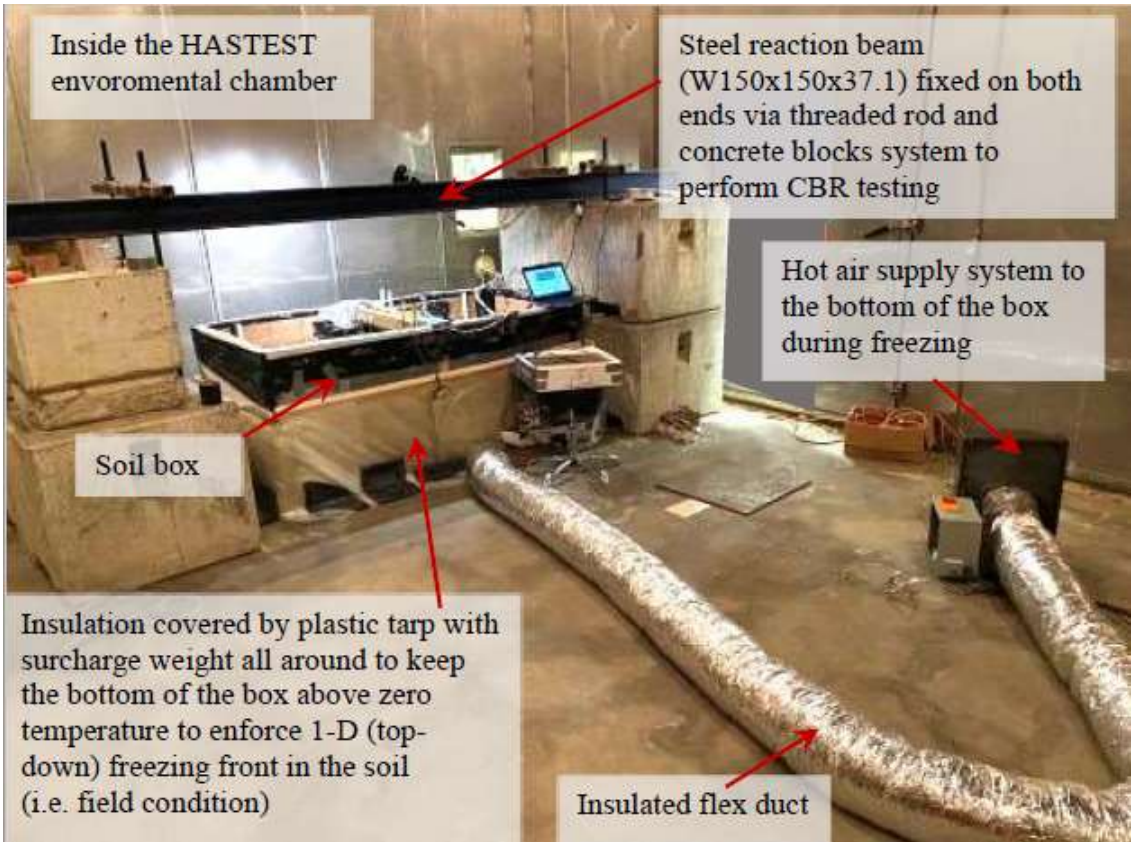

Figure 24. Overview of experimental setup and equipment used for the large-scale freeze-thaw experiments in the HASTEST environmental chamber, including insulation and heating system used to heat underside of the box and the beam and reaction blocks used for field CBR testing at different stages of testing.

A total of two FT cycles were performed, which has been shown to be the number of cycles required to capture the detrimental effects of frost action on soil (Cook 1963, Chamberlin 1981, Boynton and Daniel 1985, Graham and Au 1985, Leroueil et al. 1991, Othman and Benson 1993, Lee et al. 1995, Viklander 1998, Hazirbaba and Gullu 2010). During each freeze cycle the environmental chamber was maintained at -20 C or lower until the entirety of the soil column reached -10 C. During freezing cycles warm air was supplied from a heating system through a flex duct at the bottom of the insulated box (Figure 24) to maintain a bottom boundary temperature between 5 and 10 C (just above freezing). The introduction of warm air at the bottom of the box combined with the insulated box perimeter was sufficient to maintain a thermal differential between the top and bottom of the soil layer and achieve a desired top-down freezing front. During thaw cycles the temperature in the environmental chamber was increased to at least 23 C. In addition to increasing the relative humidity in the chamber to 85%, a plastic tarp was placed over

the soil box to limit surface evaporation and potential drying of the soil. Thawing temperatures were maintained until the entire soil column reached approximately 20 C. After completion of the two FT cycles the soil box was left exposed at the surface for 12 weeks to permit some drying to assess the resilience of the carbonated silt after exposure to harsh environmental conditions (i.e. soaking and frost action).

3.2 Experimental Observations

Accelerated Surface Carbonation

Figure 25 shows the flowmeter data during carbonation, including the absolute gas pressure and temperature where CO_2 entered the soil box (Figure 25a) and the corresponding flow rate (in standard liters/minute) and total mass of CO_2 that entered the box (Figure 25b). The accuracy of the mass flow rate and total mass is ± 2% of the reading (not full scale). Standard liters refers to the mass of gas occupying a volume at a standard pressure P_{std} = 101.3 kPa and standard temperature T_{std} = 21.1 C. Temperature and pressures are accounted for in the readings. The standard liters of CO_2 can be converted to mass using the ideal gas law,

$$m_{CO_2} = \frac{P_{std} V_g}{R T_{std}} \times M_{CO_2} \tag{14}$$

where R is the universal gas constant, V_g is the volume of gas, and M_{CO2} = 44.01 g/mol is the molar mass of carbon dioxide. For reference, the corresponding amount of gas that is theoretically required to fully carbonate the available $Ca(OH)_2$ over different depth intervals, assuming carbonation progresses top-down in the soil column, is also shown; e.g. 0–50 mm, 0–100 mm, 0–150 mm, etc. (see Figure 25b).

Gas was continuously supplied to the box without making any adjustments to the pressure regulator at the manifold for approximately 10 h under a low absolute pressure between 101 and 102 kPa (≈ 0 gauge pressure). Flow rate, pressure, and temperature fluctuations after 10 h reflect user adjustments made to the pressure regulator after 10 h of continuous flow (see Figure 25b). During the period where no adjustments were made to the pressure regulator (t_c < 10 hours), the flow rate steadily increased for approximately 8 h and then steadied out. The greatest fluctuations in flow rate were observed at the beginning of the test, presumably due to the influence of an ongoing reaction, which diminished over the course of the first 5 h when enough gas had been introduced to carbonate the upper 150 mm of soil (Figure 25b). Thereafter, the flow rate steadily increased, but with limited fluctuations (discussed more later).

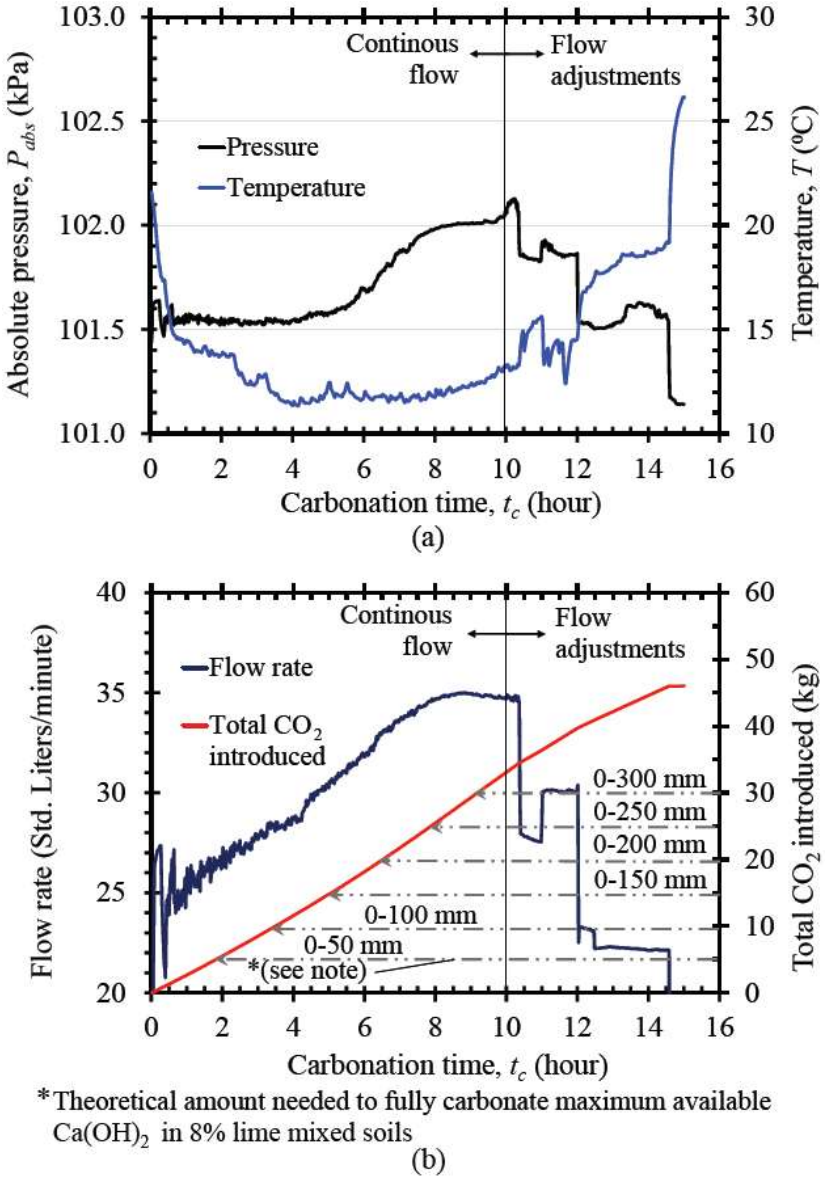

Figure 25. Flowmeter readings during the surface carbonation experiment: a.) absolute pressure and temperature readings during the carbonation period; b.) CO2 mass flow rate and total mass of CO2 introduced. Also indicated is the theoretical amount of CO2 required to fully carbonate available Ca(OH)2 at various depth intervals, assuming carbonation progressed vertically from the soil surface downward (from Gallant et al. 2024).

Figure 26 shows the temperature readings (data collected every 2 min) on each side of the box at various depths (Figure 26a), the rate of temperature change throughout the carbonation period, dT/dt_c (Figure 26b), and changes in shear wave velocity (Figure 26c). The temperature rate changes shown in Figure 26b were "smoothed" using a cell-centered average applied across ten data points. It's worth noting here that the acute temperature fluctuations observed at all locations from 10 to 12 h (Figure 26a) are attributed to the aforementioned flow adjustments made after 10 h of carbonation that decreased the rate that cooler CO_2 gas was being introduced into the box (Figure 26). Temperature rate fluctuations are not shown in Figure 26b through this period because they are not indicative of the carbonation reaction, which is discussed herein.

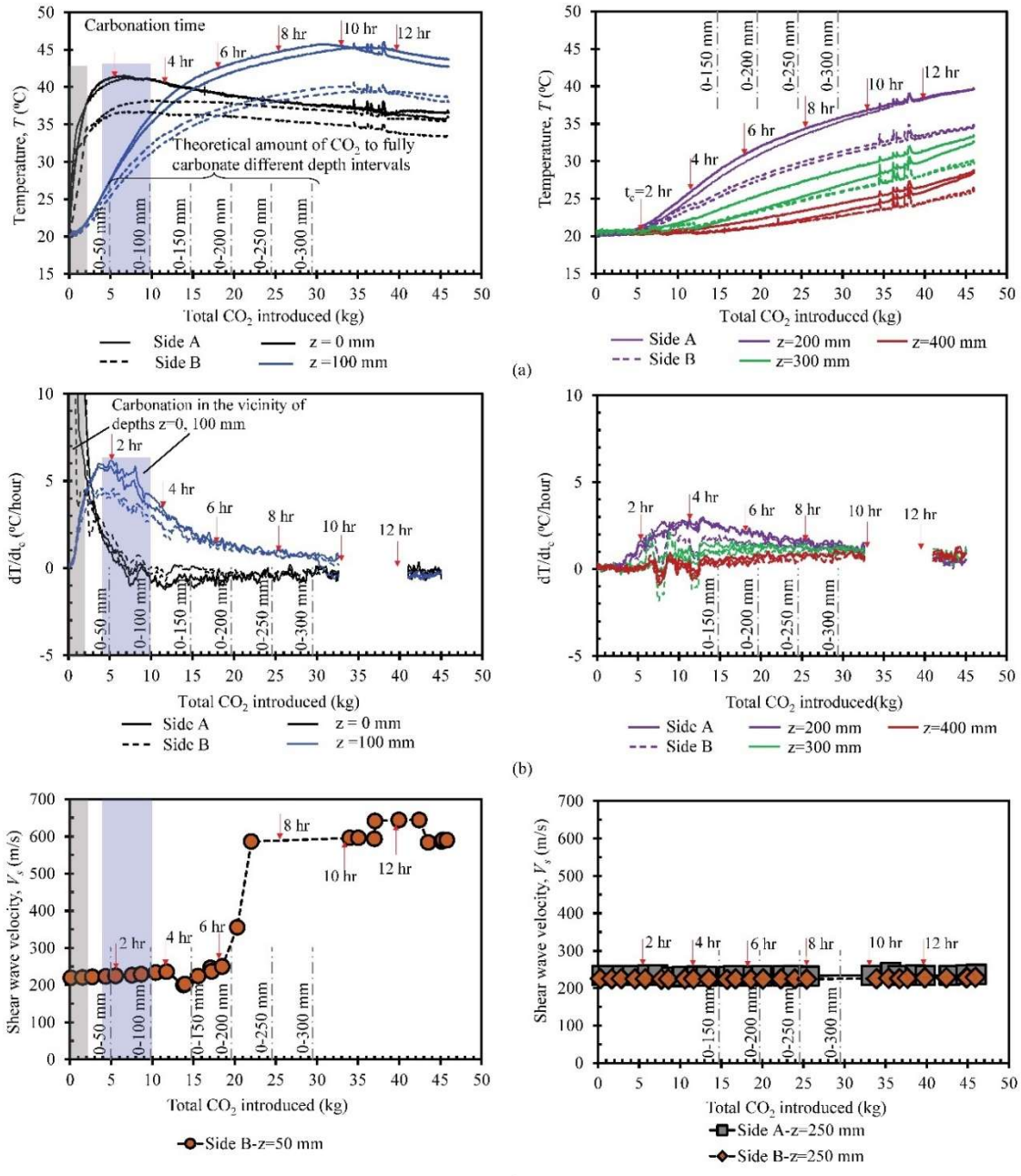

Figure 26. Changes in temperature readings and shear wave velocity at various depths in the soil as a function of the total CO_2 gas introduced and carbonation time (red arrows) during surface carbonation: a.) temperature readings at 0 and 100 mm (left) and 200, 300, and 400 mm (right); b.) rate of temperature change at 0 and 100 mm (left) and 200, 300, and 400 mm (right); c.) changes in shear wave velocity at 50 mm (left) and 250 mm (right). All plots also indicate the theoretical amount of CO_2 required to fully carbonate available $Ca(OH)_2$ to different depths (dashed gray lines), assuming carbonation progressed vertically from the soil surface downward (from Gallant et al. 2024).

Recall that the carbonation reaction with hydrated lime is an exothermic reaction that generates heat (Eq. 4). Temperatures first increased rapidly near the ground surface (z = 0 mm) followed by an increase in temperature at z = 100 mm. The corresponding rate of temperature change is greatest at the beginning of the test at the ground surface, but continuously decreased with time, suggesting that the reaction first occurred at shallow depths (expected) and then progressed vertically

downward. The decreased rate of temperature increase at z = 0 mm, followed by an increase in the temperature and the rate of temperature increase at z = 100 mm (Figure 26a,b), also support that carbonation generally progressed top-down through the soil column.

The rate of temperature increase serves as a proxy for when the reaction is occurring in the vicinity of the thermocouple; this is indicated for shallow depths by the light gray and blue shading in Figure 26 for thermocouple measurements at z = 0 and 100 mm. Notably, the rate of temperature rise in the vicinity of the z = 100 thermocouples was greatest when the theoretical amount of gas needed to fully carbonate to depths approaching 50 to 100 mm had been introduced. Thus, it is likely that the majority of CO_2 gas being introduced up to this stage of the test was being sequestered because of the reaction.

The temperature also increased at greater depths in the soil (z = 200 to 400 mm). However, the increases in temperature rise were not as pronounced as at shallower depths, likely signaling that the reaction was not occurring as rapidly, if at all, at those locations. Though all temperatures increased from z = 200 to 400 mm, which is undoubtedly due in part to the diffusion of heat within the soil layer, there was a noticeably higher rate of temperature increase at z = 200 mm than locations at greater depths (Figure 26b). It's possible that this was due to carbonation occurring and/or the proximity of the thermocouples at z = 200 mm to shallower regions where carbonation had progressed (discussed more later).

At all depths, temperature increases on side A (S_r = 30%) were higher than side B (S_r = 40%). As water has a high specific heat capacity, lower temperatures on side B may be attributed to a lower thermal conductivity expected in an identical soil with a greater volumetric water content; i.e. more heat energy generated by the carbonation reaction was likely absorbed on Side B by water. Nonetheless, changes in temperature measured on each side of the box occurred simultaneously, suggesting that carbonation progressed top-down at approximately the same rate on both Sides A and B. Thus, it is not believed that differences in S_r applied in this experiment had a significant impact on the rate or extent of carbonation—which was not unexpected based on elemental testing conducted on silt soils carbonated at similar S_r values (Hossen 2020, Gallant et al. 2025).

Figure 26c illustrates the shear wave velocity measurements at z = 50 and 250 mm in the soil box. Shear wave velocities measured at z = 50 mm increased substantially from initial values of approximately Vs = 200 m/s to Vs = 600 m/s after carbonation; i.e. in the upper portion of the soil column, the carbonated silt transitioned to a material akin to very hard soil or soft rock (NEHRP 2003, Weil et al. 2012, Loehr et al. 2016). However, based on the measured temperature changes that served as a proxy for the reaction (Figure 26a,b), the soil stiffness increased at z = 50 mm approximately 3 to 4 h after it is believed carbonation had occurred. Therefore, there was likely a short delay between the formation of the $CaCO_3$ binder and the subsequent agglomeration and solidification (i.e. crystallization) of the precipitating mineral on the soil grains that stiffened the soil matrix. During the reaction there can be metastable calcium carbonate phases, including amorphous calcium carbonate (ACC), that precede the transformation to more stable, lower energy, crystalline polymorph phases. Formation of different polymorphs of calcium carbonate follows the Ostwald's rule of stages Hadjittofis et al. (2022); that is, the least stable ACC Polymorph is the first to nucleate, which then crystallizes to form vaterite or aragonite (also metastable), and finally, forms calcite—the most thermodynamically stable polymorph. Therefore,

in such carbonation reactions, calcite is the final polymorph theoretically, which has also been confirmed experimentally for calcium hydroxide carbonation (Rodriguez-Navarro et al. 2023).

Regardless, for most practical construction applications, the rate of improvement during carbonation was effectively "immediate." No changes in shear wave velocity were observed on either side of the soil box at z = 250 mm. This further indicates that any carbonation was limited below z = 200 mm and that the temperature changes observed at greater depths were likely due to diffusion of heat from the reaction occurring above.

Figure 27 shows the gravimetric $CaCO_3$ binder content and unreacted hydrated lime contents on Sides A and B of the soil box after surface carbonation. As expected, the maximum binder content measurements correspond to the initial $Ca(OH)_2$ contents, indicating carbonation occurred rapidly enough and successfully bypassed the slow pozzolanic reactions that form hydration products with lime. The binder contents on each side of the box indicate that soil was fully carbonated in the upper 150 mm of the soil column on both sides of the soil box (i.e. all $Ca(OH)_2$ reacted) and was lightly carbonated from 150 to 200 mm. No carbonation occurred from 200 to 300 mm in the lime-mixed soil.

The post-carbonation binder content and $Ca(OH)_2$ content measurements align well with the temperature and shear wave velocity measurements observed during the experiment. The greatest spikes in temperature and rates of temperature increase were observed at depths (Figure 26a,b) where the soil was fully carbonated (Figure 27). Moreover, the greatest fluctuations in the gas flow rate, which can likely be attributed to an ongoing carbonation reaction occurring in the soil column, cease after 4 to 5 h (Figure 25b). Notably, this amount of time corresponds to the theoretical amount of gas required to fully carbonate the upper 150 mm of soil (Figure 26), where complete carbonation was observed (Figure 27). Thus, the majority of CO_2 gas introduced in the first 4 to 5 h was likely sequestered to generate a carbonate binder.

The less pronounced spike in temperature and temperature rate increases at z = 200 mm (Figure 26a,b) aligns well with depths where the silt was lightly carbonated (Figure 27). The gradual increases in temperature at z = 300 and 400 mm, where no carbonation occurred and the rates of temperature increase were much lower (Figure 26b), were due to diffusion of heat generated in soil at shallower depths. Based on spatial differences in carbonate content and the magnitude and rate of temperature changes observed in the soil column, temperature provides a strong indication of when and where accelerated carbonation is occurring.

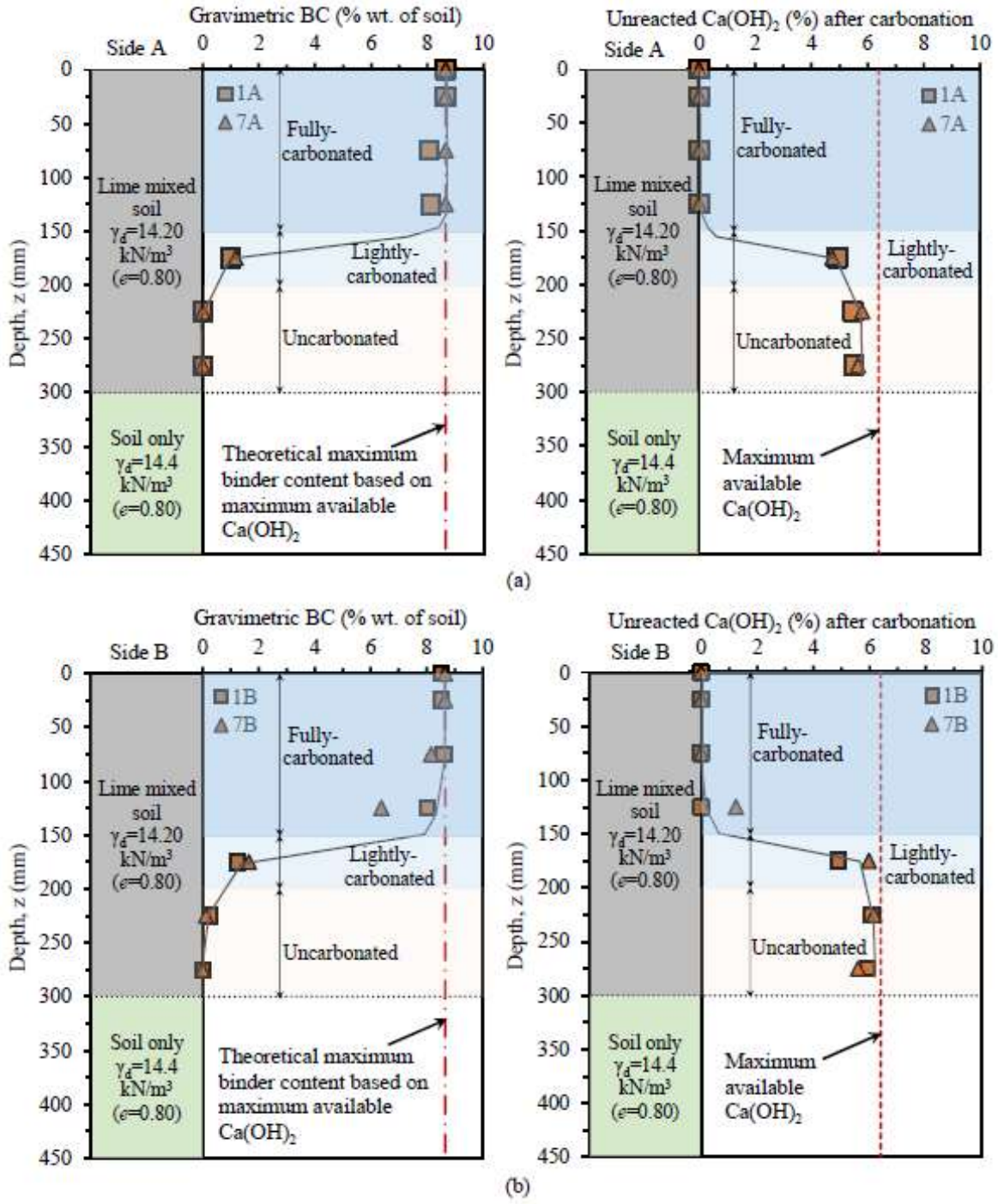

Figure 27. Gravimetric CaCO3 binder contents and unreacted hydrated lime contents on a.) side A and b.) side B of the soil box after surface carbonation (from Gallant et al. 2024).

Why carbonation did not progress to greater depths is unclear. Given lime was a relatively small percentage of the overall soil matrix, moisture content levels were not expected to change by more than 0.4 to 0.6 percent due to the carbonation reaction, which was reflected in post-carbonation measurements throughout the box (i.e. effectively unchanged). Therefore, increases in saturation

were not responsible for obstructing the flow of gas and limiting the depth where carbonation occurred. However, the experiment was designed to simulate surface carbonation near the perimeter of a treated area, where a surface seal might not exist along an embankment slope; i.e. an attempt was made to simulate carbonation at a critical location where gas could flow through soil, beneath the seal, and out of the system. Thus, the gas permeation depth may have been limited to z ≈ 150 to 200 mm because there was also lateral flow of gas towards the perimeter of the box. If that were the case, simulating surface carbonation "away" from the perimeter and near the center of a treated area may have resulted in carbonation at greater depths. This study also deliberately focused on the efficacy of accelerated surface carbonation using very low CO_2 gas pressures (≈ 0 gauge) beneath a seal, which would be easier to achieve in the field. Imposing higher gas pressures beneath a seal at the soil surface would likely enforce greater penetration of CO_2 gas as well. Due to the time and expense associated with this experimental setup, the aforementioned issues could not be systematically addressed at this scale. However, understanding these issues will facilitate development of enablement strategies and should be addressed in future work.

Regardless, chemical stabilization is typically applied to soil thicknesses ranging from 150 to 300 mm for transportation applications (Little 1999, Gross and Adaska 2020). Though carbonation was achieved to depths at the lower end of this range, the experiment provided proof of concept that accelerated surface carbonation has the potential to achieve practical targets. Though the introduction of CO_2 would be an added step, the occurrence of a chemical reaction over a few hours is practically "immediate" in a construction setting. Conventional chemical stabilization of soil relies on a hydration reaction associated with chemical additives (e.g. cement or lime) to bind the soil; this can require days, weeks, or even months in the case of lime. The large soil box experiment demonstrated that a binder can be generated rapidly via accelerated carbonation—so long as CO_2 penetrates the soil matrix.

Figure 28 shows the pre- and post-carbonation CBR measurements throughout the soil column for both sides of the soil box. For reference, qualitative descriptions provided by Schaefer et al. (2008) for subbase and subgrade soils constituting parts of a pavement system are shown. At the surface, CBR values increased from values considered fair to good for a subgrade material to very good or excellent subbase material, where stiffer, higher quality material is typically utilized. The CBR values ranged from 60 to 80 at the ground surface, remained elevated through the fully carbonated zone, but decreased with depth to pre-carbonation measurements where no carbonation occurred or where the soil was not mixed with lime. Thus, the CBR values demonstrate that accelerated surface carbonation with hydrated lime can substantially improve the mechanical properties.

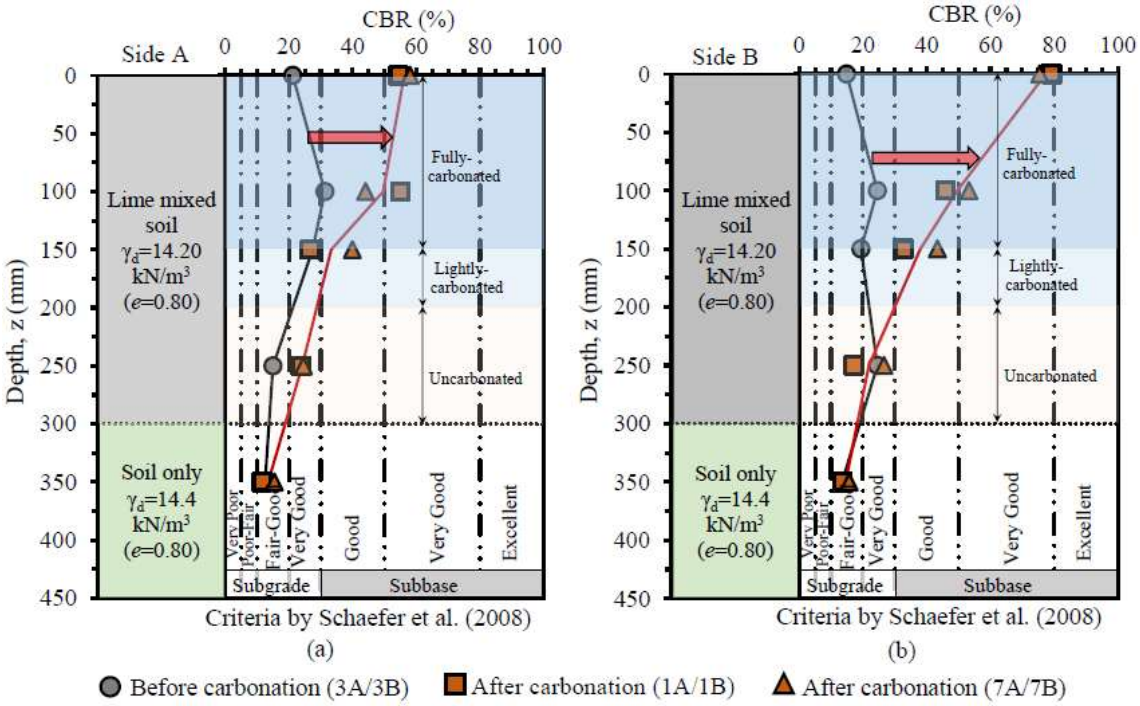

Figure 28. Pre- and post-carbonation CBR values throughout the soil column on a.) side A and b.) side B of the soil box (from Gallant et al. 2024).

Soaking and Freeze-Thaw Cycling after Carbonation

Recall that after carbonation, the soil box was soaked seven days later to fully saturate the soil, which caused CBR values at the surface to decrease to values between 20 and 30, which was expected (measurements weren't taken at depth after soaking). It's widely understood that soaking subgrade materials reduces bearing capacity and CBR measurements (e.g. Feng et al. 2020, Hazirbaba and Gullu 2010, Leelavathamma et al. 2005). Thus, the post-soaking CBR measurements served as a baseline to assess the durability of the carbonated silt after exposure to two freeze-thaw cycles in the large HASTEST environmental chamber.

Figure 29 summarizes the temperature and settlement data with time, t_{FT} , monitored throughout the duration of freeze-thaw (FT) testing. The combination of cold temperatures provided by the environmental chamber and heat provided to the underside of the soil box successfully enforced the intended 1D (top-down) freezing front in the soil on both sides of the box (Figure 29a). The soil generally thawed in a top-down manner as well, especially through fully carbonated soil; though soil at depths of 200, 300, and 400 mm typically reached the 0 C horizon at the same time, and the z = 300 mm depth was the last to rise above the 0 C threshold during thaw cycles (Figure 8a). This was due to the warmer temperatures on the bottom of the box, which were exposed to the warmer temperatures during thaw cycles, and the associated thermodynamics of heat exchange occurring within the box—which is not an unrealistic scenario in the subgrade as there are typically two thaw fronts (Konrad and Roy 2000). The cooling rate is also an important consideration and should attempt to reflect field conditions and the conditions most detrimental to soils (Dempsey and Thompson 1972, Konrad and Morgenstern 1980, 1984). In the state of Illinois, which can be considered representative for many regions in the northern United States, cooling rates of 0.1 to 0.6 C/h have been observed (Thompson and Dempsey 1970). The most detrimental effects to chemically stabilized can be expected to occur at freezing rates between 0.1 to 1.2 C/h (Dempsey

and Thompson 1972), which was generally achieved within the soil column. Thus, the test methods, which also incorporated a water supply made available throughout the test, replicated some important aspects of an expected field condition.

During both freezing phases, there was limited vertical movement (Figure 29b) and associated compression or expansion (Figure 29c) observed at different depth intervals within the soil column. Note that relative vertical deformations are expressed as a percentage of the thickness of soil between settlement plates for the subsurface depth intervals of 0 to 100, 100 to 200, 200 to 300, and 300 to 450 mm; i.e. expansion or compression indicates overall changes in layer thickness as a whole, but do not necessarily represent the compression or expansive strains of the entire depth interval. Notably, the greatest amount of upward vertical movement was observed at the start of a thaw cycle followed by downward vertical movement of the settlement plates embedded in the soil layers (Figure 29b).

As the top-down freezing front advanced in saturated soil, there was likely some adhesion between the side walls of the box and frozen water. Any adhesion would effectively impose a higher overburden stress on soils below the freezing front, which decreases the segregation potential and amount of heave where ice lens formation occurs during freezing (Konrad and Morgenstern 1984). Thus, the sidewall adhesive forces may have restricted the amount of movement at greater depths in the soil box as the frost front advanced; i.e. ice lens segregation and heave in unstabilized material at the bottom may have been greater otherwise.

During a thaw period there are typically two thaw fronts—one that progresses from the top of the soil column and other one that progresses from beneath the depth of frost penetration—which was simulated in these experiments. As summarized by Konrad and Roy (2000), the lower thaw front advances upward, and melted ice water under the weight of overburden material cannot escape (i.e. drain) upward due to the existence of an overlying impervious ice barrier. A hydraulic gradient can develop under the weight of overburden, driving downward groundwater flow and redistribution of pore water that results in “swelling” of unfrozen soils below the thaw front, a mechanism that contributes to the weakening of subgrade soils. After the complete thaw, consolidation is typically observed (Konrad and Roy 2000). Both swelling and consolidation were observed during each thaw cycle based on deformations shown in Figure 29b. However, it can be seen that the settlement platens generally move together, signaling that the greatest amount of expansion due to swelling was observed in the untreated layer from z = 300-450 mm (see Figure 29c).

Though there was little difference in the amount of deformations observed at all depths through the first FT cycle, there was substantially more swelling/expansion observed from 0 to 100 mm during the second thaw cycle on both sides of the box (Figure 29c). At the upper thaw front, an impermeable ice boundary below forces upward flow of groundwater when excess pore water pressures exist, which can contribute to the redistribution of pore water and increases in water content to overlying soils, similar to unfrozen soils underlying the lower thaw front (Konrad and Roy). There was also compression from 100 to 200 mm during the second thaw cycle (Figure 29c), which may have arisen due to the combination of pore water redistribution to the soil above and swelling of the underlying soil below. Notably, some of the material through this depth interval is

lightly carbonated. The least amount of relative movement was observed from 200 to 300 mm, which was sandwiched between the two thaw fronts (Figure 29c).

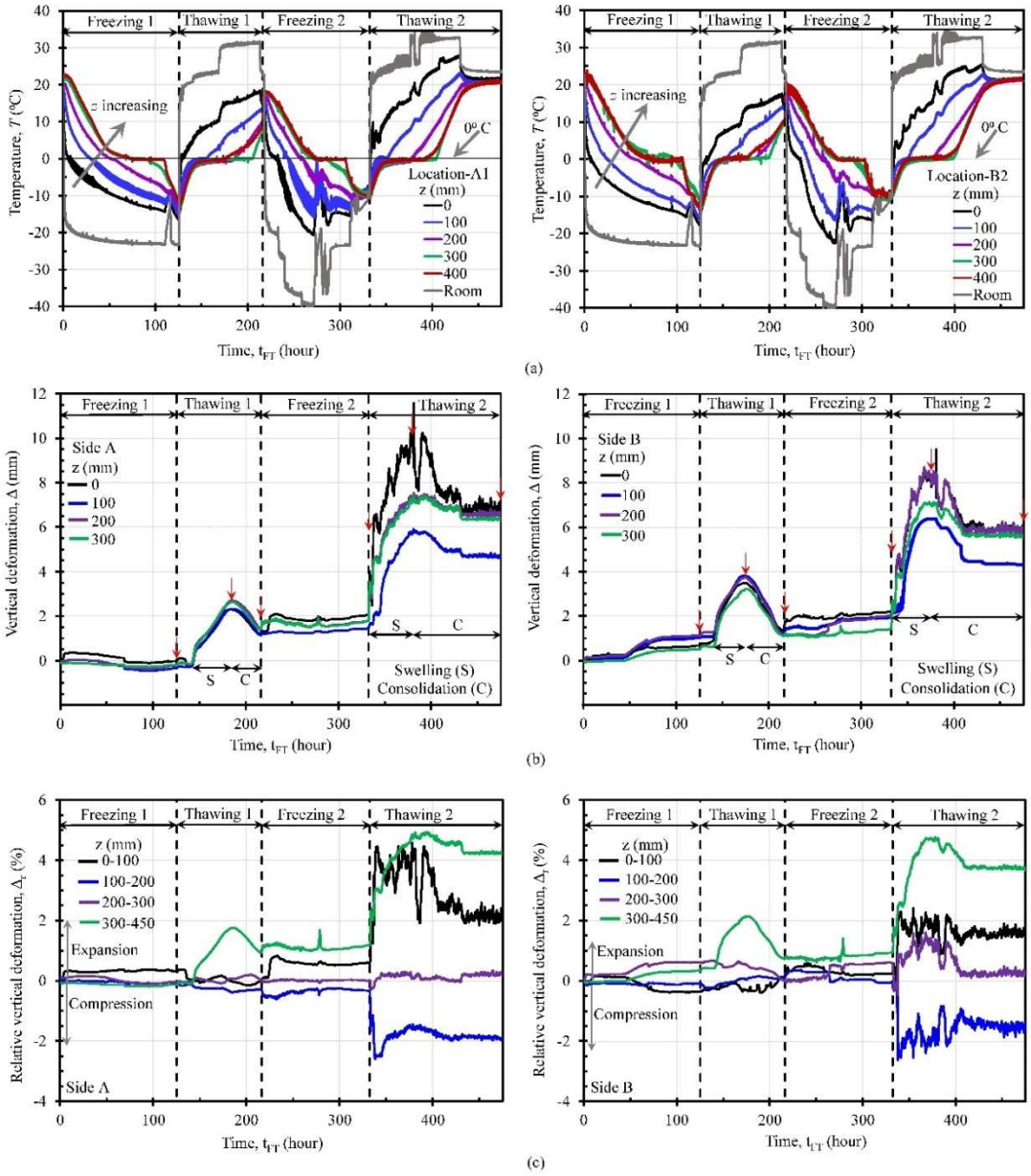

Figure 29. Summary of information continuously monitored during two freeze-thaw cycles on Side A (left) and Side B (right) of the soil box: a.) temperatures monitored in the environmental chamber (room) and at soil depths z = 100, 200, 300, and 400 mm; b.) subsurface vertical deformations measured via settlement plate at soil depths z = 100, 200, 300, and 400 mm; c.) relative vertical deformations expressed as a per-centage of the thickness of soil between settlement plates for the subsurface depth intervals of 0-100, 100-200, 200-300, and 300-450 mm.

Shear wave velocity measurements in the fully carbonated material (z = 50 mm) were initially 659 m/s prior to beginning the FT experiments. The shear wave velocity decreased to 461 m/s after the first FT cycle, but effectively remained unchanged thereafter. Thus, there was a modest drop due to weathering imposed by frost action after the first FT cycle in the carbonated silt, though it remained substantially elevated from pre-carbonation levels (Vs = 228m/s). At z = 250 mm, a

decrease to Vs = 165m/s was observed after the first FT cycle, but remained unchanged after the second FT cycle, similar to the shallower measurement.

Figure 30 shows the CBR values and water contents measured after two freeze-thaw cycles, which are compared with surface measurements after soaking, but before freeze-thaw testing, and before surface carbonation was performed (i.e. at low water contents). As expected, the strength and stiffness of fully-carbonated silt had the greatest strength and stiffness, and generally decreased in the lightly carbonated and uncarbonated soil below. According to CBR-based frost susceptibility criteria (ASTM 2013), measurements indicate fully carbonated silt had a very low susceptibility to frost action. Below the fully-carbonated soil, CBR values generally decreased with depth and the frost-susceptibility rating ranged from medium to high. Decreasing CBR values with depth can be attributed to the decreasing thickness of carbonated soil below the depth where CBR testing was conducted. CBR values in the untreated silt were very low with high to very high frost-susceptibility rating, as expected. The results from deeper tests, where loading likely resulted in some interaction with the untreated material, are also compared with CBR values before carbonation when water contents were lower. This further highlights: i.) the substantial impact that environmental stressors can have on the strength and bearing resistance of frost-susceptible soils; and ii.) that CBR values based on compaction alone should not be relied on as an indicator of the quality of subgrade material supporting surface transportation infrastructure where frost action occurs. CBR values based on compaction only would be considered a "very good" subgrade material (Schaefer et al. 2008) (see criteria presented in Figure 28).

After the 12-week drying period of the soil column to allow moisture contents to decrease, which is expected for roadway foundation materials after seasonal periods where frost action occurs, CBR testing and sampling were performed to assess the resilience of carbonated material and potential changes in the gravimetric binder content (BC). Figure 31 illustrates representative changes in CBR and water content observed throughout the drying period. CBR values fully recovered, and in most cases, exceeded values observed after carbonation, but prior to soaking and FT testing. Thus, carbonated soil is resilient to soaking and frost-action.

The notable increases in CBR, especially in the lightly carbonated soil, was not expected. Sampling and TGA results revealed a continued increase in the BC and associated decrease in unreacted $Ca(OH)_2$ from depths z = 150 to 300 mm (Figure 31b). Immediately after carbonation there was limited $CaCO_3$ formed below 150 mm. However, one week elapsed between the accelerated carbonation phase and full saturation of the silt during the soaking phase, which would have left water contents relatively low and substantial "air pipes" in the soil matrix during that time. Thus, any lime remaining after accelerated carbonation had the potential to react with atmospheric CO_2 between the end of accelerated surface carbonation and soaking, which is likely why there was some increase in the BC (and decrease in $Ca(OH)_2$) between carbonation and soaking (Figure 31b). However, diffusion of CO_2 into the voids would have been effectively halted once the box was soaked because water significantly obstructs the mobility of gas (Moldrup et al. 2000, 2001, Mahmoodi and Gallant 2020, 2021). Therefore, carbonation could not have been occurring after soaking and during freeze-thaw testing. During the 12-week drying period it is believed that the decreasing water content opened pathways for atmospheric CO_2 to diffuse into the soil and react with lime in the previously lightly carbonated soil (z = 150 to 300 mm). Given this additional

carbonation increases the effective thickness of cemented soil, it explains the increase in CBR observed (Gallant et al. 2024).

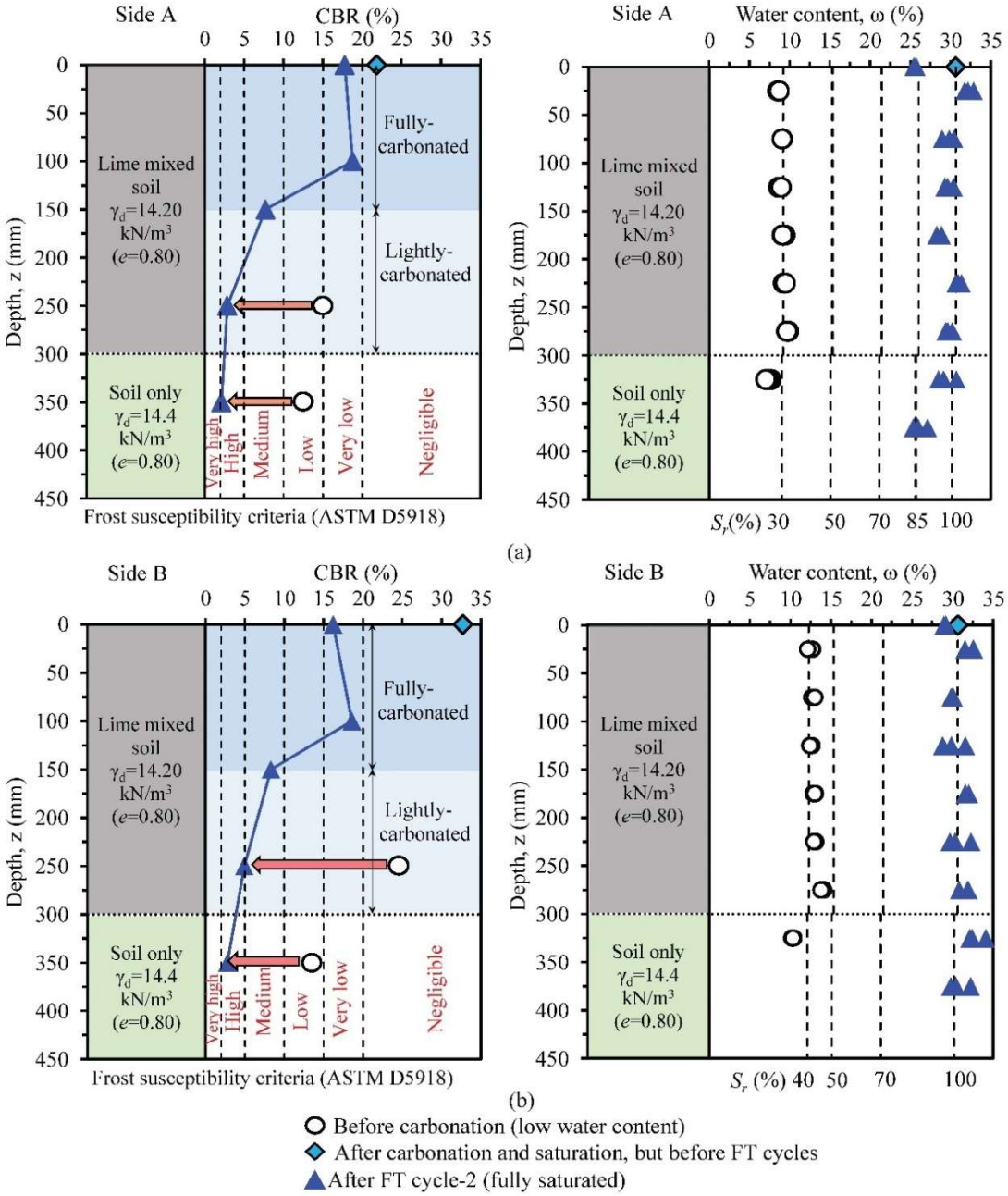

Figure 30. CBR values and water contents measured after two freeze-thaw cycles compared with surface measurements after soaking, but before freeze-thaw testing, and before surface carbonation was performed in a.) Side A and b.) Side B. The frost-susceptibility criteria according to ASTM D5918 are also indicated.

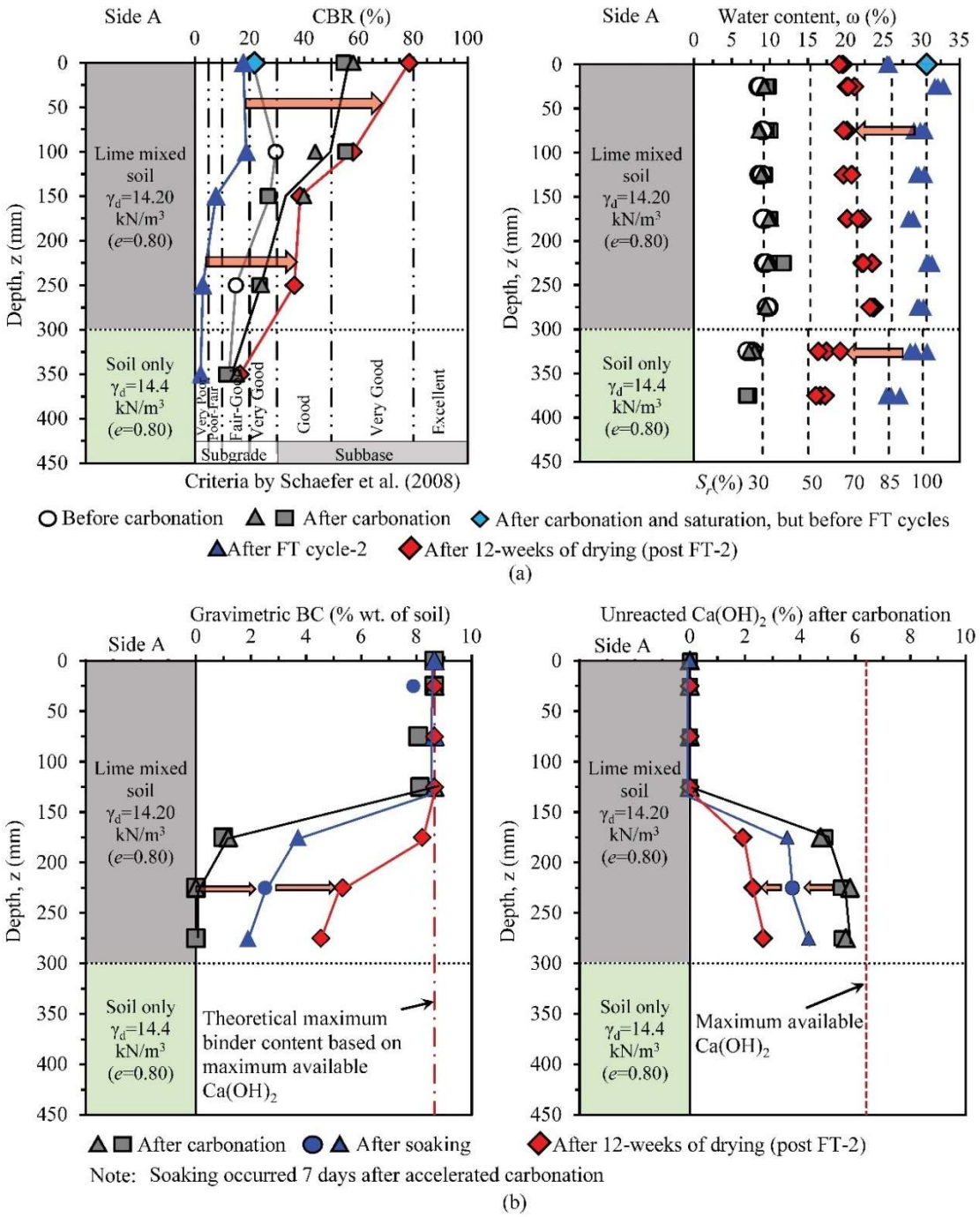

Figure 31. Comparison summary for Side A of the soil box: a.) highlighted comparison between CBR values observed after two-freeze thaw cycles with values after a 12-week drying period (left); changes in water content (right); b.) highlighted changes in gravimetric binder content (left) and unreacted calcium hydroxide during the drying period. Also shown in (a) and (b) are measurements before carbonation, after accelerated carbonation, and soaking.

Chapter 4: Benefits and Challenges of Accelerated Carbonation

Conventional lime-stabilization can take months, or even years, for the binding hydration products to fully form. It is typically only applied to "reactive" soils with soluble pozzolans—which were not present in the soil tested. Accelerated carbonation offers a means to utilize lime for "non-reactive" granular or low plasticity materials as well.

During production of materials derived from limestone ($CaCO_3$), like cement and lime, limestone is quarried and then calcinated in kilns, where it decomposes into quick lime ($CaCO_3$+Heat→CaO + CO_2). Water is simply added to quick lime to form hydrated lime ($Ca(OH)_2$) used in this study. The carbon dioxide generated due to the decomposition of limestone is referred to as "process-based" carbon emissions. As illustrated in Figure 32, accelerated carbonation of lime has the potential to sequester the same amount of CO_2 attributed to process-based emissions when lime is converted back to $CaCO_3$. Calcination and the associated decomposition of limestone remain the most carbon-intensive component of lime and cement production, where process-based emissions are also accompanied by "combustion- based" emissions attributed to the energy/fuels required to heat kilns. However, process-based emissions account for approximately two-thirds of CO_2 emissions during this process (Stork et al. 2014, Campo et al. 2021). Thus, accelerated soil carbonation has the potential to permanently sequester the majority of CO_2 attributed to calcination—assuming adequate methods are applied to achieve complete mineral carbonation with this chemical additive. In this study, it has demonstrated that the available $Ca(OH)_2$ can be completely converted to $CaCO_3$ in soil; i.e. the amount of CO_2 sequestered was equivalent to approximately 100% of process-based emissions associated with production of the lime. However, getting CO_2 into the soil is likely to be the greatest challenge.

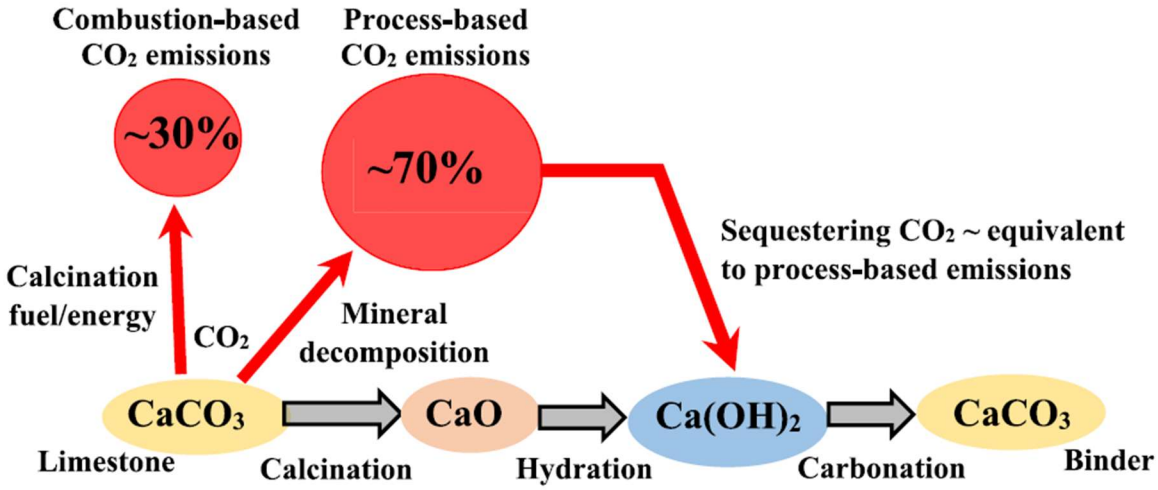

Figure 32. Flow chart illustrates carbon dioxide emissions during production and sequestration of carbon dioxide during soil carbonation, which has the potential to be equivalent to process-based emissions (from Gallant et al. 2025).

The enablement of soil carbonation remains in its infancy. An obvious drawback is the required step to introduce gas, which is not required with conventional chemical stabilization methods that rely on traditional hydration products to bind the soil. Field-scaling processes will need to consider techniques to supply large amounts of gas, which are not yet readily available, but soon may be. Additionally, strategies will likely either need to: a.) have some control over water content in the

field to ensure sufficient permeability of gas in the soil, which is sometimes the case for shallow subgrade stabilization; or b.) utilize pressurized systems or develop techniques that can overcome the challenges associated with carbonation of soil with high water contents. This study attempted to leverage the first concept by using low degrees of saturation because gas otherwise diffuses very slowly through soil with a continuous water-phase in the voids (Moldrup et al. 2000, 2001, Fredlund et al. 2012 Mahmoodi and Gallant 2020, 2021, Feng et al. 2023), which is attributed in part to the rate of carbonation (Li et al. 2023, Rodriguez-Navarro et al. 2023, Gallant et al. 2025). If gas can get into the soil, the carbonation reaction happens rapidly, and the rate of binder formation is governed primarily by the rate that CO_2 gas is introduced and the ability of the gas to penetrate into a soil–lime-water mixture. It was demonstrated via both elemental and large-scale testing that full carbonation can be achieved on the order of a few hours under certain conditions.

However, substantial increases in the carbonate content were observed in the week between accelerated carbonation and soaking and then during the 12-week drying period that followed environmental testing for the large soil box experiment. While these findings were unintended, they indicate that substantial amounts of binder can form so long as water in the soil matrix does not obstruct the diffusion of atmospheric CO_2 into the soil. This observation opens the possibility to passively carbonating soil in a reasonable time frame without the complexity of developing systems and processes to introduce CO_2 directly, which may be suitable for some applications. This of course relies on ensuring that lime-mixed soil is prepared (mixed and compacted) at water contents that permit the diffusion of CO_2 gas.

To fully exploit the potential environmental benefits, it will also be necessary to optimize the required thickness of treated material, mixing methods, and the lime content. The logistics associated with these challenges will need to be overcome prior to widespread adoption of soil carbonation in practice. However, the need to mitigate CO_2 emissions may hasten the advancement of carbonation solutions for soil stabilization.

Chapter 5: Summary and Conclusions

This report investigated the feasibility of using accelerated mineral carbonation of hydrated lime to stabilize non-plastic soils, with the dual objectives of improving mechanical performance and reducing the carbon footprint associated with conventional cement-based stabilization. Elemental laboratory testing and large-scale soil box experiments were conducted to evaluate reaction kinetics, strength and stiffness gains, scalability, and environmental durability.

Elemental testing demonstrated that accelerated carbonation can generate substantial strength and stiffness gains in sands and silts through the formation of a calcium carbonate binder. The degree of mechanical improvement was governed primarily by density, volumetric binder content, and soil type, consistent with trends observed in cement-stabilized soils. Carbonated soils exhibited strength–binder–porosity relationships that closely matched established predictive frameworks for cement-treated materials, indicating that carbonation-based stabilization can achieve comparable performance. Stiffness was strongly correlated with strength, confirming that the binder phase dominates mechanical behavior.

The rate of carbonation was found to be intrinsically linked to gas mobility within the soil matrix. Specimens prepared at intermediate degrees of saturation (approximately 30–50%) carbonated most rapidly due to the coexistence of sufficient pore water to host reactions and a continuous gas phase to facilitate CO_2 transport. High degrees of saturation substantially suppressed carbonation rates due to gas-phase obstruction, while very low water contents limited reaction kinetics.

Large-scale soil box experiments demonstrated that accelerated surface carbonation can be implemented under near-atmospheric pressure and can propagate downward through the soil profile. Field-representative testing showed measurable increases in strength and stiffness with depth, supported by temperature monitoring, shear wave velocity measurements, and field CBR testing. Following saturation and freeze–thaw cycling, the carbonated soils retained improved mechanical performance, indicating strong resistance to frost-related degradation.

Overall, the findings confirm that accelerated mineral carbonation of lime-treated non-plastic soils is a potential stabilization technique with performance comparable to cement-based methods from a mechanical perspective. Importantly, carbonation offers the potential to substantially offset process-based CO_2 emissions associated with lime production, positioning it as a promising pathway for decarbonizing geotechnical and transportation infrastructure. While additional research is needed to refine field implementation strategies and expand validation across a broader range of soil types and conditions, the results presented establish a strong technical foundation for to develop enablement schemes for carbonation-based soil stabilization.

References

Apodaca LE. 2021. Lime statistics and information. URL: https://pubs.usgs.gov/periodicals/mcs2021/mcs2021-lime.pdf last accessed 25 June 2021.

Ashraf W. Carbonation of cement-based materials: challenges and opportunities. 2016. Constr Build Mater 120: 558–70.

ASTM 2009. Standard test methods for unconfined compressive strength of compacted soil–lime mixtures. ASTM D5102. ASTM, West Conshohocken, PA.

ASTM 2012. Standard test methods for laboratory compaction characteristics of soil using standard effort (12,400 ft-lbf/ft3 (600 kNm/m3)). ASTM D698. ASTM, West Conshohocken, PA.

ASTM. 2013. Standard Test Methods for Frost Heave and Thaw Weakening Susceptibility of Soils. *ASTM D5913*. West Conshohocken, PA: ASTM.

ASTM 2014. Standard test method for rapid determination of carbonate content of soils. ASTM D4373. ASTM, West Conshohocken, PA.

ASTM 2017a. Standard practice for classification of soils for engineering purposes (unified soil classification system). ASTM D2487. ASTM, West Conshohocken, PA.

ASTM 2017b. Standard practice for laboratory preparation of soil–lime mixtures using mechanical mixer. ASTM D3551. ASTM, West Conshohocken, PA.

ASTM 2017c. Standard specification for standard sand. ASTM C778. ASTM, West Conshohocken, PA.

Barman, D., and Dash, S.K. 2022. Stabilization of expansive soils using chemical additives: a review. Journal of Rock Mechanics and Geotechnical Engineering, 14(4): 1319–1342. doi:10.1016/j.jrmge.2022.02.011.

Behnood A. 2018. Soil and clay stabilization with calcium-and non-calcium-based additives: A state-of-the-art review of challenges, approaches and techniques. *Transport Geotech* 17: 14–32.

Boynton, S.S. and D.E. Daniel. 1985. Hydraulic conductivity tests on compacted clay. *Journal of Geotechnical Engineering* 111 (4): 465–478.

Burland, J. 1990. On the compressibility and shear strength of natural clays. Géotechnique, 40(3): 329–378. doi:10.1680/geot.1990.40.3.329.

Cai H, Du G, Liu JY, YS, Singh ND. 2015. Physical properties, electrical resistivity, and strength characteristics of carbonated silty soil admixed with reactive magnesia. *Canadian Geotech J* 52: 1699–1713.

Cai, G., Liu, S., Zhong, Y., Poon, C., and Li, J. 2023. Model investigation of the low-carbon mgo-treated soil foundation based on Co2 overall carbonation. Journal of Rock Mechanics and Geotechnical Engineering, 15(11): 2901–2916. doi:10.1016/j.jrmge.2023.02.018.

Campo FP, Tua C, Biganzoli L, Pantini S, Grosso M. 2021. Natural and enhanced carbonation of lime in its different applications: a review. *Environ Technol Rev* 10: 224–237.

Cizer, Ö., Rodriguez-Navarro, C., Ruiz-Agudo, E., Elsen, J., Van Gemert, D., and Van Balen, K. 2012. Phase and morphology evolution of calcium carbonate precipitated by carbonation of hydrated lime. Journal of Materials Science, 47(16): 6151–6165. doi:10.1007/s10853-012-6535-7.

Chamberlain, E.J. 1981. *Frost susceptibility of soil, review of index tests*. Technical report, Cold Regions Research and Engineering Lab Hanover NH.

Consoli NC, Foppa D, Festugato L, Heineck KS. 2007. Key parameters for strength control of artificially cemented soils. *J Geotech Geoenviron Eng.* 133: 197–205.

Consoli, N.C., Lopes, D.S.L., Jr., and Heineck, K.S. 2009. Key parameters for the strength control of lime stabilized soils. Journal of Materials in Civil Engineering, 21(5): 210–216. doi:10.1061/(ASCE)0899-1561(2009)21:5(210).

Consoli, N.C., Lopes, L.D.S., Jr, Prietto, P.D.M., Festugato, L., and Cruz, R.C. 2011a. Variables controlling stiffness and strength of lime-stabilized soils. Journal of Geotechnical and Geoenvironmental Engineering, 137(6): 628–632. doi:10.1061/(ASCE)GT.1943-5606.0000470.

Consoli, N.C., Rosa, A.D., and Saldanha, R.B. 2011b. Variables governing strength of compacted soil–fly ash–lime mixtures. Journal of Materials in Civil Engineering, 23(4): 432–440. doi:10.1061/(ASCE)MT.1943-5533.0000186.

Consoli NC, Vaz Ferreira PM, Tang CS, Veloso Marques SF, Festugato L, Corte MB. 2016. A unique relationship determining strength of silty/clayey soils–Portland cement mixes. *Soils Found* 56: 1082–1088.

Consoli, N.C., Winter, D., Leon, H.B., and Scheuermann Filho, H.C. 2018. Durability, strength, and stiffness of green stabilized sand. Journal of Geotechnical and Geoenvironmental Engineering, 144(9): 04018057. doi:10.1061/(ASCE)GT.1943-5606.0001928.

Consoli, N.C., BittarMarin, E.J., Quiñónez Samaniego, R.A., Scheuermann Filho, H.C., and Cristelo, N.M.C. 2020. Field and laboratory behaviour of fine-grained` soil stabilized with lime. Canadian Geotechnical Journal, 57(6): 933–938. doi:10.1139/cgj-2019-0271.

Consoli, N.C., da Silva Carretta, M., Festugato, L., Leon, H.B., Tomasi, L.F., and Heineck, K.S. 2021. Ground waste glass–carbide lime as a sustainable binder stabilising three different silica sands. Géotechnique, 71(6): 480–493. doi:10.1680/jgeot.18.P.099.

Cook, R.D. 1963. *Some Effects of Closed System Freeze-thaw Cycles on a Compacted, Highly Plastic Clay*. Ph. D. thesis, University of Alberta.

Cunningham, M., Ridley, A., Dineen, K., and Burland, J. 2003. The mechanical behaviour of a reconstituted unsaturated silty clay. Géotechnique, 53(2): 183–194. doi:10.1680/geot.2003.53.2.183

Das G, Razakamanantsoa A, Herrier G, Saussaye L, Lesueur D, Deneele D. 2021. Evaluation of the long-term effect of lime treatment on a silty soil embankment after seven years of atmospheric exposure: mechanical, physicochemical, and microstructural studies. *Eng Geol* 281: 105986.

Das G, Razakamanantsoa A, Saussaye L, Losma F, Deneele D. 2022. Carbonation investigation on atmospherically exposed lime-treated silty soil. *Case Stud Constr Mater* 17: e01222.

Dash SK, Hussain M. 2012. Lime stabilization of soils: Reappraisal. *J Mater Civ Eng* 24: 707–714.

Dempsey, B.J. and M.R. Thompson. 1972. *Effects of freeze-thaw parameters on the durability of stabilized materials*. University of Illinois.

De Silva P, Bucea L, Moorehead DR, Sirivivatnanon V. 2006. Carbonate binders: Reaction kinetics, strength and microstructure. *Cem Concr Compos* 28: 613–620.

De Silva P, Bucea L, Sirivivatnanon V. 2009. Chemical, microstructural and strength development of calcium and magnesium carbonate binders. *Cem Concr Res* 39: 460–465.

Diambra, A., Ibraim, E., Peccin, A., Consoli, N., and Festugato, L. 2017. Theoretical derivation of artificially cemented granular soil strength. Journal of Geotechnical and Geoenvironmental Engineering, 143(5): 04017003. doi:10.1061/(ASCE)GT.1943-5606.0001646.

dos Santos, C.P., Bruschi, G.J., Mattos, J.R.G., and Consoli, N.C. 2022. Stabilization of gold mining tailings with alkali-activated carbide lime and sugarcane bagasse ash. Transportation Geotechnics, 32: 100704.

Dowling A, O'Dwyer J, Adley CC. 2015. Lime in the limelight. *J Clean Prod* 92: 13–22.

Escario, V., and Saez, J. 1986. The shear strength of partly saturated soils. Géotechnique, 36(3): 453–456. doi:10.1680/geot.1986.36.3.453.

Fan W, Chen W, Zhang Q, Wu G. 2023. Effects of sticky rice on the carbonation reaction of lime-treated soil in earthen sites. *Constr Build Mater* 378: 131164.

Fasihnikoutalab MH, Asadi A, Huat BK, Westgate P, Ball RJ, Pourakbar S. 2016. Laboratory-scale model of carbon dioxide deposition for soil stabilisation. *J Rock Mech Geotech Eng* 8: 178–86.

Fasihnikoutalab MH, Asadi A, Huat BK, Ball RJ, Pourakbar S, Singh P. 2017. Utilisation of carbonating olivine for sustainable soil stabilisation. *Environ Geotech* 4: 184–198.

Feng, R., L. Wu, D. Liu, Y. Wang, and B. Peng. 2020. Lime-and cement- treated sandy lean clay for highway subgrade in china. *Journal of materials in civil engineering* 32 (1): 04019335.

Feng S, Sun J, Zhan L, Liu H. 2023. A new method and instrument for measuring in situ gas diffusion coefficient and gas coefficient of permeability of unsaturated soil. *J Geotech Geoenviron Eng* 149: 04023041.

Fredlund, D.G., Xing, A., Fredlund, M., and Barbour, S. 1996. The relationship of the unsaturated soil shear strength to the soil–water characteristic curve. Canadian Geotechnical Journal, 33(3): 440–448. doi:10.1139/t96-065.

Fredlund DG, Rahardjo H, Fredlund MD. 2012. *Unsaturated soil mechanics in engineering practice*. John Wiley & Sons.

Gallant AP, Hossen SB, Botero-Lopez. Ashraf W. 2024. Accelerated surface carbonation of non-plastic silt mixed with lime. *Transport Geotech* 48: 101320.

Gallant AP, Hossen SB, Ashraf W. 2025. Accelerated carbonation of non-plastic soils mixed with hydrated lime: index properties influencing binder formation rate and mechanical improvement. *Can Geotech J* 00: 1-19.

Graham, J. and V. Au. 1985. Effects of freeze–thaw and softening on a natural clay at low stresses. *Canadian Geotechnical Journal* 22 (1): 69–78.

Gross, J., & Adaska, W. 2020. *Guide to cement-stabilized subgrade soils*. Portland Cement Association: Washington, DC, USA.

Hadjittofis E, Vargas SM, Litster JD, Campbell KLS. 2022. Exploring the role of crystal habit in the ostwald rule of stages. *Proc Royal Soc A* 478: 20210601.

Han, S.J., Yoo, M., Kim, D.W., andWee, J.H. 2011. Carbon dioxide capture using calcium hydroxide aqueous solution as the absorbent. Energy & Fuels, 25(8): 3825–3834.

Haque MI, Borno IB, Khan RI, Ashraf W. 2023. Reducing carbonation degradation and enhancing elastic properties of calcium silicate hydrates using biomimetic molecules. *Cem Concr Compos* 136: 104888.

Hay, R., Kashwani, G., and Celik, K. 2021. Carbonation, strength development, and characterization of calcined limestone as a potential construction material. Cement and Concrete Research, **139**: 106263. doi:10.1016/j.cemconres.2020.106263.

Hazirbaba, K. and H. Gullu. 2010. California bearing ratio improvement and freeze–thaw performance of fine-grained soils treated with geofiber and synthetic fluid. *Cold regions science and technology* 63 (1-2): 50–60.

Higgins D. 2005. *Soil stabilisation with ground granulated blastfurnace slag*. UK Cementitious Slag Makers Association (CSMA) 1:15.

Hossen SB, Gallant AP, Ashraf W. 2020. Elemental testing of carbonated silty sand treated with lime. *In Geo-Congress 2020: Foundations, Soil Improvement, and Erosion*. VA: American Society of Civil Engineers, Reston, VA: 562–571.

Hossen SB. 2023. Laboratory Study of Accelerated Carbonation with Hydrated Lime for Soil Stabilization. Maine: University of Maine Orono. Ph.D. thesis.

Jang, J.G., Kim, G.M., Kim, H.J., and Lee, H.K. 2016. Review on recent advances in CO2 utilization and sequestration technologies in cement-based materials. Construction and Building Materials, 127: 762–773. doi:10.1016/j.conbuildmat.2016.10.017.

Konrad, J.M. and N.R. Morgenstern. 1980. A mechanistic theory of ice lens formation in fine-grained soils. *Canadian Geotechnical Journal* 17 (4): 473–486.

Konrad, J.M. and N. Morgenstern. 1984. Frost heave prediction of chilled pipelines buried in unfrozen soils. *Canadian Geotechnical Journal* 21 (1): 100–115.

Konrad, J.M. and M. Roy. 2000. Flexible pavements in cold regions: a geotechnical perspective. *Canadian Geotechnical Journal* 37 (3): 689–699.

Lee, W., N. Bohra, A. Altschaeffl, and T. White. 1995. Resilient modulus of cohesive soils and the effect of freeze–thaw. *Canadian Geotechnical Journal* 32 (4): 559–568.

Leelavathamma, B., K. Mini, and N. Pandian. 2005. California bearing ratio behavior of soil-stabilized class f fly ash systems. *Journal of Testing and Evaluation* 33 (6).

Leroueil, S., J. Tardif, M. Roy, P.L. Rochelle, and J.M. Konrad. 1991. Effects of frost on the mechanical behaviour of champlain sea clays. *Canadian Geotechnical Journal* 28 (5): 690–697.

Li M, Cai G, Wang Q, Liu S, He H, Liu X, Shi W. 2023. The state of the art of carbonation technology in geotechnical engineering: A comprehensive review. *Renew Sustain Energy Rev* 171: 112986.

Little DN. 1999. *Evaluation of structural properties of lime stabilized soils and aggregates*. In: summary of findings, Volume 1. Arlington, VA: The National Lime Association (NLA).

Little, D.N., & Nair, S. 2009. *Recommended practice for stabilization of subgrade soils and base materials*. Washington, DC: National Cooperative Highway Research Program, Transportation Research Board of the National Academics.

Liu, S.-Y., Cai, G.-H., Du, G.-Y.,Wang, L., Li, J.-S., and Qian, X.-C. 2021. Field investigation of shallow soft-soil highway subgrade treated by mass carbonation technology. Canadian Geotechnical Journal, 58(1): 97– 113. doi:10.1139/cgj-2020-0008.

Loehr, J.E., Lutenegger, A., Rosenblad, B.L., Boeckmann, A., & Brinckerhoff, P. 2016. *Geotechnical Site Characterization Geotechnical Engineering Circular No. 5*. Technical Report National Highway Institute (US).

Mahmoodi, B. and A.P. Gallant. 2020. Efficient determination of aqueous-phase gas diffusion coefficients and tortuosity in soil. *Geotechnique Letters* 10 (4): 575–581.

Mahmoodi, B. and A. Gallant. 2021. Assessing persistence of entrapped gas for induced partial saturation. *Journal of Geotechnical and Geoenvironmental Engineering* 147 (3): 04020184.

Moldrup, P., T. Olesen, J. Gamst, P. Schjønning, T. Yamaguchi, and D. Rolston. 2000. Predicting the gas diffusion coefficient in repacked soil water-induced linear reduction model. *Soil Science Society of America Journal* 64 (5): 1588–1594.

Moldrup, P., T. Olesen, T. Komatsu, P. Schjønning, and D. Rolston. 2001. Tortuosity, diffusivity, and permeability in the soil liquid and gaseous phases. *Soil Science Society of America Journal* 65 (3): 613–623.

Merrill, A. 2021. Magnesium compounds statistics and information. URL: https://pubs.usgs.gov/periodicals/mcs2021/mcs2021-lime.pdf last accessed 25 June 2021.

Miller, S.A., John, V.M., Pacca, S.A., and Horvath, A. 2018. Carbon dioxide reduction potential in the global cement industry by 2050. Cement and Concrete Research, 114: 115–124. doi:10.1016/j.cemconres.2017.08.026.

Moldrup, P., Olesen, T., Gamst, J., Schjønning, P., Yamaguchi, T., and Rolston, D. 2000. Predicting the gas diffusion coefficient in repacked soil water-induced linear reduction model. Soil Science Society of America Journal, **64**(5): 1588–1594. doi:10.2136/sssaj2000.6451588x.

Moldrup, P., Olesen, T., Komatsu, T., Schjønning, P., and Rolston, D. 2001. Tortuosity, diffusivity, and permeability in the soil liquid and gaseous phases. Soil Science Society of America Journal, **65**(3): 613–623. doi:10.2136/sssaj2001.653613x.

Mooney, M.A., Finno, R.J., and Viggiani, M.G. 1998. A unique critical state for sand? Journal of Geotechnical and Geoenvironmental Engineering, 124(11): 1100–1108. doi:10.1061/(ASCE)1090-0241(1998)124:11(1100).

NEHRP. 2003. *Recommended provisions for seismic regulations for new buildings and other steel structures. part 1: Provisions*. Federal Emergency Management Agency, (p. 338).

Olesen, T., Moldrup, P., and Gamst, J. 1999. Solute diffusion and adsorption in six soils along a soil texture gradient. Soil Science Society of America Journal, **63**(3): 519–524. doi:10.2136/sssaj1999. 03615995006300030014x.

Olesen, T., Moldrup, P., Henriksen, K., and Petersen, L. 1996. Modeling diffusion and reaction in soils: iv. new models for predicting ion diffusivity. Soil science, **161**(10): 633–645. doi:10.1097/00010694-199610000-00001.

Othman, M.A. and C.H. Benson. 1993. Effect of freeze–thaw on the hydraulic conductivity and morphology of compacted clay. *Canadian Geotech J* 30 (2): 236–246.

Perbawa, A., Gramajo, E., Finkbeiner, T., and Santamarina, J. 2021. Rock triaxial tests: global deformation vs local strain measurements implications. Rock Mechanics and Rock Engineering, 54(7): 3527–3540. doi:10.1007/s00603-021-02389-z.

Puppala AJ. 2016. "Advances in ground modification with chemical additives: From theory to practice. *Transport Geotech* 9: 123–138.

Reis, D.C., Quattrone, M., Souza, J.F.T., Punhagui, K.R.G., Pacca, S.A., and John, V.M. 2021. Potential CO2 reduction and uptake due to industrialization and efficient cement use in Brazil by 2050. Journal of Industrial Ecology, 25(2): 344–358. doi:10.1111/jiec.13130.

Rodriguez-Navarro C, Ili´c T, Ruiz-Agudo E, Elert K. 2023. Carbonation mechanisms and kinetics of lime-based binders: An overview. *Cem Concr Res* 173: 107301.

Schaefer, V.R., White, D.J., Ceylan, H., & Stevens, L.J. 2008. *Design guide for improved quality of roadway subgrades and subbases*. Iowa Highway Research Board (IHRB Project TR-525), 7, 8–72.

Schjønning, P., Thomsen, I.K., Møberg, J.P., de Jonge, H., Kristensen, K., and Christensen, B.T. 1999. Turnover of organic matter in differently textured soils: I. physical characteristics of structurally disturbed and intact soils. Geoderma, 89(3–4): 177–198. doi:10.1016/S0016-7061(98)00083-4.

Sherwood P. 1993. *Soil stabilization with cement and lime. Transport Research Laboratory (TRL) State-of-the Art Review*. Berkshire, UK: Her Majesty Stationary Office.

Silva, B., Pinto, A.F., Gomes, A., and Candeias, A. 2021. Effects of natural and accelerated carbonation on the properties of lime-based materials. Journal of CO2 Utilization, 49: 101552. doi:10.1016/j.jcou.2021.101552.

Stork M, Meindertsma W, Overgaag M, Neelis M. 2014. *A competitive and efficient lime industry-cornerstone for a sustainable Europe*. In: Technical report by The European Lime Association (EuLA). Brussels, Belgium: EuLA.

Thompson, M.R. and B.J. Dempsey. 1970. Quantitative characterization of cyclic freezing and thawing in stabilized pavement materials. *Highway Research Record* (304).

Toohey NM, Mooney MA, Bearce RG. 2013. Stress-strain-strength behavior of lime-stabilized soils during accelerated curing. *J Mater Civ Eng* 25: 1880–1886.

UNEP-GEAS 2010. Greening cement production has a big role to play in reducing greenhouse gas emissions. United Nations Environment Programme (UNEP) Global Environmental Alert Service (GEAS). UNEPGEAS, Sioux Falls, SD.

Vanapalli, S.K., Fredlund, D.G., and Pufahl, D.E. 1996. The relationship between the soil–water characteristic curve and the unsaturated shear strength of a compacted glacial till. Geotechnical Testing Journal, 19:259–268. doi:10.1520/GTJ10351J.

Viklander, P. 1998. Permeability and volume changes in till due to cyclic freeze/thaw. *Canadian Geotechnical Journal* 35 (3): 471–477.

Weil MH, DeJong JT, Martinez BC, Mortensen BM. 2012. Seismic and resistivity measurements for real-time monitoring of microbially induced calcite precipitation in sand. *ASTM Geotech Test J* 35: 330–41.

Worrell, E., Price, L., Martin, N., Hendriks, C., and Meida, L.O. 2001. Carbon dioxide emissions from the global cement industry. Annual Review of Energy and the Environment, 26: 303–329. doi:10.1146/annurev.energy.26.1.303.

Xu L, Zha F, Liu C, Kang B, Liu J, Yu C. 2020. Experimental investigation on carbonation behavior in lime-stabilized expansive soil. *Adv Civil Eng* 2020: 1–14.

Yi Y, Liska M, Akinyugha A, Unluer C, Al-Tabbaa A. 2013a. Preliminary laboratory-scale model auger installation and testing of carbonated soil-mgo columns. Geotech Test J 36: 384–93.

Yi Y, Liska M, Unluer C, Al-Tabbaa A. 2013b. Carbonating magnesia for soil stabilization. *Can Geotech J* 50:899–905.

Yi Y, Liska M, Al-Tabbaa A. 2014. Properties of two model soils stabilized with different blends and contents of GGBS, MgO, lime, and PC. *J Mater Civ Eng* 26: 267–274.

Transportation Infrastructure Durability Center
AT THE UNIVERSITY OF MAINE

35 Flagstaff Road
Orono, Maine 04469
tidc@maine.edu
207.581.4376

www.tidc-utc.org